ERDC/CHL TR-00-10

Coastal and Hydraulics Laboratory

US Army Corps
of Engineers.
Engineer Research and
Development Center

Lower St. Johns River and Estuary, Florida, Numerical Model Study

Jose A. Sanchez and Robert A. Evans, Jr.

July 2000

ERDC/CHL TR-00-10
July 2000

Lower St. Johns River and Estuary, Florida, Numerical Model Study

by Jose A. Sanchez

Coastal and Hydraulics Laboratory
U.S. Army Engineer Research and Development Center
3909 Halls Ferry Road
Vicksburg, MS 39180-6199

Robert A. Evans, Jr.

U.S. Army Engineer District, Jacksonville
P.O. Box 4970
Jacksonville, FL 32232-0019

Final report

Approved for public release; distribution is unlimited

Prepared for U.S. Army Engineer District, Jacksonville
Jacksonville, FL 32232-0019

Engineer Research and Development Center Cataloging-in-Publication Data

Sanchez, Jose A.
Lower St. Johns River and estuary, Florida, numerical model study / by Jose A. Sanchez, Robert A. Evans, Jr. ; prepared for U.S. Army Engineer District, Jacksonville.
96 p. : ill. ; 28 cm. — (ERDC/CHL ; TR-00-10)
Includes bibliographic references.
1. Saint Johns River (Fla.) — Mathematical models. 2. Salinity — Florida — Saint Johns River. 3. Hydrodynamics — Florida — Saint Johns River. I. Evans, Robert A. II. United States. Army. Corps of Engineers. Jacksonville District. III. Engineer Research and Development Center (U.S.) IV. Coastal and Hydraulics Laboratory (U.S.) V. Title. VI. Series: ERDC/CHL TR ; 00-10.
TA7 E8 no.ERDC/CHL TR-00-10

CONTENTS

Preface

The study described herein was conducted during 1999 for the U.S. Army Engineer District, Jacksonville, and the St. Johns River Water Management District, Palatka, FL, by personnel of the Coastal and Hydraulics Laboratory (CHL) of the U.S. Army Engineer Research and Development Center (ERDC), Vicksburg, MS. General supervision was provided by Dr. James R. Houston, former Director of CHL; Mr. Thomas W. Richardson, Acting Director, CHL; and Dr. Robert T. McAdory, Chief of Tidal Hydraulics Branch (HE-T), CHL.

Messrs. Jose A. Sanchez, of CHL, and Robert A. Evans, Jr. of the Jacksonville District conducted the study and prepared this report.

At the time of publication of this report, Dr. James R. Houston was Director of ERDC and COL Robin R. Cababa, EN, was Commander.

This report should be cited as follows:

Sanchez, Jose A., and Evans, Robert A. Jr. (2000). "The Lower St. Johns River and Estuary Numerical Model Study," Technical Report ERDC/CHL TR-00-10, U.S. Army Engineer Research and Development Center, Vicksburg, MS.

1 Introduction

The U.S. Army Engineer Research and Development Center (ERDC) was asked to develop a multidimensional hydrodynamic and salinity model for the Lower St. Johns River and Estuary (LSJRE), Florida. The developed model was intended as a general planning tool to gain insight into the hydrodynamics and transport mechanisms of the system.

The LSJRE has some salinity stratification in some of its lower reaches and is well mixed in the upper reaches. To adequately duplicate this stratification and the associated hydrodynamics, a multidimensional model is needed. In a previous effort,[1] the modeling approach was recommended based on expected model needs. This report describes the implementation of those recommendations.

Project Objectives

The objective of this study was to develop a verified multidimensional model of hydrodynamics and salinity transport in the Lower St. Johns River and Estuary. The work was accomplished in the following steps:

a. Develop a working, yet unverified, multidimensional model of hydrodynamics and salinity transport in the LSJRE.

b. Verify the multidimensional model of hydrodynamics and salinity transport against field measurements of tidal elevation, velocity, and salinity concentrations.

Task 1 was the model development phase of the project. Model development encompasses defining questions to be posed, creating the numerical mesh, testing the mesh using synthetic boundary conditions, refining and reworking of the mesh to improve model accuracy and stability, and assigning initial model parameters. To improve performance, modifications of the numerical code were included.

Task 2 was the verification phase of the project. Verification includes:

[1] Roig, Lisa C. (1994). "Review and evaluation of hydrodynamic modeling for the Lower St. Johns River Estuary," Technical Report HL-94-15, U.S. Army Engineer Waterways Experiment Station, Vicksburg, MS.

a. the development of synoptic, comprehensive field (prototype) data sets for boundary conditions and model adjustment,
b. model spin-up to achieve realistic initial conditions,
c. performance of model runs,
d. comparison of simulation results against prototype data,
e. analysis of simulation results,
f. adjustments to improve model performance,
g. comparison of the adjusted model against prototype data,
h. repeat steps e through g until satisfactory results are obtained.

Lower St. Johns River and Estuary Description

The Lower St. Johns River and Estuary extends from the mouth approximately 161 km (100 miles), to just north of Welaka, FL. The mean range of the tide is 1.67 m (5.49 ft) at the mouth, and 0.11 m (0.35 ft) at Welaka. Between these two points, the mean tide range varies from 0.22 m (0.71 ft) at Julington Creek to 0.33 m (1.09 ft) at Palatka. These differences are due mainly to considerable variations of the channel width.

The salinity distribution varies depending on the distance from the ocean. At the ocean, the salinity is between 30 - 35 ppt; at Buffalo Bluff, the salinity is less than 0.5 ppt. The vertical salinity distribution varies between a well mixed structure and a slightly stratified structure. Based on the data collected June 1995 - February 1996, the stretch of the river above the Shands Bridge is well mixed; below the Buckman Bridge there are periods when the salinity is stratified. In between these locations, it is assumed that the salinity varies between stratified and well mixed.

The 1994 bathymetric survey covered only the main stem of the river. Bathymetric data for the tributaries were taken from the National Oceanic and Atmospheric Administration (NOAA) charts, which is referenced to mean lower low water (mllw). The nodes of the initial finite element mesh for the tributaries were digitized from these maps. The Surface Water Modeling System (SMS) Graphical Users Interface (GUI) was then used to unite the tributary meshes with the main stem mesh. Discrepancies among the datums of the bathymetric data from the various sources were carefully corrected. The bathymetry of the model was referenced to the National Geodetic Vertical Datum (NGVD). The difference between mllw and NGVD was obtained from published data[2] (it must be noted that the published data were preliminary).

The character of the St. Johns River itself influenced many of the mesh decisions. For example, a large expanse of tidal marshes exists to the north of the river near its mouth. These tidal marshes are known to store and release tidal waters entering and exiting the marshes through several inlets. The volume of this tidal exchange is unknown and difficult to measure.

[2] National Oceanic and Atmospheric Administration (1993). "Final Report, St. Johns River, Florida, Tide control and tidal characteristics".

In a two-dimensional, channel deepening study of the Lower St. Johns River conducted by ERDC for the U. S. Army Engineer District, Jacksonville during 1994 and 1995, it was noted that the simulation model had difficulty matching velocity measurements in the vicinity of the entrance to the Intracoastal Waterway. It was thought that the major factors affecting these currents were the tidal volume stored in the adjacent marshes and the modulation of the tidal signal resulting from this storage. A numerical experiment was carried out during this earlier study bearing out these assumptions.

For this modeling effort, the magnitude of the water discharge interchange between the main stem of the river and the tidal marshes through two tributaries, Browns Creek and Clapboard Creek, was estimated using discharge data collected during 1994. The same was done for the northern and southern sections of the Intracoastal waterway.

A second characteristic of the St. Johns River influencing the level of mesh resolution is the number of tributaries and inlets. For reasons of model accuracy, it is necessary to increase the resolution around bends, corners, peninsulas, islands, channel expansions and channel contractions to maintain smooth mesh transitions. Geometric features that have a significant influence on the overall circulation of the estuary should be adequately resolved to represent the flow patterns caused by the feature. If the feature does not have a significant influence on the overall circulation, then it is better to ignore the feature and preserve the smoothness of the mesh. Irregular regions of the mesh can cause spurious oscillations of the numerical model solution and degrade solution accuracy. The sinuosity of the main stem, the numerous branch points and inlets, and the numerous large tributaries contribute to the complex geometry of this system. Thus, the level of resolution necessarily increases with the number of features included. Unfortunately, as the level of resolution is increased, the computer time required for processing increases.

It was determined that the mesh must extend into the main tributaries for several reasons. First, inflow boundary conditions must be specified at each of the major tributaries to properly account for the mixing of fresh and brackish waters having more saline water masses. Boundary locations were moved upstream to points along the tributaries where inflow salinities were thought to be known. The St. Johns River Water Management District (SJRWMD) specified the locations of the boundary data points. Second, the circulation patterns of the main stem in the vicinities of the tributaries is generally unknown. The solution domain must be contiguous through the zone of influence of the main stem to properly calculate the tidal circulation.

2 Numerical Hydrodynamic/Salinity Model

RMA10-WES

The generalized numerical hydrodynamic model used in this project is known as RMA10-WES. The model was originally developed under contract to Waterways Experiment Station, now known as ERDC, by Dr. Ian King of Resource Management Associates of Suisun City, CA. The version known as RMA10-WES has been modified significantly by ERDC personnel and is described in Appendix A. A summary of technical specifications of the model is given below:

a. Galerkin finite element formulation,
b. Unstructured mesh composed of bricks, tetrahedral elements, prism, and pyramids in 3-D, triangles and quadrilaterals in 2-D (horizontal averaging or vertical averaging), and line elements in 1-D;
c. Mixed interpolation scheme for pressures and velocities (linear and quadratic);
d. Z - based vertical coordinate transform;
e. Governing equations of the nonlinear Reynolds form of the Navier-Stokes equations, including baroclinic forcing, wind forcing, tidal forcing, Coriolis effect, and bed friction;
f. Three-dimensional, two-dimensional vertically averaged, two-dimensional laterally averaged, and one-dimensional approximations within the same numerical mesh;
g. Time integration via an implicit Crank-Nicholson finite difference operator;
h. Eddy viscosity formulation for horizontal turbulence closure;
i. Mellor-Yamada Level 2 vertical turbulence closure model;
j. Non-linear acceleration and friction terms of the governing equations;
k. Newton-Raphson iteration for the solution of the non-linear system of

equations;

l. Frontal solver for the solution of the matrix equations; and
m. Two algorithms available for wetting and drying of 2-D vertically averaged elements.

Numerical Model Mesh

The numerical model mesh boundary of the Lower St. Johns River is shown in Figures 1a to 1e. The elements of the mesh were divided into 57 categories, called material types. In general, these material types were defined by size, location, and average depth. Table 1 lists the material types and the associated hydraulic and transport parameters. Table 1 also lists the number of layers specified for each material type when the model is used in 3-D mode.

The ocean area is classified with material types 2, 15, 16, and 17. When run in 3-D mode, all of these, with the exception of Material 15, are three-dimensional elements. Material 15 is specified as two-dimensional, because it is on the ocean boundary. Specifying the ocean tidal boundary along two-dimensional elements aids in model stability. In addition, eddy viscosity and Manning's n values in the ocean are artificially high to control instability near the boundaries. These values are numerically, rather than physically based, but do not compromise results in the interior part of the model. Additionally, the region just outside of the jetties has been schematized to insure a smooth boundary. The reason for not including the jetties precisely is to reduce the front width of the model, and thereby the execution time.

The numerical mesh is defined by 5696 1-D/2-D elements and 16457 1-D/2-D nodes. Extending the model to three-dimensions increases the total number to 15,780 elements and 37,187 nodes. The three-dimensional region of the model only includes the main stem up to Shands Bridge and part of the ocean. In areas where the stratification is significant, the three-dimensional area is defined by two, three, or four layers; in areas where the stratification is less significant, there is only one layer; and, in areas where there is no stratification, the elements are two-dimensional. For finite-element, quadratic elements of the type used in RMA10-WES, the number of vertical computation nodes is greater than the number of layers. The number of vertical computation nodes in an area is found using the following formula:

$$N_V = 2 N_L + 1$$

where

N_V = number of vertical computation nodes,

N_L = number of layers specified in the area.

Some of the minor tributaries and marsh areas are represented by one-

dimensional elements. This approach minimizes the computer simulation time requirements.

Boundary Conditions

Figure 1a shows the location of nine inflow data stations used as model boundary conditions. The SJRWMD provided average daily discharge values for Big Davis Creek, Black Creek, Buffalo Bluff, Cedar River, Deep Creek, Dunns Creek, Ortega River, Rice Creek, and Six Mile Creek. The data covered the period 1 April 1996 to 31 January 1997. Recording of discharge data at Cedar River stopped on 30 September 1996. Discharge records of Deep Creek, Dunns Creek, Ortega River, and Six Mile Creek showed several gaps in the data starting during the first days of October 1996. Gaps were also found in the salinity and water surface elevation data provided. Based on the system data on hand and in consultation with the SJRWMD, 120 days were selected, starting on 29 May 1996 as the verification period to avoid major gaps in the field data driving the model. The cumulative total stream inflow to the model is shown in Figure 2. The period represented begins on 29 April 1996 and ends on 26 September 1996. Thirty days were added to the beginning of the verification period as spin-up time to eliminate any residual effects of the initial conditions assigned during the start of the simulation. The actual flow rates are shown in Figures 3 – 11. The primary inflow sources are Dunns Creek and Buffalo Bluff. The discharge at Buffalo Bluff contributes more inflow than all other streams combined.

Still, flow data for Cedar River and Six Mile Creek were incomplete. No flow measurements were collected for Cedar River between 15 June and 9 July. Forty-four days worth of data, starting on 29 May, were missing from the Six Mile Creek data. Gaps were filled with flow values derived from the rest of the tributaries. Daily factors were calculated for each tributary based on the formula:

daily factor = (daily average flow) / (average flow for the verification period, excluding days when data was missing at Cedar River or Six Mile Creek).

Average daily factors were calculated using all tributaries and were then applied to estimate daily flows at Cedar River and Six Mile Creek.

The tidal head (water level) boundary is shown in Figure 1a. The tidal elevations are applied along the northern and southern edges of the ocean boundary of the model, corresponding to the area in front of Fernandina Beach and Jacksonville Beach respectively. The elevations specified are equal and in phase. The elevations along the boundary are representative of the tide at U.S. Coast Guard Base at Mayport. Real tide data measured every hour at Mayport was provided by the SJRWMD and was applied using half hour time steps at the model boundary, after increasing the tide range by 18 percent. This amplification of the tide range was necessary to account for the energy loss between the

boundary and Mayport. A wave travel time of 15 minutes between the tide boundary and Mayport was calculated. The travel time was subtracted from the model time after extracting results for the sake of compatibility with the prototype. The salinity at the ocean was set at a constant value of 35 ppt.

Originally, predicted tide signals for the tide boundary conditions at Jacksonville Beach and Fernandina Beach were to be used. This approach would have yielded variation between the two tidal boundaries to more accurately drive the currents in the ocean area of the mesh. The difference between predicted and measured tide at Mayport was calculated to account for atmospheric events not included in the predicted tide signal. This difference was then applied to the predicted tide signals used as boundary condition at Jacksonville Beach and Fernandina Beach. A long-term simulation (five months) showed that the modeled tide signal diverged from the prototype. This fact repeated itself at all tide stations used for verification. The problem was caused by a defect in the predicted tide data. After plotting the daily average tide during the five month period, a downward curve was observed. As a consequence, this approach was discarded.

The ocean region of the mesh is the area of the model outside the jetties. It extends approximately 18 km (11 miles) east beyond the end of the jetties and approximately 14.5 km (9 miles) north and south of the jetties. These dimensions were required to minimize occurrences of fresher water from the river reaching the ocean boundary, which could have caused numerical instabilities.

In addition to stream flow and tidal boundaries, wind, rainfall, and evaporation were considered. Historically, the period of May-August has more rainfall than other seasons. It is also, however, considered the low flow period. This apparent contradiction is a result of evaporation rates exceeding rainfall rates. To account for this gain and loss, it is necessary to compute the net flow into the system due to rain and evaporation.

Flow in and out of the mesh caused by rainfall/evaporation is accomplished by specifying a rate (m/sec) into (positive) or out of (negative) the specific elements. The inflow caused by rainfall was computed converting the recorded rainfall rate in units of inches/day into meters/second. Rainfall intensity measured at thirteen District sites in the St. Johns River Basin varied from site to site, but the frequency of rainfall events for all stations and their relative intensity within each station were similar. The same fact was observed for wind speed and direction measured at six sites. These observations demonstrate that the major meteorological events affecting the behavior of the Lower St. Johns River and Estuary are regional and can be assumed uniform over the entire model. Daily median values of rainfall from among the 13 District sites were used. Hourly wind data used were measured at Shands Bridge, with missing records filled using Dames Point data. Shands Bridge was selected, since that is where the river is at its widest. Monthly evaporation rates were obtained from a NOAA gauge located in Gainesville. A pan correction factor of 0.78 was used.

Figures 12 and 13 show the rainfall and evaporation data for the time period under study. Volumes were obtained by multiplying the flow rate by the area of

the river, excluding the ocean and 1-D elements. Figure 14 illustrates the cumulative flow into and out of the system during the study period. The low flow and high flow periods are easily delineated. Wind speed and direction are shown in Figure 15.

Marsh Approximation with One-Dimensional Elements

To increase computer efficiency, some marsh areas and streams were approximated using one-dimensional elements. These areas included:

a. Pablo Creek and marshes,
b. Chicopit Bay,
c. Greenfield Creek,
d. Sisters Creek and marshes
e. Cedar Point Creek and marshes,
f. Ribault River,
g. Moncrief Creek,
h. Parts of the Ortega River and Fishing Creek,
i. Part of Arlington River, Pottsburg Creek, Little Pottsburg Creek, and Strawberry Creek,
j. Black Creek,
k. Murphy Creek,
l. Dunns Creek,
m. St. Johns River between Lake George and Buffalo Fluff, and
n. Lake George

3 Results

Field Data

Tide and salinity data for verification were supplied by SJRWMD. These data cover a period of approximately 300 days, starting 1 April 1996. The data set included hourly tidal elevation data at nine locations and hourly temperature and conductivity (used to compute salinity) data at five locations.

The nine tidal stations were located at the following locations, which span the length of the LSJRE and provide a continuous set of verification data (see Figure 16): Mayport, Dames Point, U.S. Army Corps of Engineer Dredge Depot, Main Street Bridge, Buckman Bridge, Shands Bridge, Racy Point, Palatka, and Buffalo Bluff. The salinity stations were located at Dames Point, Acosta Bridge, Buckman Bridge, Shands Bridge, and Buffalo Bluff (see Figure 17).

The salinity data were collected at the surface, mid-depth, and bottom for all stations but Buffalo Bluff where only surface data were collected. Surface and bottom data were used for the verification. Gaps in the surface salinity data were: Buffalo Bluff from 1 July to 8 August, Dames Point from 24 June to 2 July, and Acosta Bridge from 3 July to 27 August. Gaps in the bottom salinity data were: Shands Bridge from 29 May to 29 August, and Dames Point from 13 July to 28 August. Measurements at Shands Bridge and Buffalo Bluff represent salinity values less than 1 ppt having no identifying shape, form, or structure.

The model was verified to water surface elevation and water discharge by adjusting the mesh and by selecting the model parameters of Manning's roughness coefficient (n) and horizontal eddy viscosity. To provide adequate flows for verification, discharge data were provided by the SJRWMD for eight locations (see Figure 18). These eight locations are located near or at: Bayard Point, Corps Dock, Dames Point, Doctors Inlet, Main Street, Mayport (Marker 22), Blount Island Channel (Marker 36), and Fulton-Dame Cutoff Range (Marker 38).

3-D Model Verification

The model was operated in three-dimensional mode. The three-dimensional mode uses one-, two-, and three-dimensional elements.

The 3-D model was run for a total of 150 days. The first 30 days represented the period 29 April to 28 May 1996 and served as the spin-up period. Spin-up is necessary, because the initial conditions are not precisely known. In studies involving hydrodynamics only, the spin-up period can consist of as little as one or two days. With hydrodynamics and transport (salinity), however, it can require weeks to months of simulation to reach equilibrium, real-world conditions of salinity. The initial salinity field for the 3-D simulation was approximated by interpolating average field salinity values to the numerical model mesh. These values were input by RMA10-WES and the salinity values assigned to the corresponding 3-D numerical mesh node. From that starting point, RMA10-WES computed the hydrodynamics and salinities.

Tidal elevation

Figure 16 shows the location of the nine prototype tidal stations. Water surface elevation data collected at Buckman Bridge, Dames Point, USCOE Dredge Depot, Palatka, and Shands Bridge contained various gaps. Figures 17-25 show the prototype data plotted with the 3-D model results for the nine stations (all locations have been plotted with reference to NGVD).

Very good agreement was observed at the Mayport station for tidal range and phasing. Moving upstream, the water surface elevation computed by the model tends to remain higher than the prototype. Several unsuccessful efforts to lower the water surface elevation of the model took place by modifying numerous model parameters. Since the model salinity was observed to be higher than the prototype downstream from Jacksonville downtown, an investigation of the model was performed by uncoupling hydrodynamic calculations to the salinity. A good match of the water surface elevation between model and prototype was obtained as a result of this change (see Figure 26). The explanation for this model behavior is that the density of the fresh water located in the upstream part of the model is lower than the density of the salty water in the downstream section of the LSJRE model. Therefore, the water surface elevation upstream is forced to increase to mass balance against heavier water located downstream. The tidal range throughout the model was also improved by uncoupling salinity. After these findings, verification efforts were concentrated on improving salinity results.

The water level datum planes add uncertainty to the verification. They are notoriously unreliable and could be responsible for some of the difference between prototype data and model results.

Water flow

Figure 43 shows the location of eight discharge measurement sites as well as the dates when the measurements took place. Figures 44-51 show the prototype discharge plotted with the 3-D model results.

The results at Bayard Point show good agreement in both magnitude and phasing. Although the magnitude of the water flowing through the Blount Island Channel (Marker 36) is well matched by the model, there is an hour lag in the phase. The difference in phase is due to the geometry simplification of the adjacent marshes and the lack of data to verify the timing of the water flow interchange between the marshes and the main stem of the river. The magnitude of the discharge at Mayport could have also been overestimated by the simplification of the marshes. Another possible factor overestimating the discharge magnitude at Mayport is the simplified geometry of the river entrance where jetties were substituted by a smooth rounded entrance.

The model and prototype discharge data at the other five locations match well. Consistently, the magnitude of the model discharges was slightly higher. This observation agrees with the fact that water surface elevations were also higher during the simulation period. Figure 52 shows how discharges are affected by uncoupling salinity to hydrodynamic computations.

Attempts to reduce discharges by increasing the bed roughness were unsatisfactory because the tide range throughout the model was compromised as a result.

Salinity

Figure 27 shows the location of the salinity stations. Data were collected at three depths at all of the stations except Buffalo Bluff. The surface and bottom salinity values for model and prototype are shown for four of the stations in Figures 28-40. Buffalo Bluff only shows surface salinity.

Referring to the Dames Point, Acosta Bridge, and Buckman Bridge data, the three-dimensional model captures the salinity trend, including isolated peaks. A good example is observed on Julian day 194. All salinity stations show a water surface elevation and salinity peak in prototype data and model results. Figure 14 shows an increase in wind speed as well as a change in direction on the same day. Winds were blowing northeast and suddenly changed to southwest. The response of the model justifies the assumption of using uniform winds for this study. At Shands Bridge and Buffalo Bluff, the model results represent well the prototype conditions with salinity values less than 1 ppt and with no identifying shape, form, or structure.

As mentioned earlier, model salinities are somewhat higher than those observed in the lower (seaward) half of the model. Two aspects of the model are considered as likely reasons for the higher average salinities computed in the

lower portion of the model: a) ungauged watershed runoff and groundwater flow into the river; and b) simplified geometry, particularly at the river entrance. Since both model aspects have an effect on the river freshwater levels, additional simulations were performed to test the sensitivity of the model to higher freshwater inflows. Results of one of the simulations are shown in Figure 41. In this simulation, 130.26 m^3/sec (4,600 cfs) of fresh water were distributed over the surface of the river. This amount of water yields a satisfactory fit between prototype and modeled salinity values at Acosta Bridge. Although the application of the additional fresh water dropped salinity considerably over the entire model, a different distribution and magnitude of freshwater inflow could yield better results. Again, the simplification in the geometry of the St. Johns River entrance could overestimate the interchange of water in the downstream section of the river. Also, the secondary, northern entrance was not modeled, and the surrounding marshes were simplified in the model.

The model still showed the same stratification trends found in the prototype, although more markedly. Stratification was found in the model as far upstream as Buckman Bridge, reproducing the same prototype behavior.

We interpret these salinity results to indicate that the model successfully reproduces the overall salinity trends within the LSJRE, with the understanding that some local areas may not be as well reproduced as the five stations shown until verification of those areas is checked and any necessary adjustments made. The model simulates salinity pulses caused by changes in freshwater flow and stratification changes, but the tidal surface elevation throughout the model is the variable playing a major roll in the overall salinity behavior, as shown in Figure 42.

Computational Speed

The 3-D geometry used to generate the results discussed is computationally time intensive, but the model solution converges with the use of only three iterations per time step, two for hydrodynamic calculations and one for salinity. Half-hour time steps were used for this study.

The platform used to run the model is an SGI Origin 2000. This is part of the ERDC High Performance Computing Center. The SGI Origin is a cc-NUMA distributed shared memory architecture that contains 112 processors, 64 Gbytes of memory, and 500 Gbytes of hard disk storage. We simulated as much as 10 days during 12 wall clock hours, or 28 sec per iteration.

4 Discussion and Conclusions

Discussion

The purpose of a numerical model is to achieve insight and understanding about the system being modeled to help in a decision making process. A complete understanding of a system cannot be obtained within ordinary constraints of time and money; therefore, a model must be designed to satisfy specific criteria in anticipation of its intended uses. For example, if a LSJRE model will be used to study the salinity and sedimentation effects of a navigation channel enlargement, the modeler will build a different model than if its purpose is to study the effects of non-point pollution on water quality. The former will portray very high resolution in the navigation channel, while the latter may ignore the exact location of the channel as long as the river cross section is adequately described.

The two aspects of waterway modeling most important for faithful reproduction of hydrodynamic and transport processes are an accurate rendering of the geometry (bank lines and bathymetry) and accurate specification of the boundary conditions (tides, river flows, etc.).

The model described here was designed to provide a satisfactory reproduction of estuarine hydraulics and salinity transport. This objective was accomplished. With presently available micro and mini computers, the model runs too slowly to be considered practical for continuous simulation periods longer than a few months. The use of a mainframe supercomputer is necessary for the feasibility of a long-term simulation study. Lower resolution versions with a more structured layout (i.e., a nearly uniform number of elements across the estuary) will run considerably faster. For water quality modeling, which typically requires multi-year simulations, such a lower resolution and, thus, a computationally more efficient version of this model is adequate and should be considered.

Accurate specification of boundary conditions is often more difficult than accurate specification of system geometry. Water level datum planes are notoriously unreliable, and they should always be subjected to critical evaluation. Even routine discharge measurements are less precise than desired. In this model, we added rain and evaporation estimates to achieve salinity verification, but did not include groundwater flows or local runoff, which can significantly affect

salinity and mixing.

Future use of the model should bear these limitations in mind and (a) revise the mesh if new uses require it, (b) recheck the local verification with high quality data if specific zones are of high interest, and (c) refine boundary conditions of the model, depending on the usage.

Conclusions

A hydrodynamics and salinity transport model of the Lower St. Johns River and Estuary has been constructed and verified. The RMA10-WES model described here satisfactorily reproduces tidal elevations, discharges, and salinity trends.

Although the model verification is satisfactory, improvements can be made:

a. More comprehensive, synoptic field data collected specifically for the purpose of modeling is needed to check local verification if detailed results are desired at locations among the verification stations used herein.
b. Improved definition of boundary conditions, including local runoff as well as groundwater interactions will improve the model.
c. A mesh geometry more closely representing the river entrance and the extensive marshes located to the north of the LSJRE is necessary. Prototype data (water velocity and discharge) collected within the marshes and their connection to the main stem of the river should complement improvements in the geometry.

The model is suitable for addressing questions of general hydrodynamics and salinity intrusion within the main body of the LSJRE. Off-channel tributaries and marshes have been modeled for their effect on the main waterway, but have not been verified to reproduce local, internal hydrodynamic behavior. For future applications, the level of verification, degree of resolution and appropriateness of boundary conditions should be carefully evaluated in each case to ensure a proper match between uses and model behavior in the areas of interest.

The model is computationally intensive. Simulations longer than a few months can be achieved with the use of a mainframe supercomputer or by optimizing the mesh for balanced accuracy and speed, matching mesh resolution to the questions posed.

References

Henderson-Sellers, B. (1984). "A simple formula for vertical eddy diffusion coefficients under conditions of nonneutral stability," *Journal of Geophysical Research* 87(C8), 5860-5864.

King, I.P. (1982). "A finite element model for three-dimensional flow," Resource Management Associates, Lafayette, CA, for U.S. Army Engineer Waterways Experiment Station, Vicksburg, MS.

_____(1985). "Strategies for finite element modeling of three-dimensional hydrodynamic systems," *Advances in Water Resources* 8, 69-76.

_____(1993). "RMA-10, a finite element model for three dimensional density stratified flow," Department of Civil and Environmental Engineering, University of California, Davis.

Krone, R.B. (1962). "Flume studies of the transport of sediment in estuarial shoaling processed, final report," Hydraulic Engineering Laboratory and Sanitary Engineering Research Library, University of California, Berkeley.

Mellor, G.L. and Yamada, T. (1982). "Development of a turbulence closure model for geophysical fluid problems," *Reviews of Geophysics and Space Physics* 20(4), 851-875.

Parthenaides, E. (1962). "A Study of erosion and deposition of cohesive soils in salt water," Ph. D. diss., University of California, Berkeley.

Pritchard, D.W. (1982). "A summary concerning the newly adopted practical salinity scale, 1978, and the international equation of state of seawater, 1980," Marine Sciences Research Center, State University of New York, Stony Brook, New York.

Stelling, G.S. and van Kester, J.A.T.M. (1993). "Horizontal gradients in sigma transformed bathymetries with steep bottom slopes", *Hydraulic Engineering* '93, Proceedings of the 1993 Conference, ASCE, 2123-2134.

Wu, J. (1980). "Wind-stress coefficients over sea surface neutral conditions-a revisit," *Journal of Physical Oceanography* 10(5), 727-740.

Table 1
Turbulent Exchange Coefficients and Manning's n Values

Material Type	Eddy Viscosity N•s/m² (lb-s/ft²)	Horizontal Diffusion m²/s (ft²/s)	Vertical Diffusion m²/s (ft²/s)	Manning's n Value	Number of 3D Layers
1	4788 (100.00)	5.57 (60.00)	0.0000929 (0.001)	0.018	4
2	11970 (250.00)	5.57 (60.00)	0.00929 (0.100)	0.024	1
3	9576 (200.00)	5.57 (60.00)	0.0000929 (0.001)	0.018	3
4	9576 (200.00)	5.57 (60.00)	0.0000929 (0.001)	0.018	2
50	11970 (250.00)	5.57 (60.00)	0.0000929 (0.001)	0.018	3
5	4788 (100.00)	5.57 (60.00)	0.0000929 (0.001)	0.018	1
6	4788 (100.00)	5.57 (60.00)	0.0000929 (0.001)	0.024	1
49	3591 (75.00)	5.57 (60.00)	0.0000929 (0.001)	0.028	1
7	11970 (250.00)	5.57 (60.00)	0.0000929 (0.001)	0.022	2
70	9576 (200.00)	5.57 (60.00)	0.0000929 (0.001)	0.018	2
8	11970 (250.00)	5.57 (60.00)	0.00929 (0.100)	0.018	0
9	11970 (250.00)	5.57 (60.00)	0.0000929 (0.001)	0.024	0
10	11970 (250.00)	5.57 (60.00)	0.0000929 (0.001)	0.018	0
11	3591 (75.00)	5.57 (60.00)	0.0000929 (0.001)	0.018	0
12	2394 (50.00)	5.57 (60.00)	0.0000929 (0.001)	0.018	2
47	1197 (25.00)	5.57 (60.00)	0.0000929 (0.001)	0.026	1
13	3591 (75.00)	5.57 (60.00)	0.0000929 (0.001)	0.012	0
14	4788 (100.00)	5.57 (60.00)	0.0000929 (0.001)	0.024	1
15	47880 (1000.00)	5.57 (60.00)	0.01858 (0.200)	0.024	0
16	35910 (750.00)	5.57 (60.00)	0.01858 (0.200)	0.024	1
17	14364 (300.00)	5.57 (60.00)	0.013935 (0.150)	0.024	1
18	2394 (50.00)	5.57 (60.00)	0.0000929 (0.001)	0.018	2
48	1197 (25.00)	5.57 (60.00)	0.0000929 (0.001)	0.026	1
19	2394 (50.00)	5.57 (60.00)	0.0000929 (0.001)	0.024	0
20	2394 (50.00)	5.57 (60.00)	0.0000929 (0.001)	0.024	0
21	2394 (50.00)	5.57 (60.00)	0.0000929 (0.001)	0.024	0
22	2394 (50.00)	5.57 (60.00)	0.0000929 (0.001)	0.024	0
23	2394 (50.00)	5.57 (60.00)	0.0000929 (0.001)	0.024	0
24	2394 (50.00)	5.57 (60.00)	0.0000929 (0.001)	0.024	0
25	2394 (50.00)	5.57 (60.00)	0.0000929 (0.001)	0.024	0
26	2394 (50.00)	5.57 (60.00)	0.0000929 (0.001)	0.024	0
27	2394 (50.00)	5.57 (60.00)	0.0000929 (0.001)	0.024	0
28	2394 (50.00)	5.57 (60.00)	0.0000929 (0.001)	0.024	0
29	2394 (50.00)	5.57 (60.00)	0.0000929 (0.001)	0.024	0
30	2394 (50.00)	5.57 (60.00)	0.0000929 (0.001)	0.024	0
31	2394 (50.00)	5.57 (60.00)	0.0000929 (0.001)	0.024	0
32	2394 (50.00)	5.57 (60.00)	0.0000929 (0.001)	0.024	0
33	2394 (50.00)	5.57 (60.00)	0.0000929 (0.001)	0.024	0
34	2394 (50.00)	5.57 (60.00)	0.0000929 (0.001)	0.024	0
35	3591 (75.00)	5.57 (60.00)	0.0000929 (0.001)	0.012	0
36	3591 (75.00)	5.57 (60.00)	0.0000929 (0.001)	0.012	0
37	3591 (75.00)	5.57 (60.00)	0.0000929 (0.001)	0.012	0
38	3591 (75.00)	5.57 (60.00)	0.0000929 (0.001)	0.012	0
39	3591 (75.00)	5.57 (60.00)	0.0000929 (0.001)	0.012	0
40	3591 (75.00)	5.57 (60.00)	0.0000929 (0.001)	0.012	0
41	3591 (75.00)	5.57 (60.00)	0.0000929 (0.001)	0.012	0
42	3591 (75.00)	5.57 (60.00)	0.0000929 (0.001)	0.012	0
43	3591 (75.00)	5.57 (60.00)	0.0000929 (0.001)	0.012	0
44	3591 (75.00)	5.57 (60.00)	0.0000929 (0.001)	0.012	0
45	3591 (75.00)	5.57 (60.00)	0.0000929 (0.001)	0.012	0
46	3591 (75.00)	5.57 (60.00)	0.0000929 (0.001)	0.012	0
51	3591 (75.00)	5.57 (60.00)	0.0000929 (0.001)	0.012	0
52	3591 (75.00)	5.57 (60.00)	0.0000929 (0.001)	0.012	0
53	3591 (75.00)	5.57 (60.00)	0.0000929 (0.001)	0.012	0
54	3591 (75.00)	5.57 (60.00)	0.0000929 (0.001)	0.012	0
55	3591 (75.00)	5.57 (60.00)	0.0000929 (0.001)	0.012	0
56	3591 (75.00)	5.57 (60.00)	0.0000929 (0.001)	0.012	0

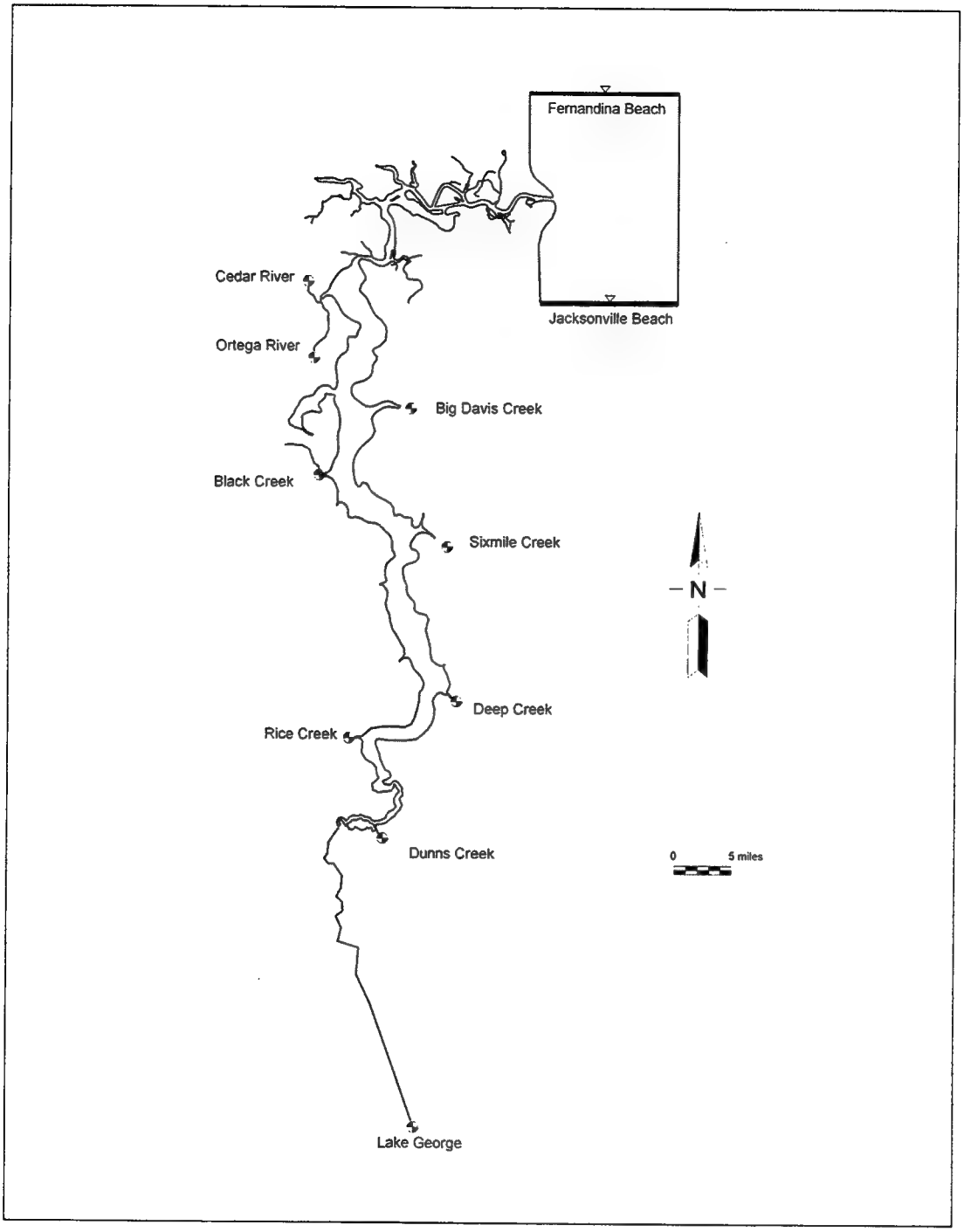

a. Mesh boundary and boundary condition locations (Sheet 1 of 5)

Figure 1. Lower St. Johns River and Estuary Model mesh

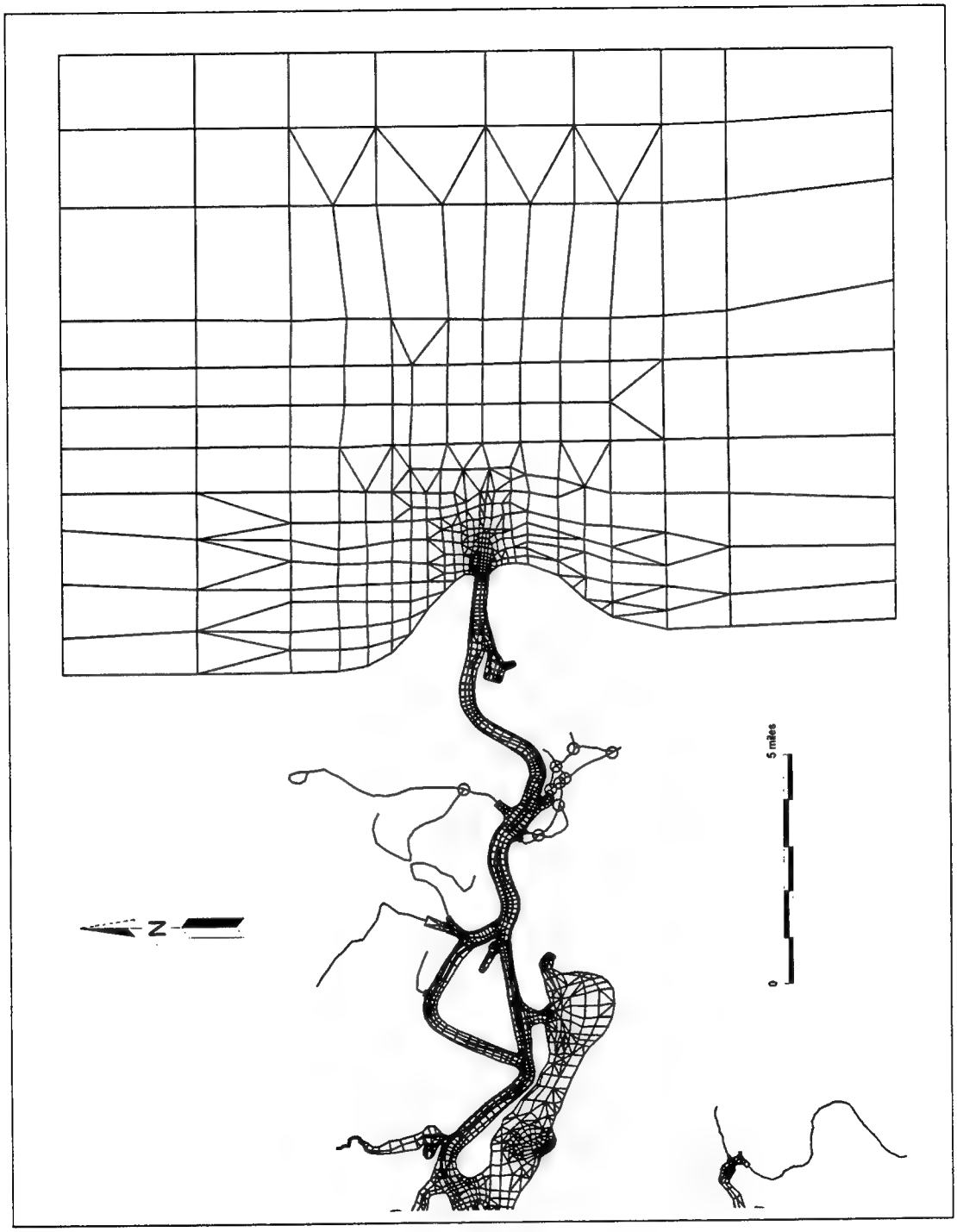

b. Lower portion of mesh

Figure 1. (Sheet 2 of 5)

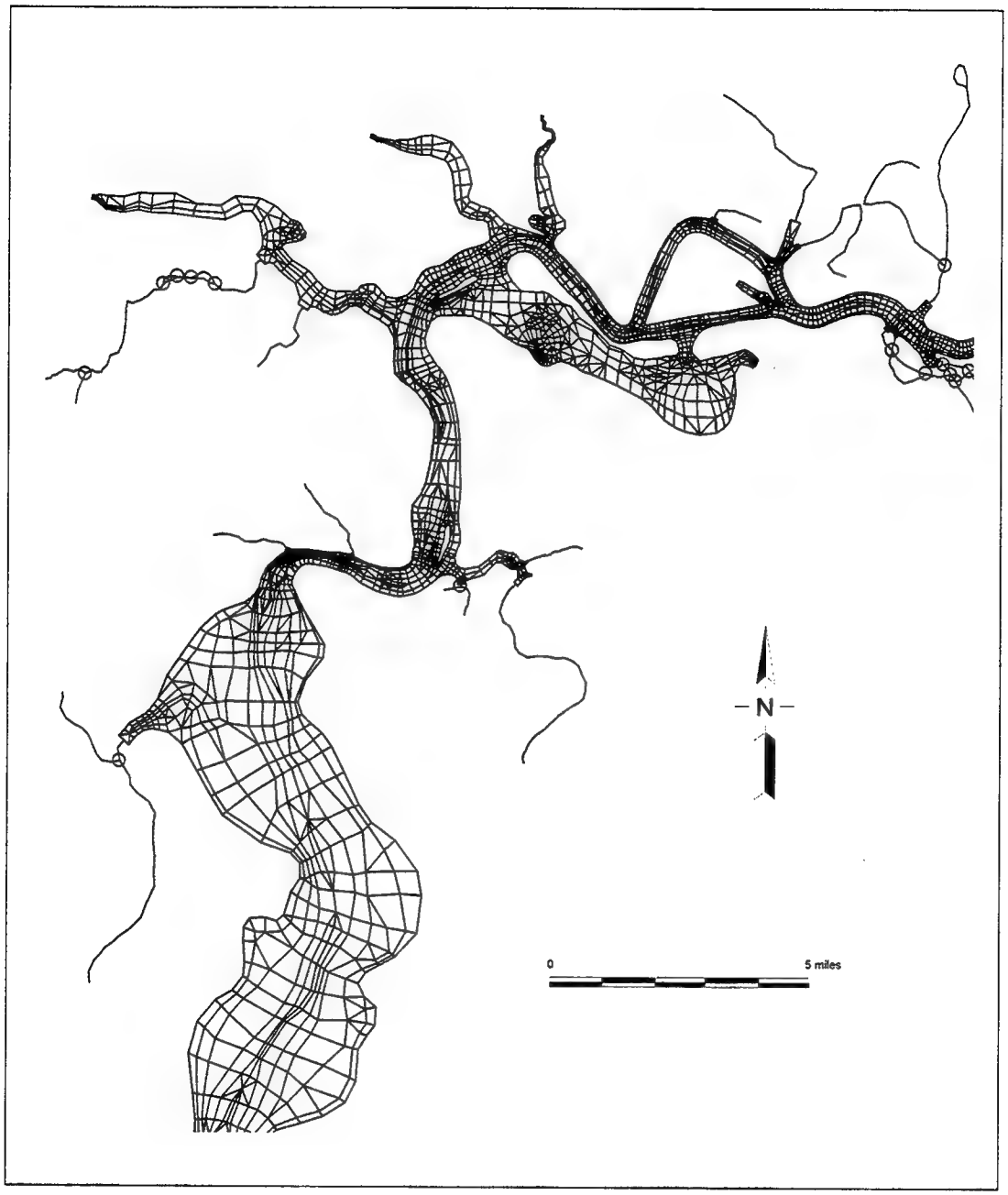

c. Lower middle portion of mesh

Figure 1. (Sheet 3 of 5)

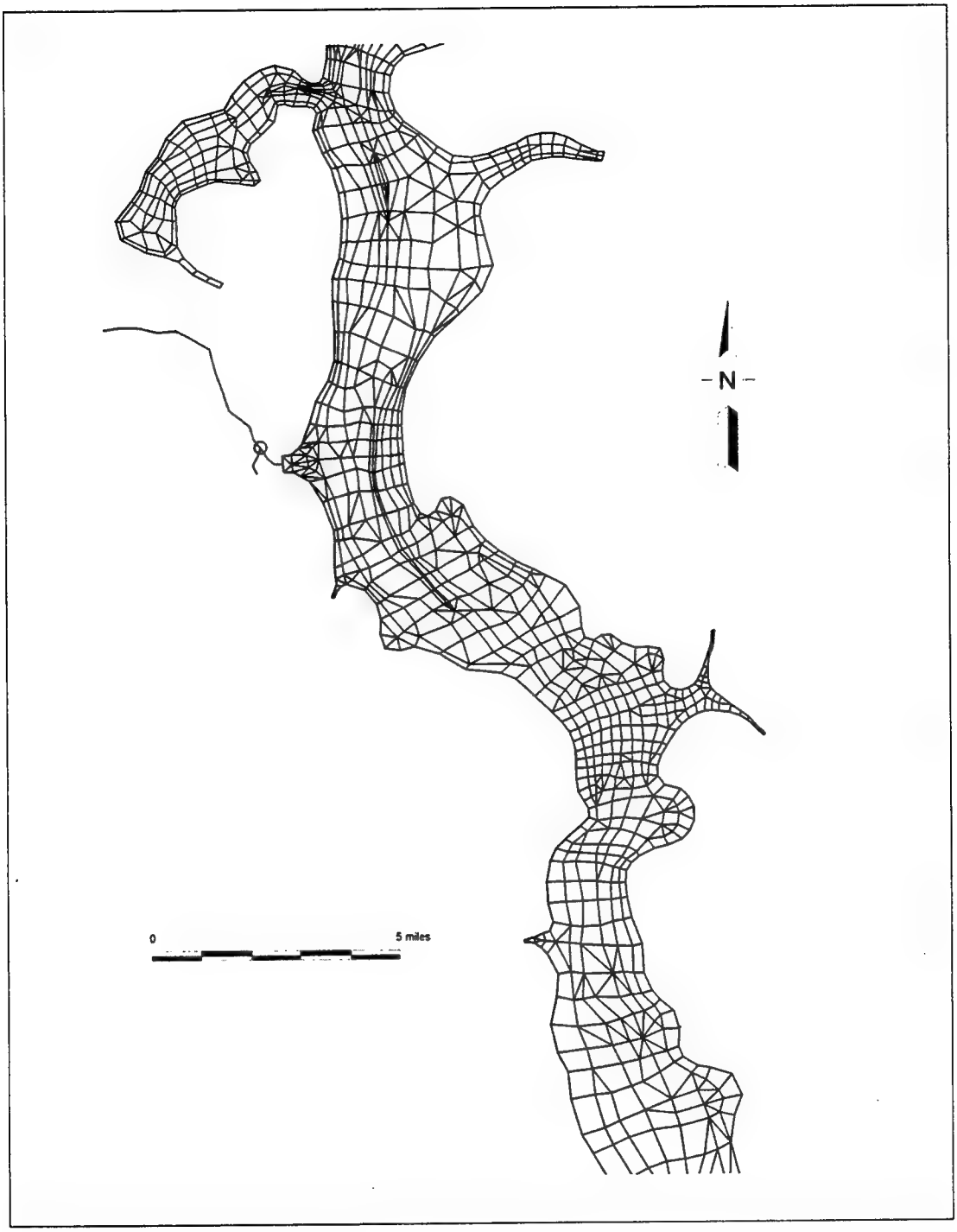

d. Upper middle portion of mesh

Figure 1. (Sheet 4 of 5)

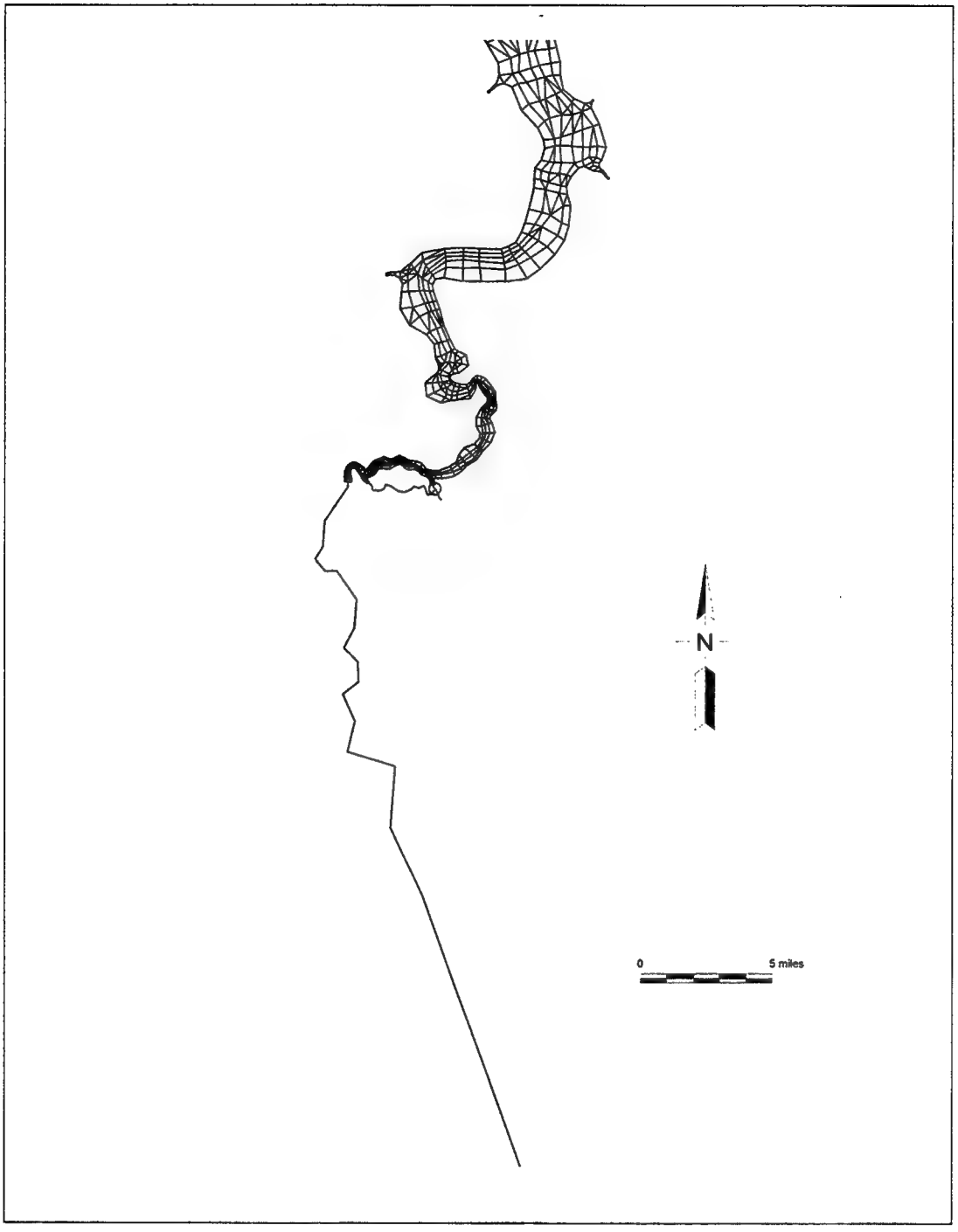

e. Upper portion of mesh

Figure 1. (Sheet 5 of 5)

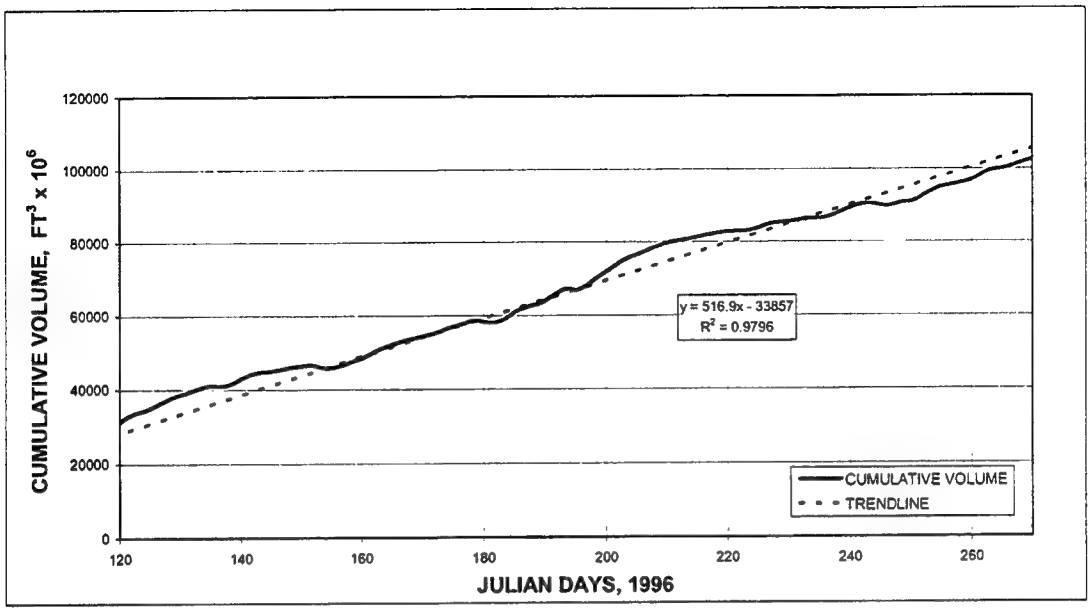

Figure 2. Cumulative inflow from tributaries into the Lower St. Johns River and Estuary (To convert volume to cubic meters, multiply by 0.02832)

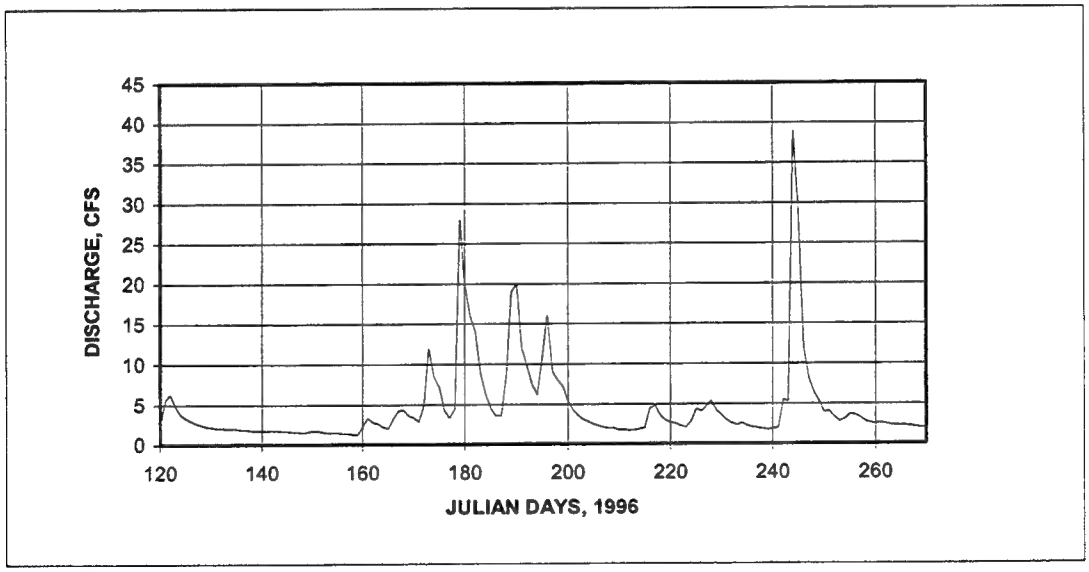

Figure 3. Big Davis Creek daily average flow (To convert discharge to cubic meters per second, multiply by 0.02832)

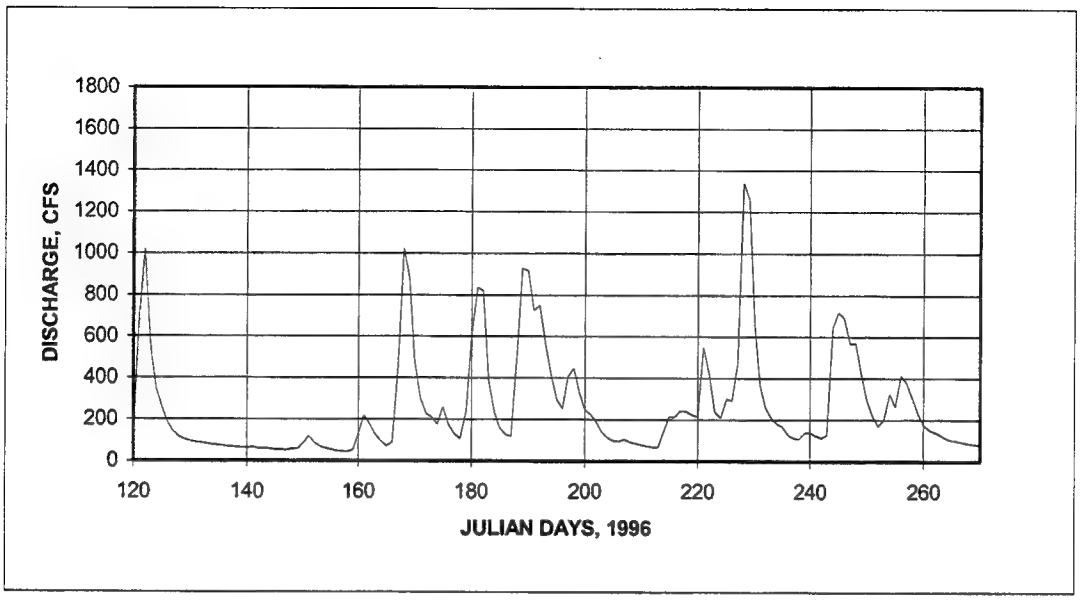

Figure 4. Black Creek daily average flow (To convert discharge to cubic meters per second, multiply by 0.02832)

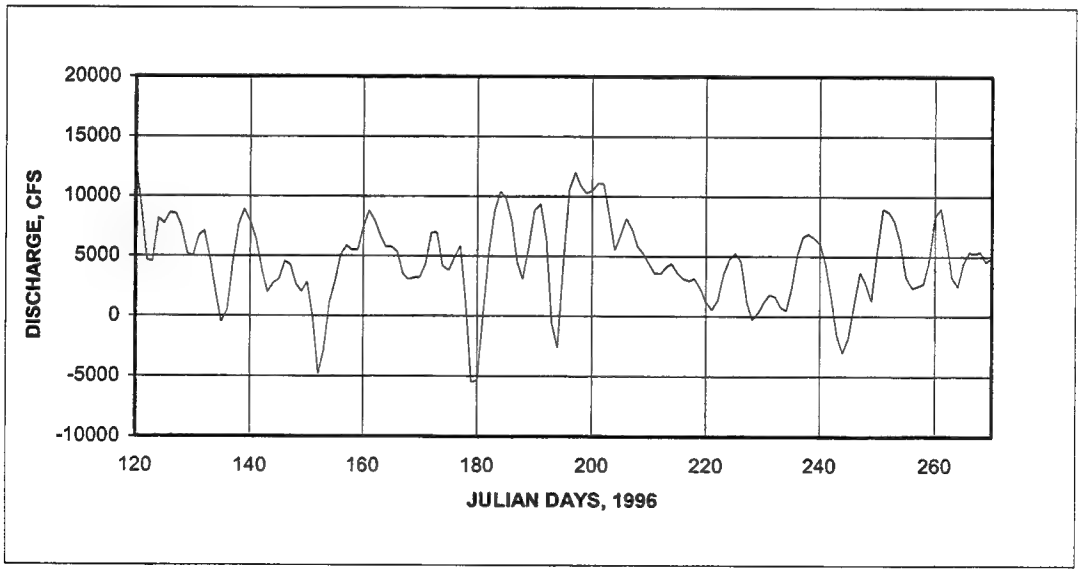

Figure 5. Buffalo Bluff daily average flow (To convert discharge to cubic meters per second, multiply by 0.02832)

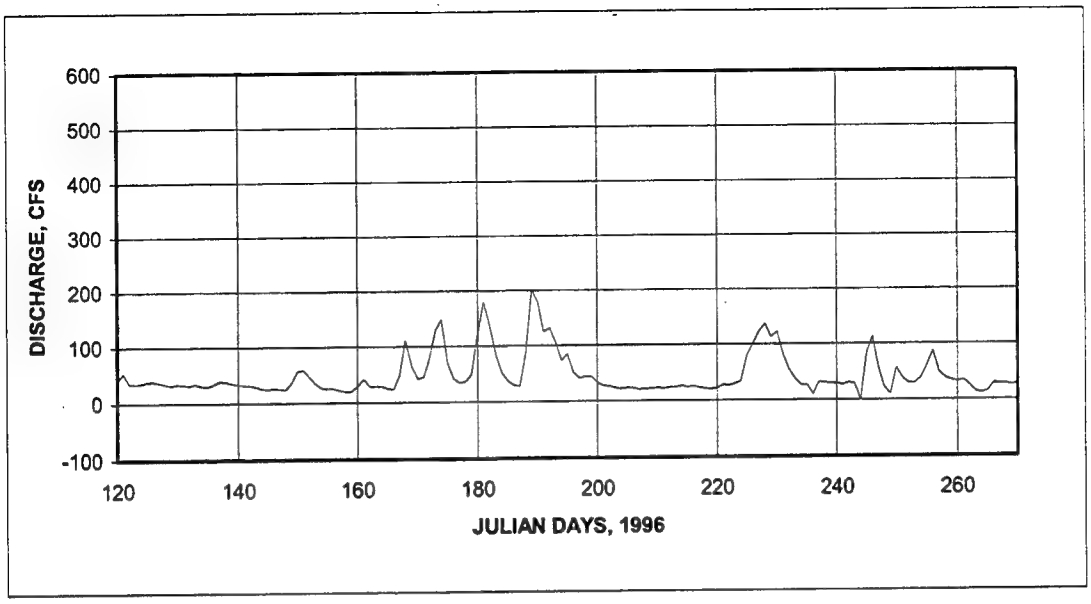

Figure 6. Deep Creek daily average flow (To convert discharge to cubic meters per second, multiply by 0.02832)

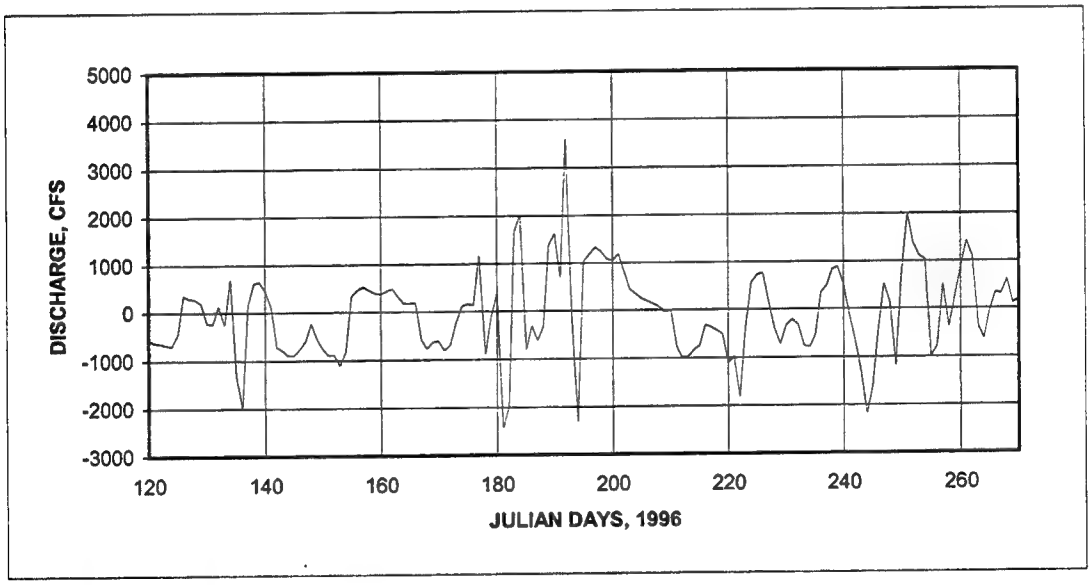

Figure 7. Dunns Creek daily average flow (To convert discharge to cubic meters per second, multiply by 0.02832)

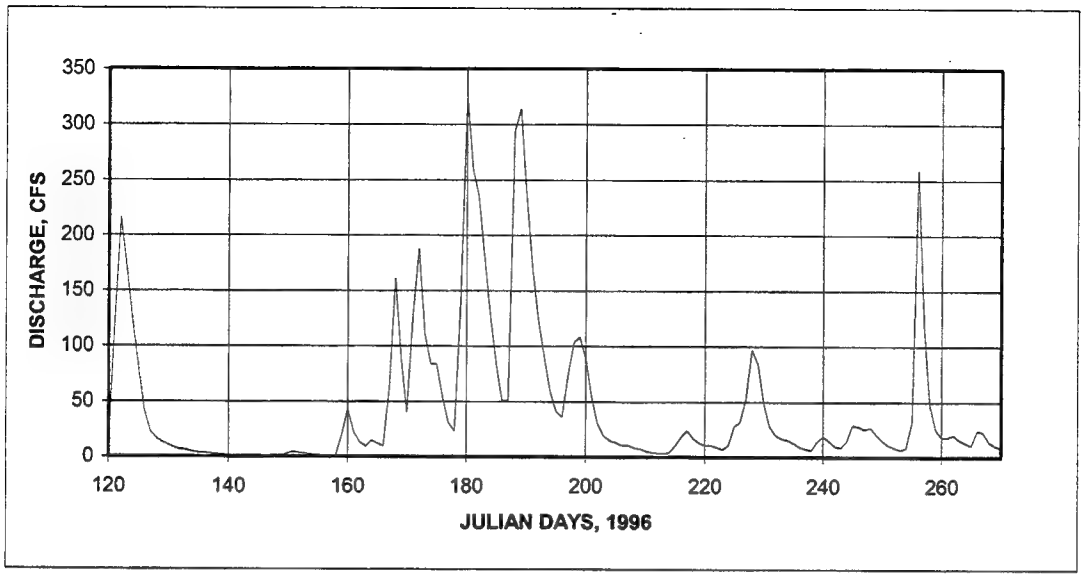

Figure 8. Ortega River daily average flow (To convert discharge to cubic meters per second, multiply by 0.02832)

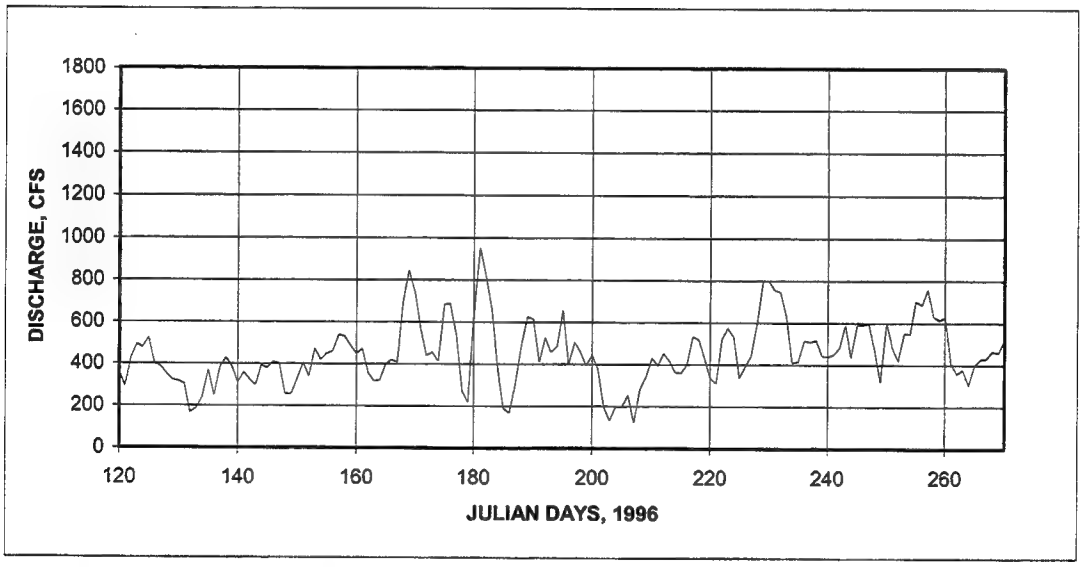

Figure 9. Rice Creek daily average flow (To convert discharge to cubic meters per second, multiply by 0.02832)

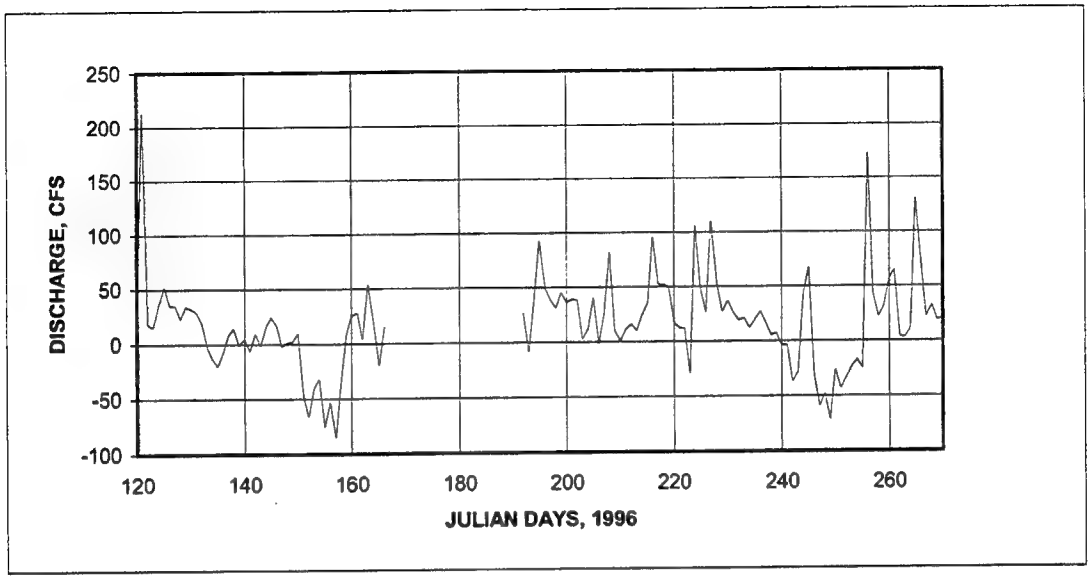

a. Daily average flow

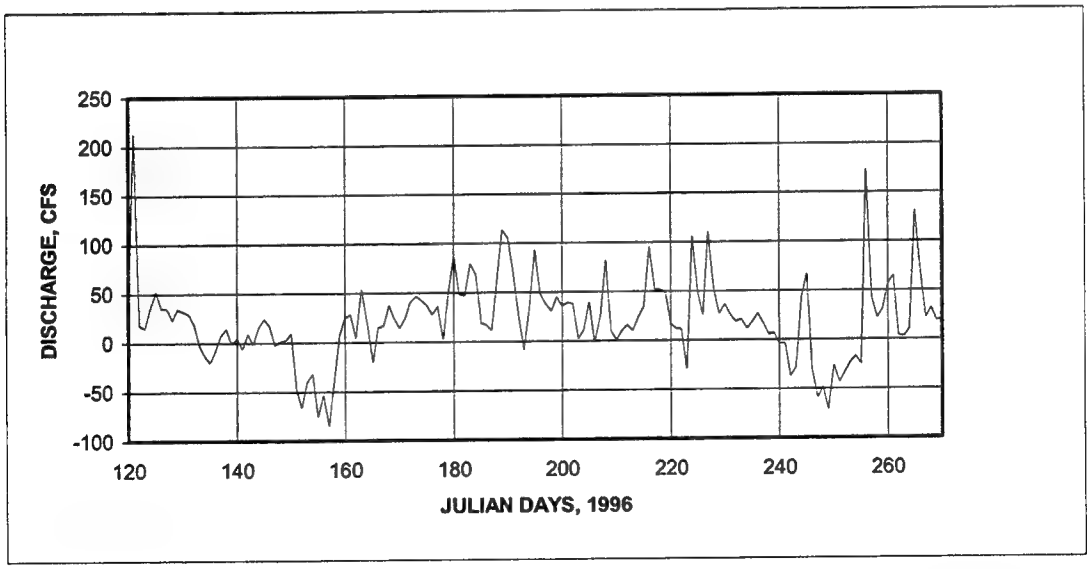

b. Corrected daily average flow

Figure 10. Cedar River average flow (To convert discharge to cubic meters per second, multiply by 0.02832)

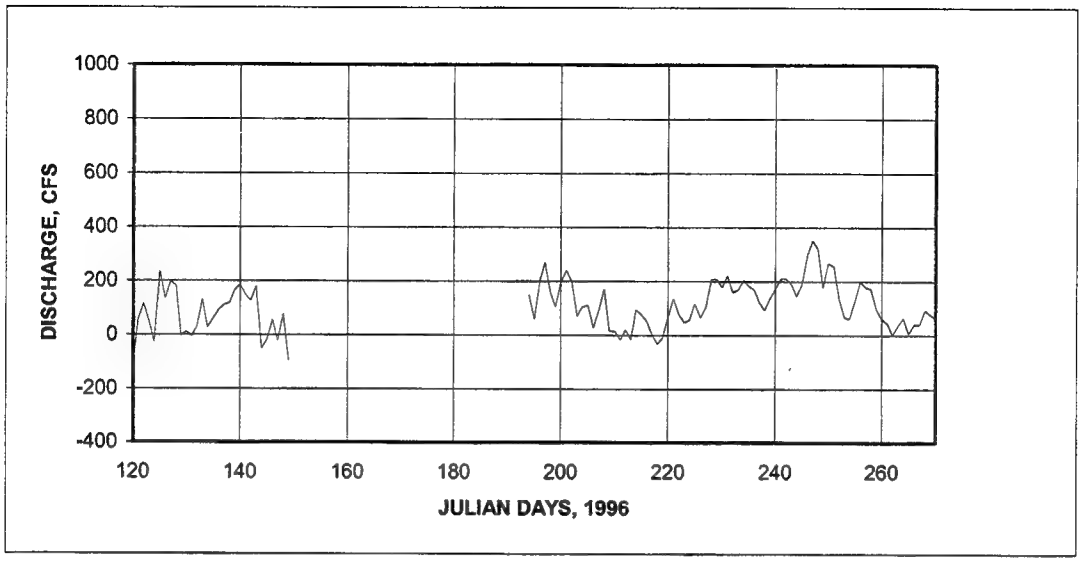

a. Daily average flow

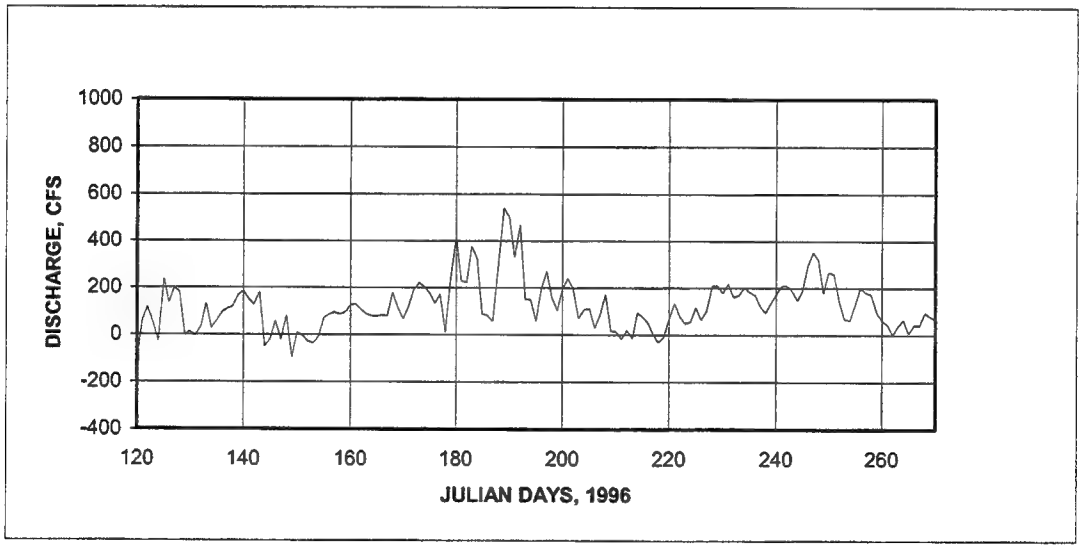

b. Corrected daily average flow

Figure 11. Six Mile Creek average flow (To convert discharge to cubic meters per second, multiply by 0.02832)

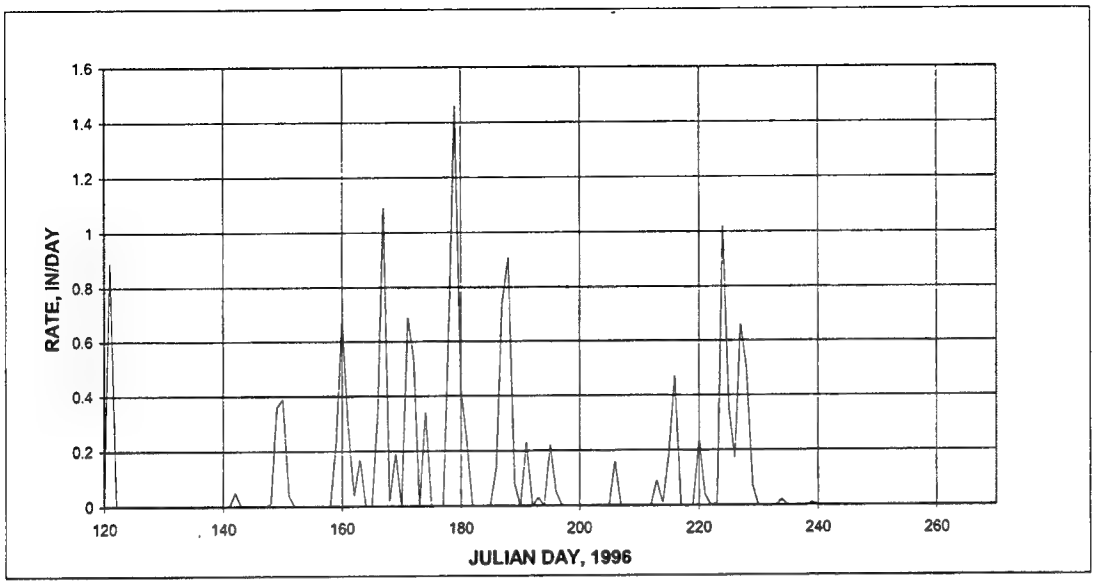

Figure 12. Rainfall (median values among 13 district sites) (To convert rainfall to mm/day, multiply by 25.4)

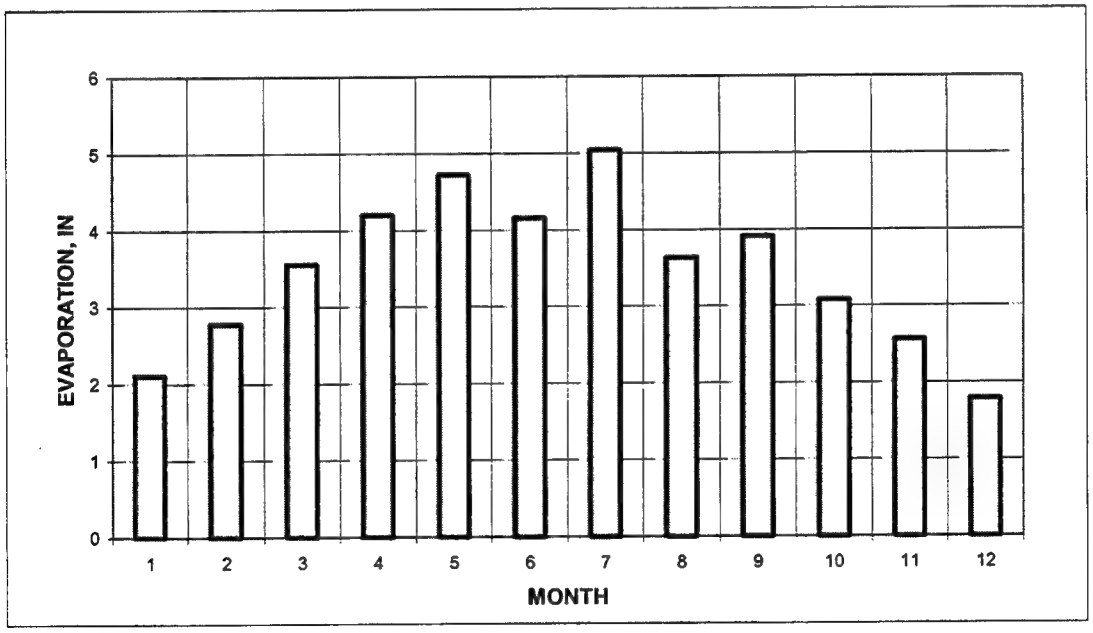

Figure 13. Evaporation at Gainesville, 1996 (To convert evaporation to mm, multiply by 25.4)

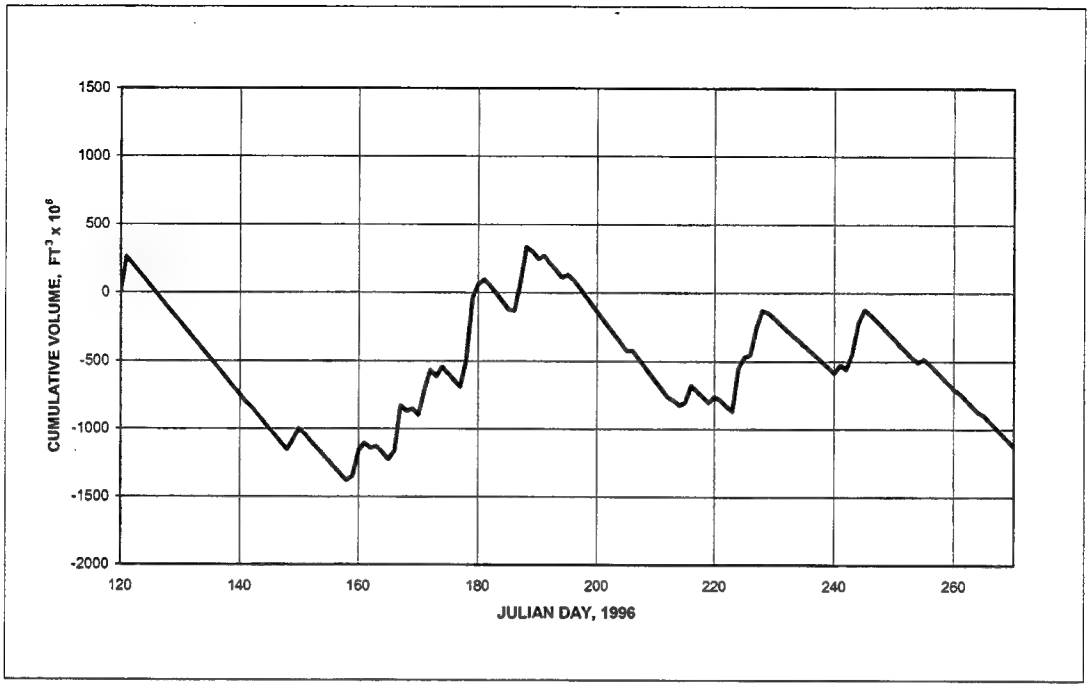

Figure 14. Cumulative rainfall/evaporation into the Lower St. Johns River and Estuary (To convert volume to m^3, multiply by 0.02831685)

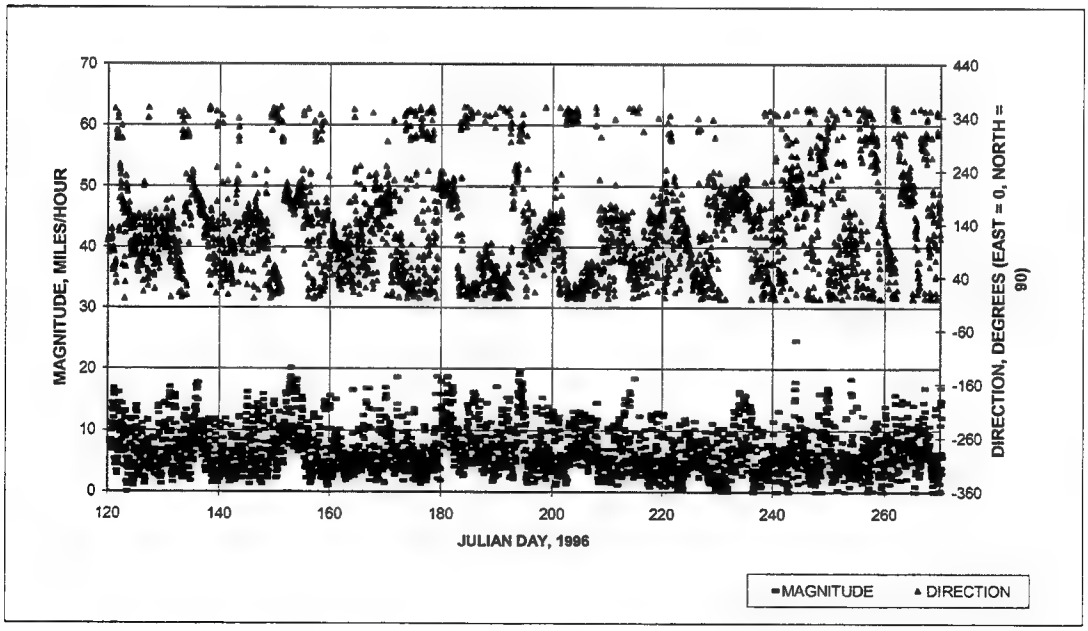

Figure 15. Wind (Shands Bridge, missing records filled using Dames Point) (To convert magnitude to km, multiply by 1.609)

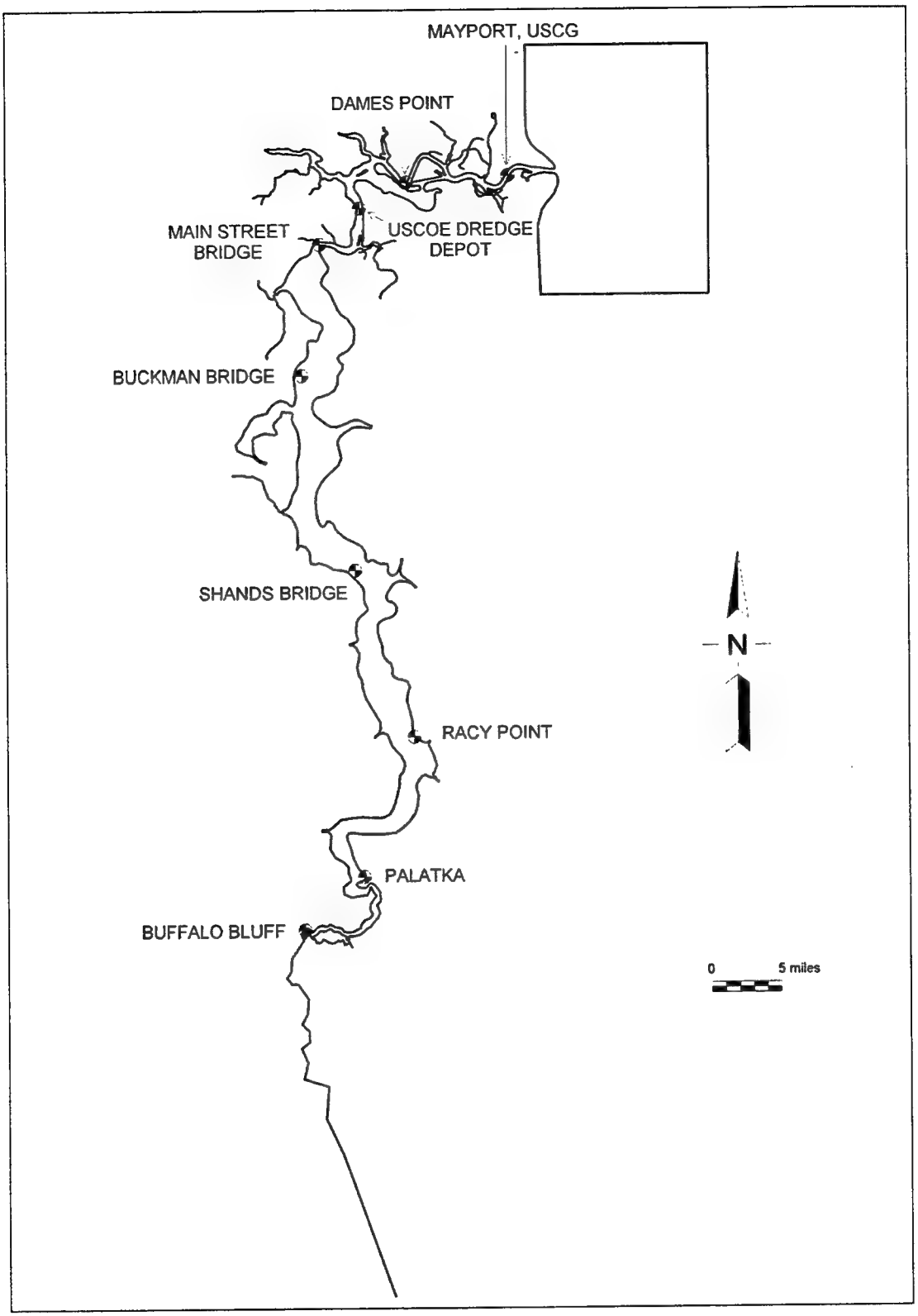

Figure 16. LSJRE tide stations

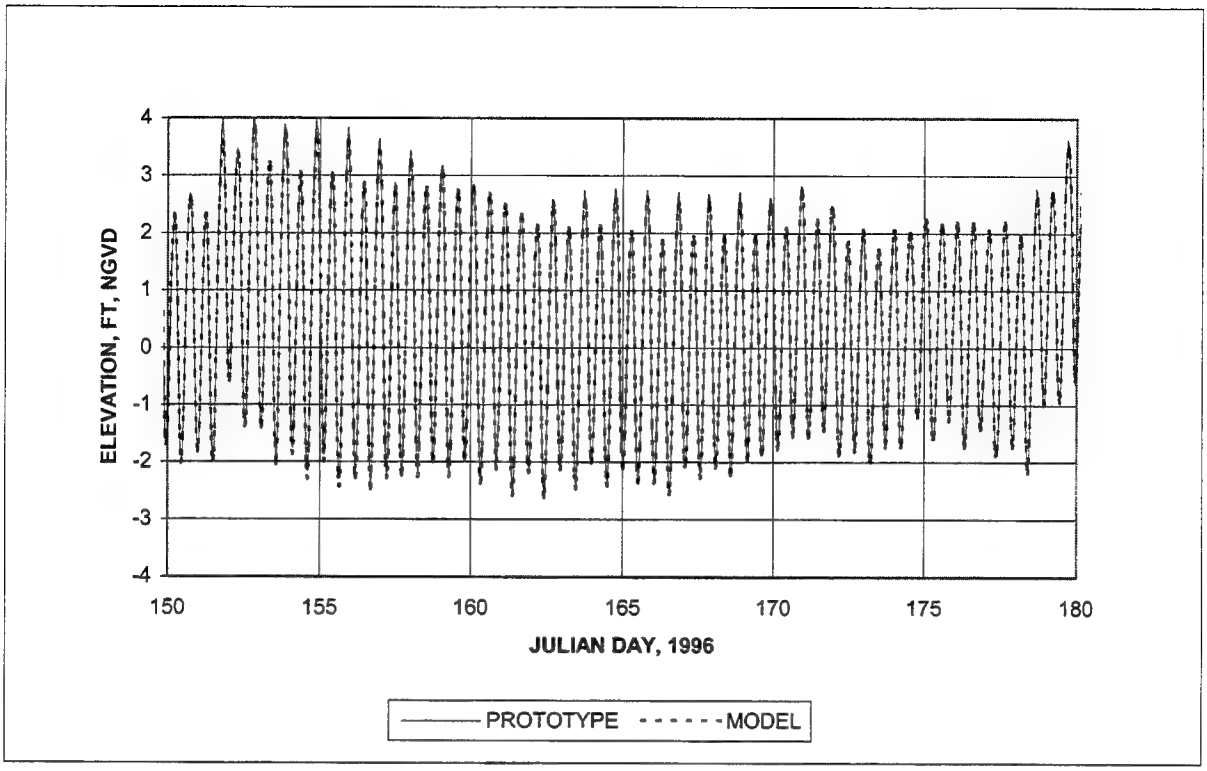

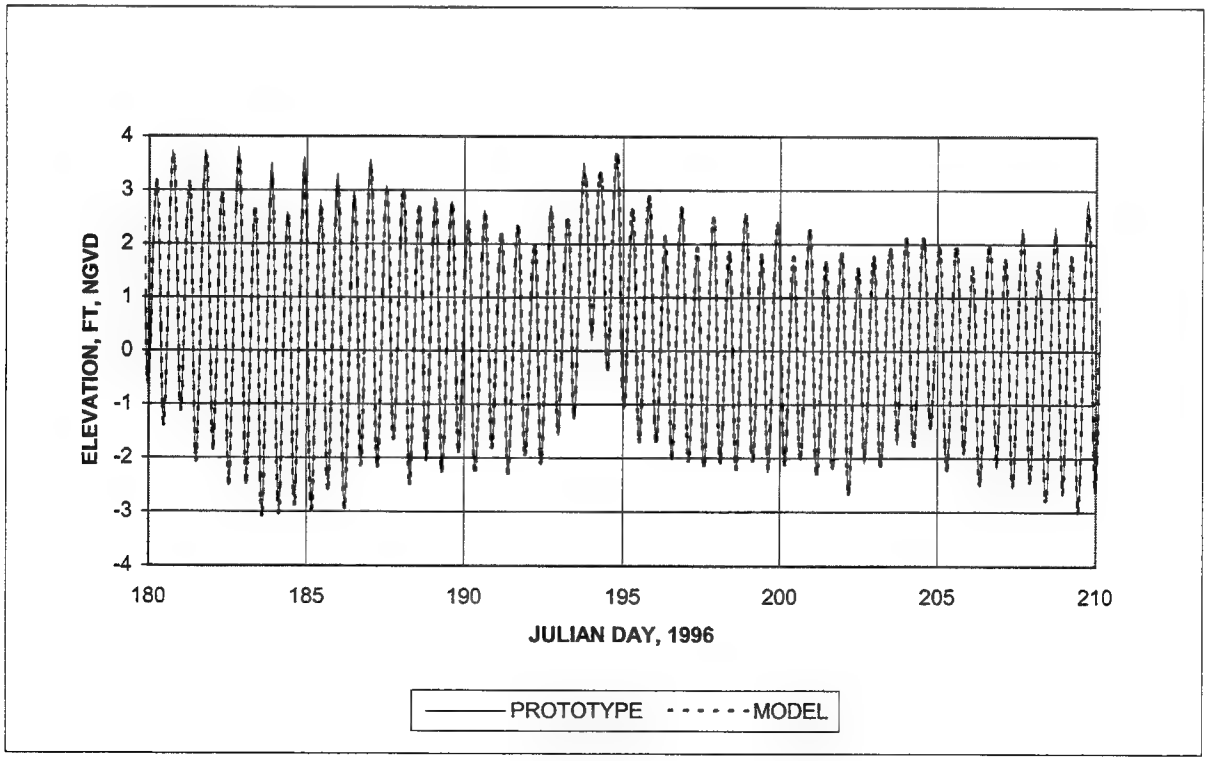

Figure 17. Water surface elevation at Mayport (Continued) (To convert elevation to meters, multiply by 0.3048)

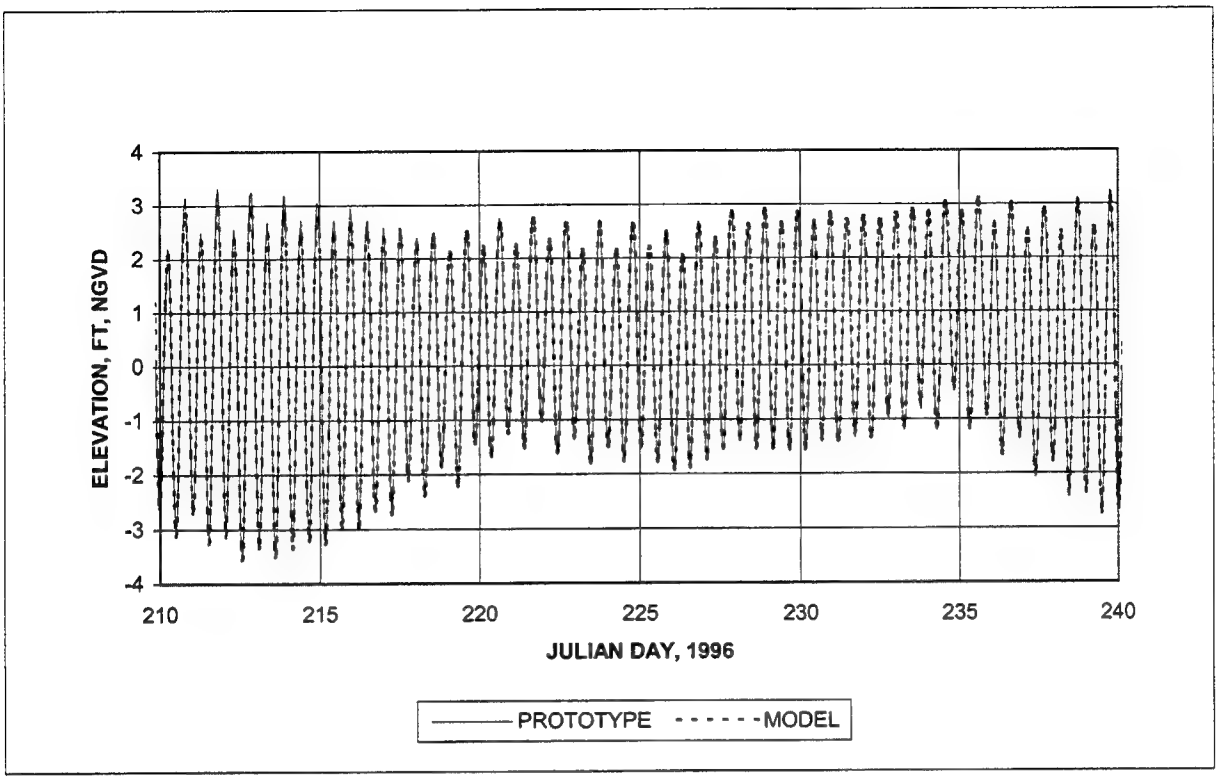

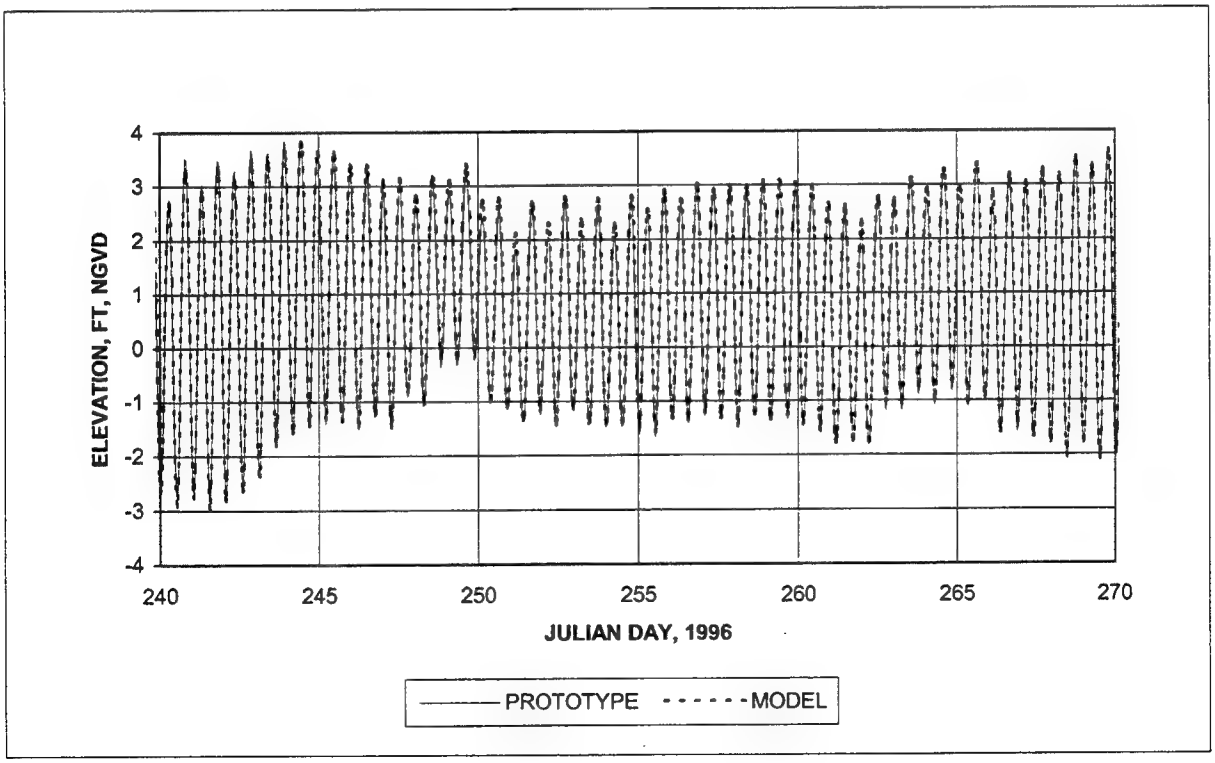

Figure 17. (Concluded)

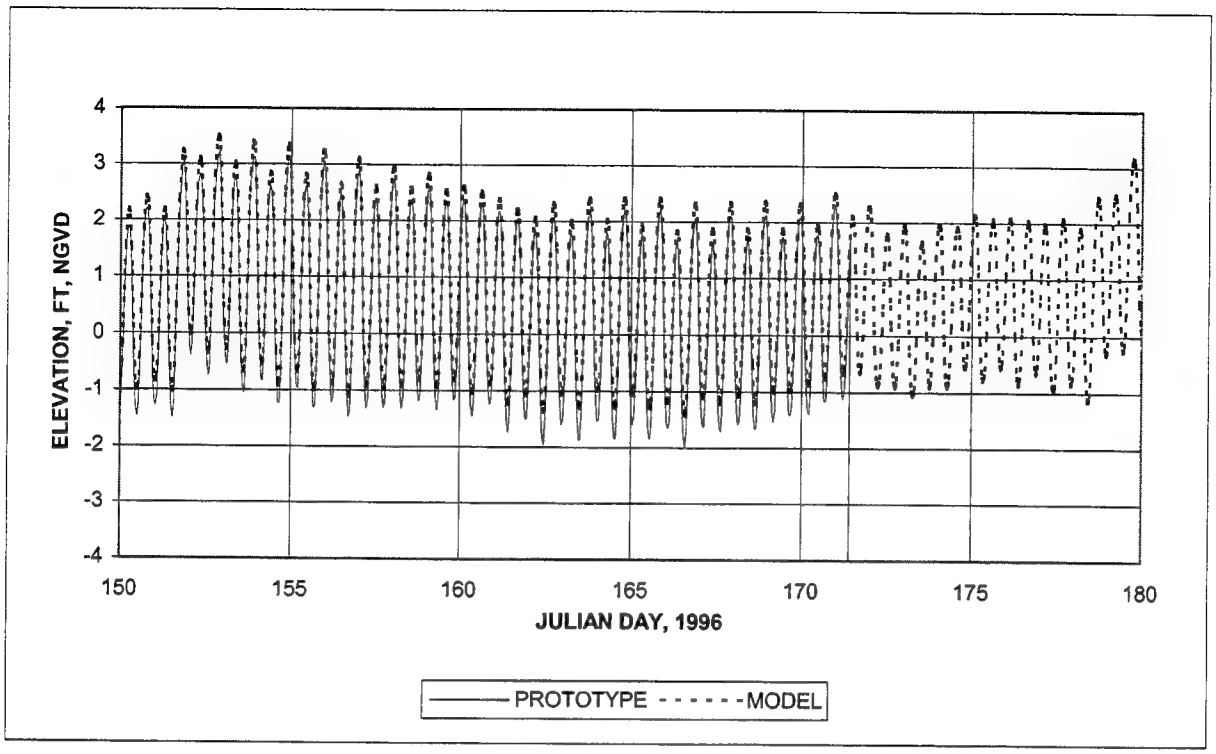

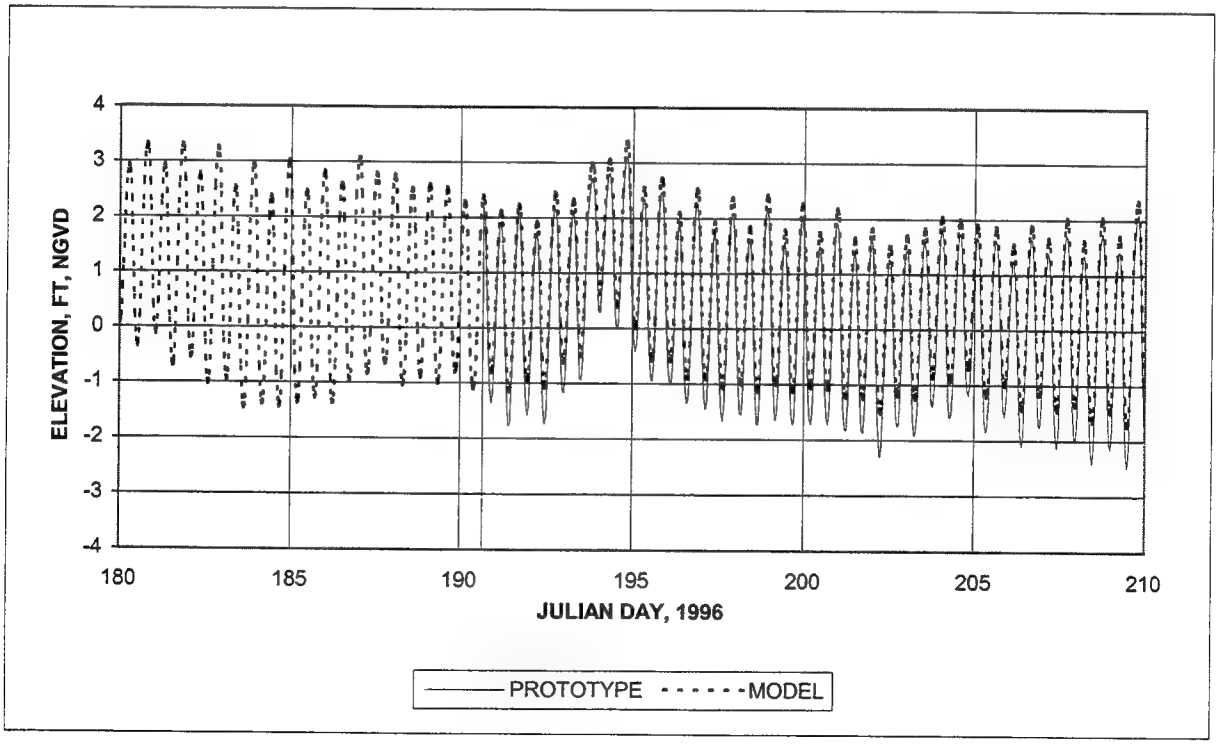

Figure 18. Water surface elevation at Dames Point (Continued) (To convert elevation to meters, multiply by 0.3048)

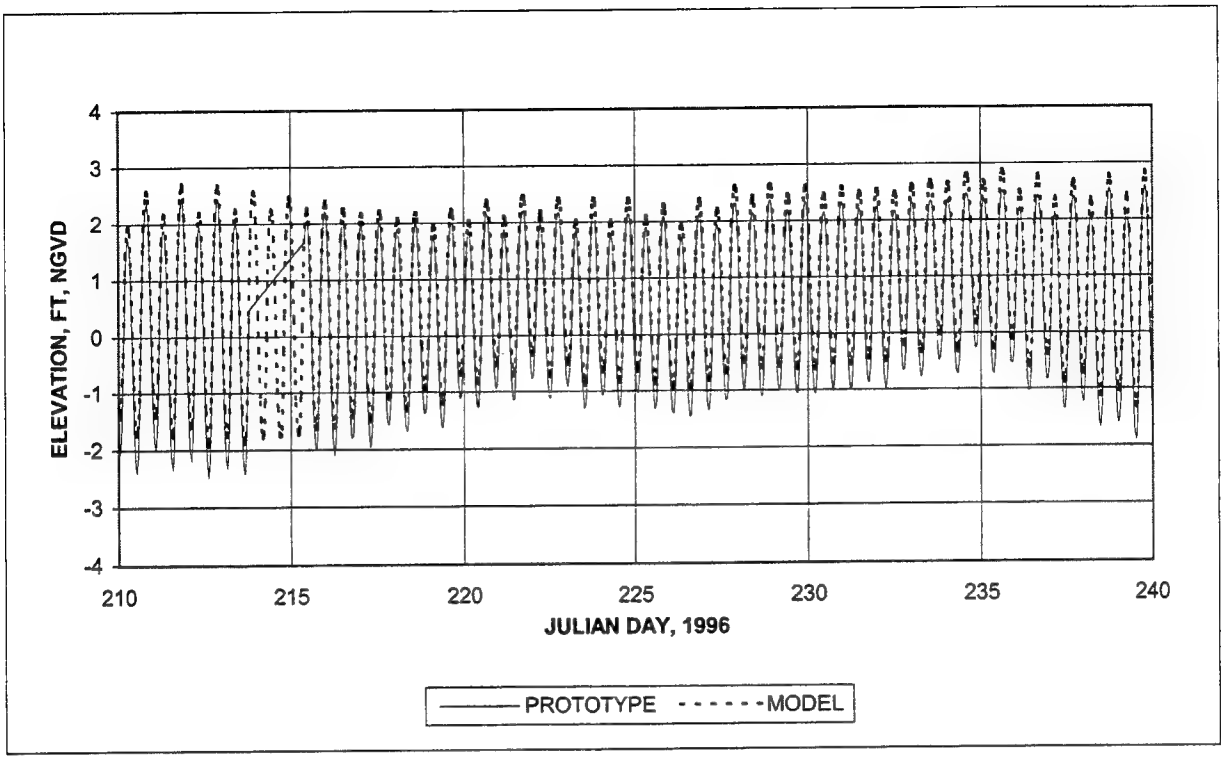

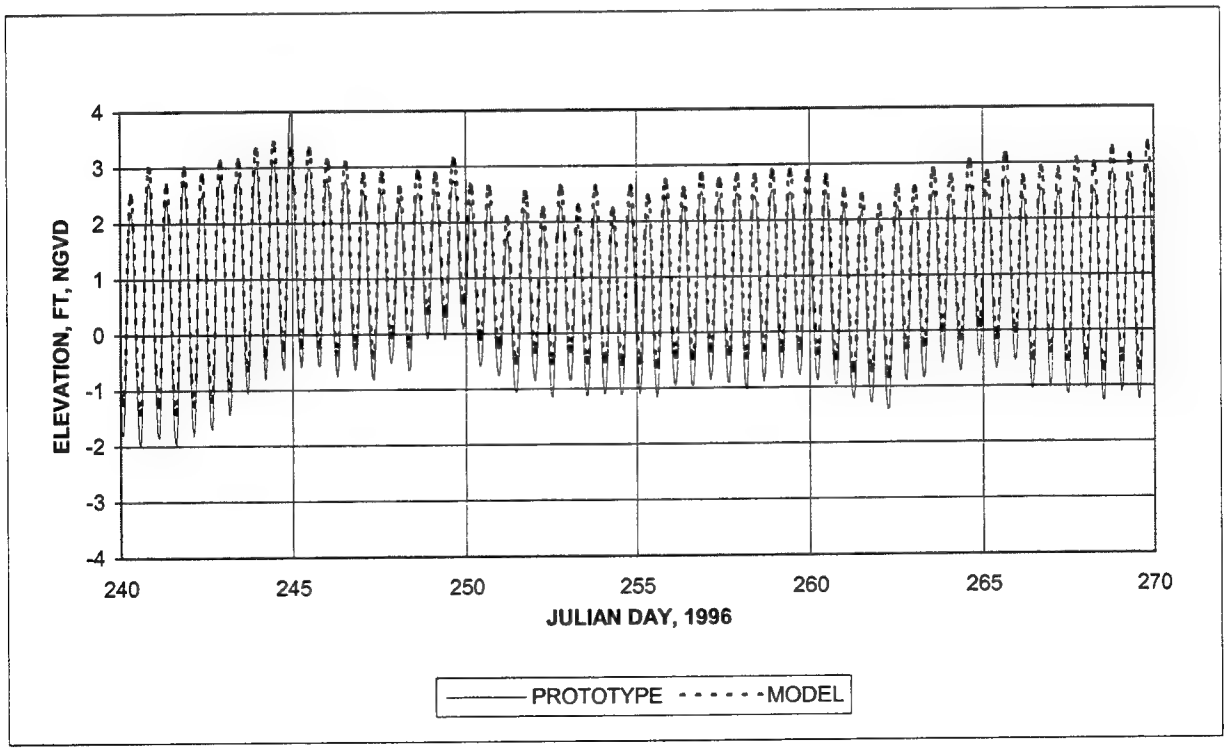

Figure 18. (Concluded)

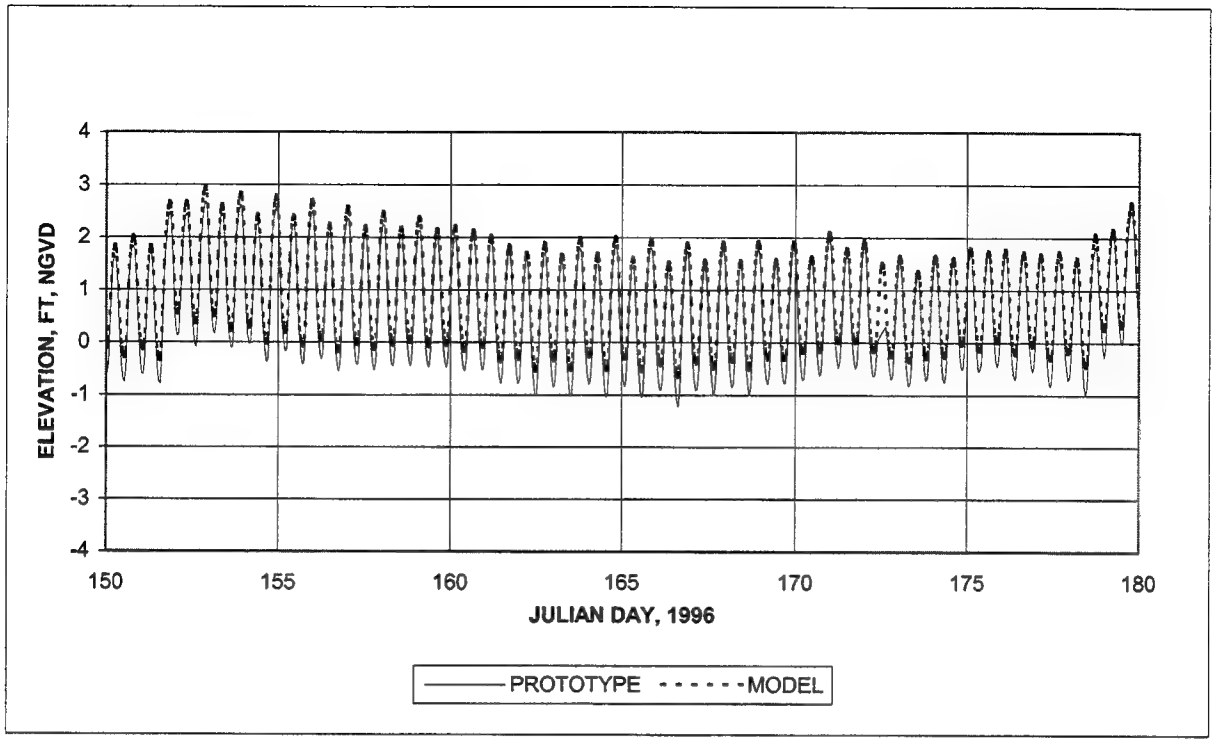

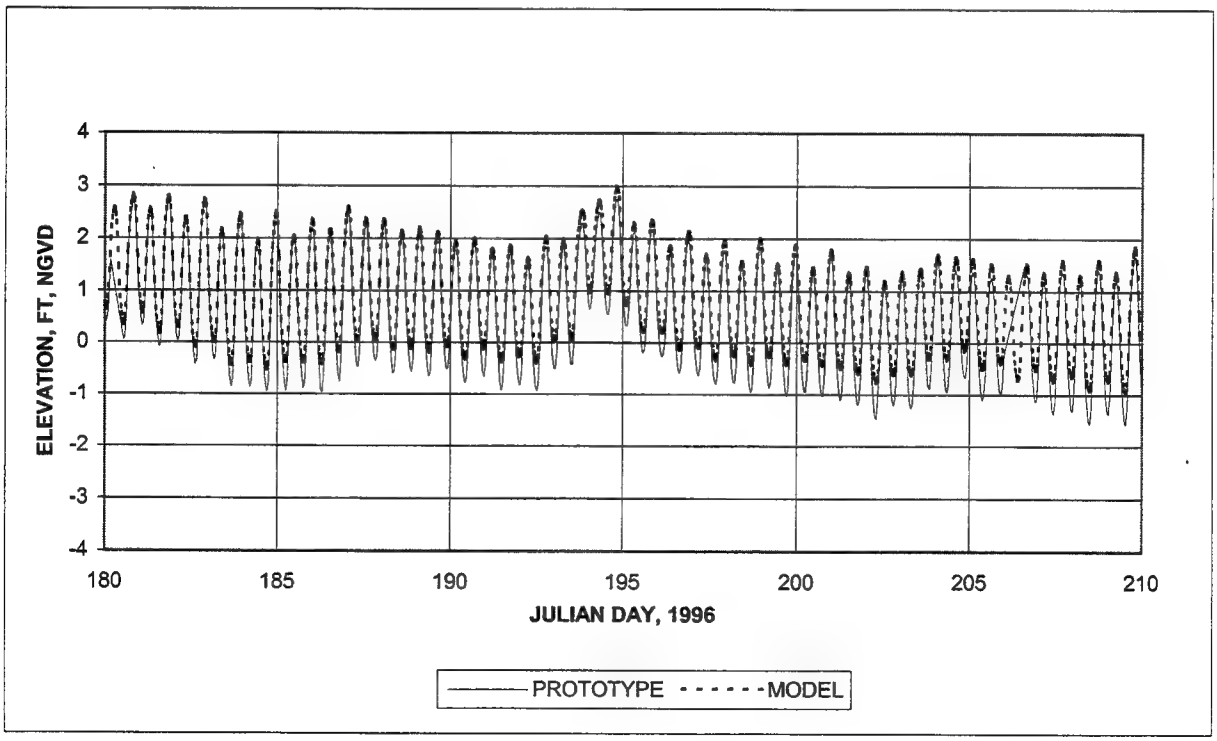

Figure 19. Water surface elevation at USCOE Dredge Depot (Continued) (To convert elevation to meters, multiply by 0.3048)

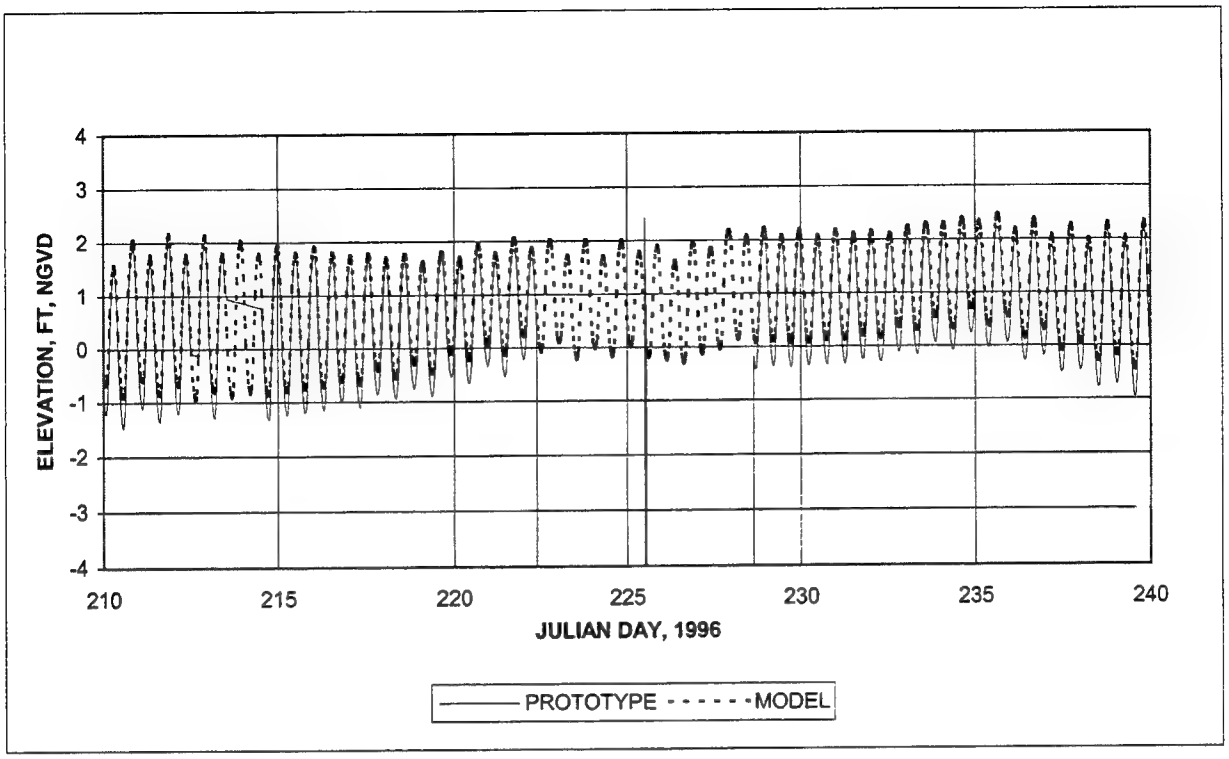

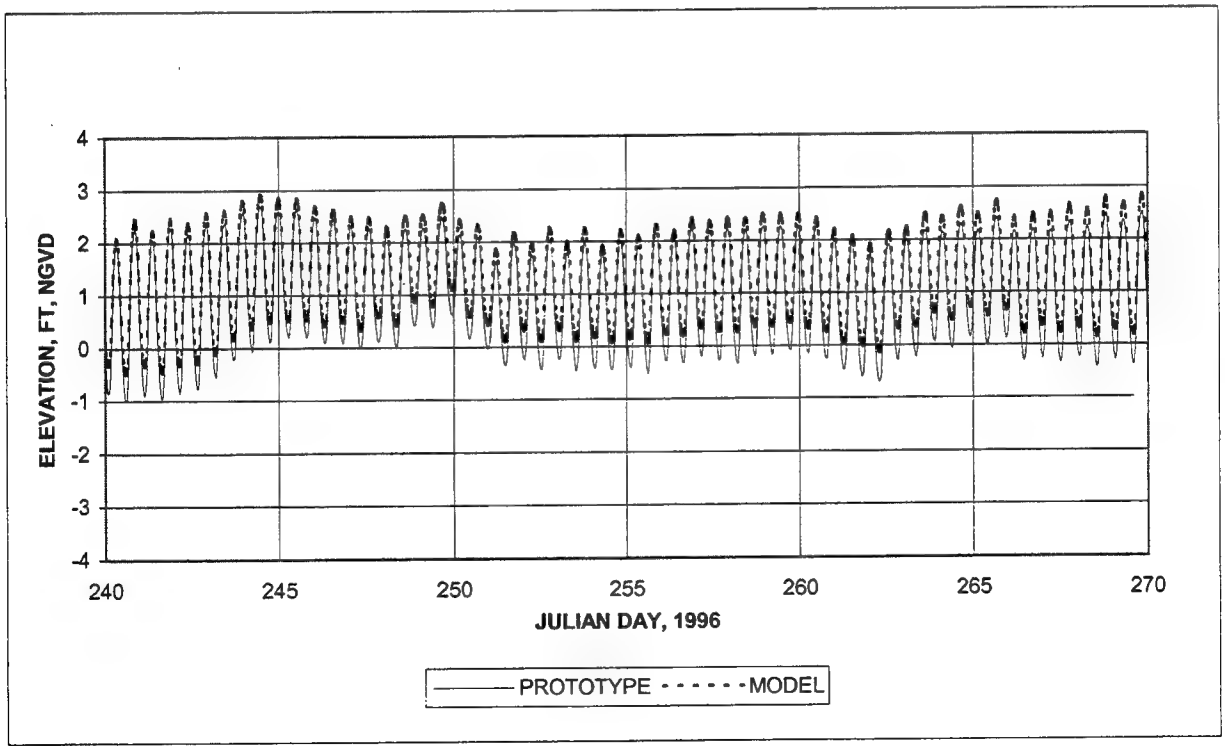

Figure 19. (Concluded)

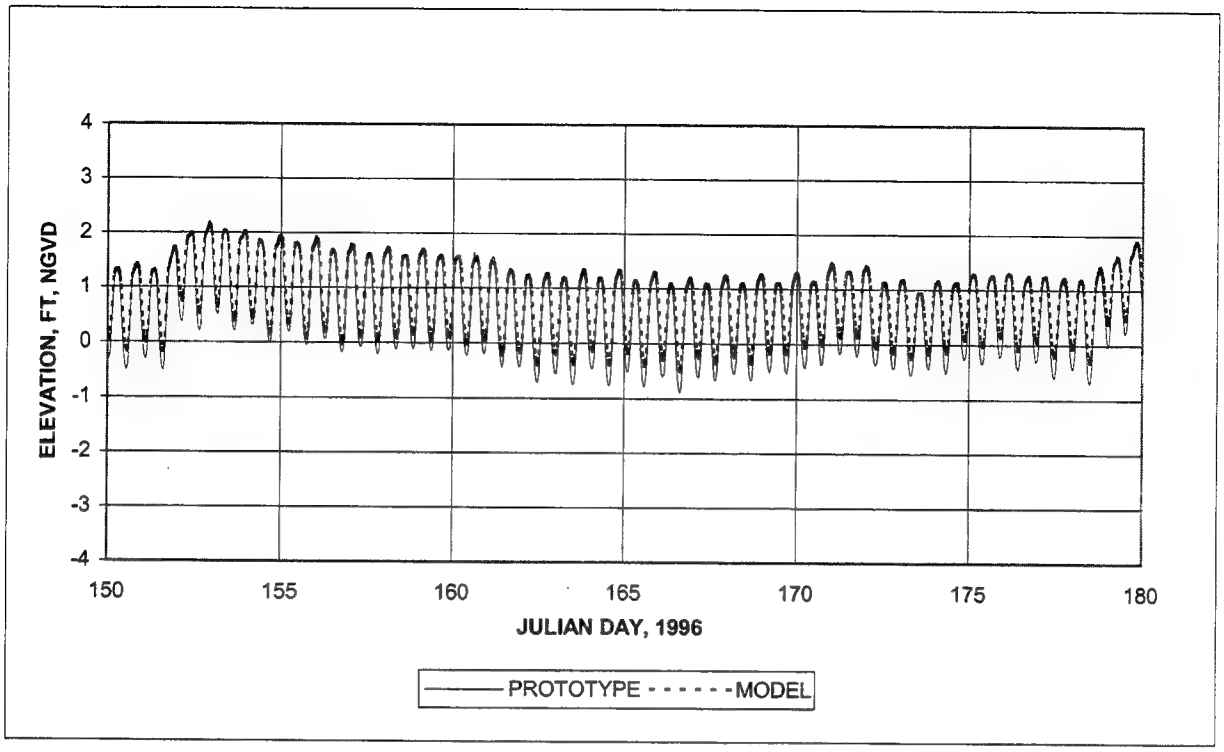

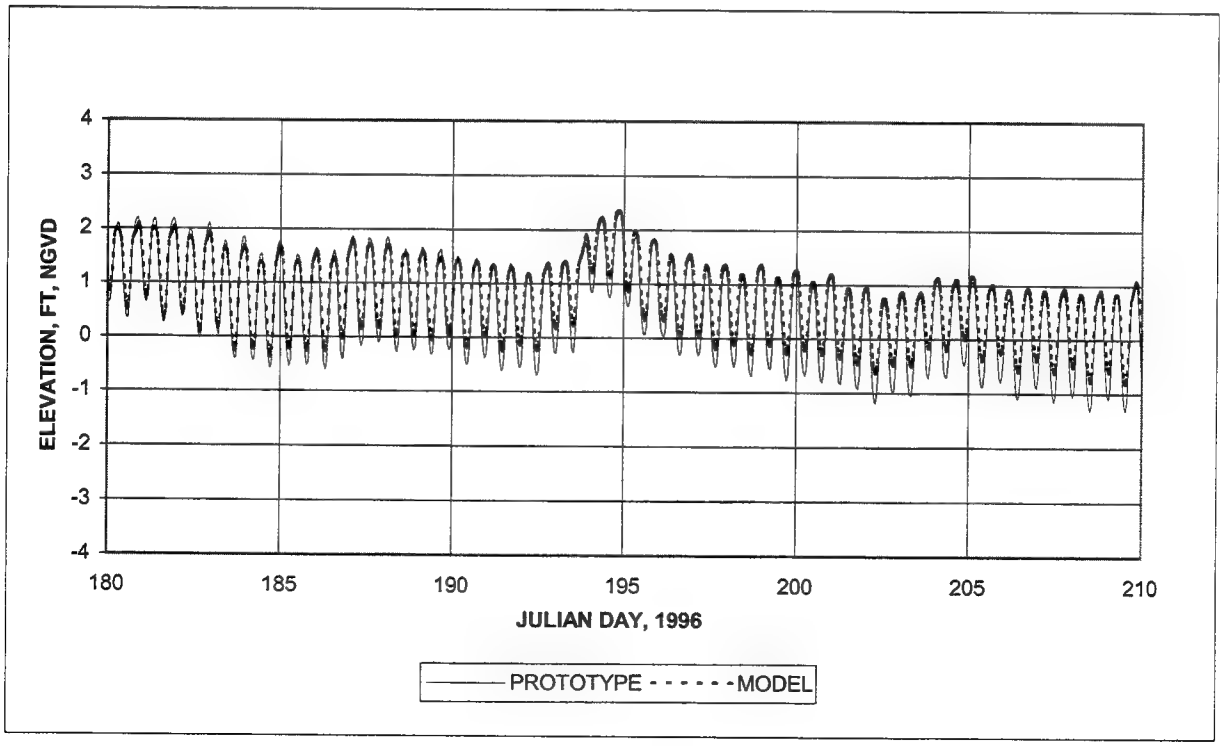

Figure 20. Water surface elevation at Main Street Bridge (Continued) (To convert elevation to meters, multiply by 0.3048)

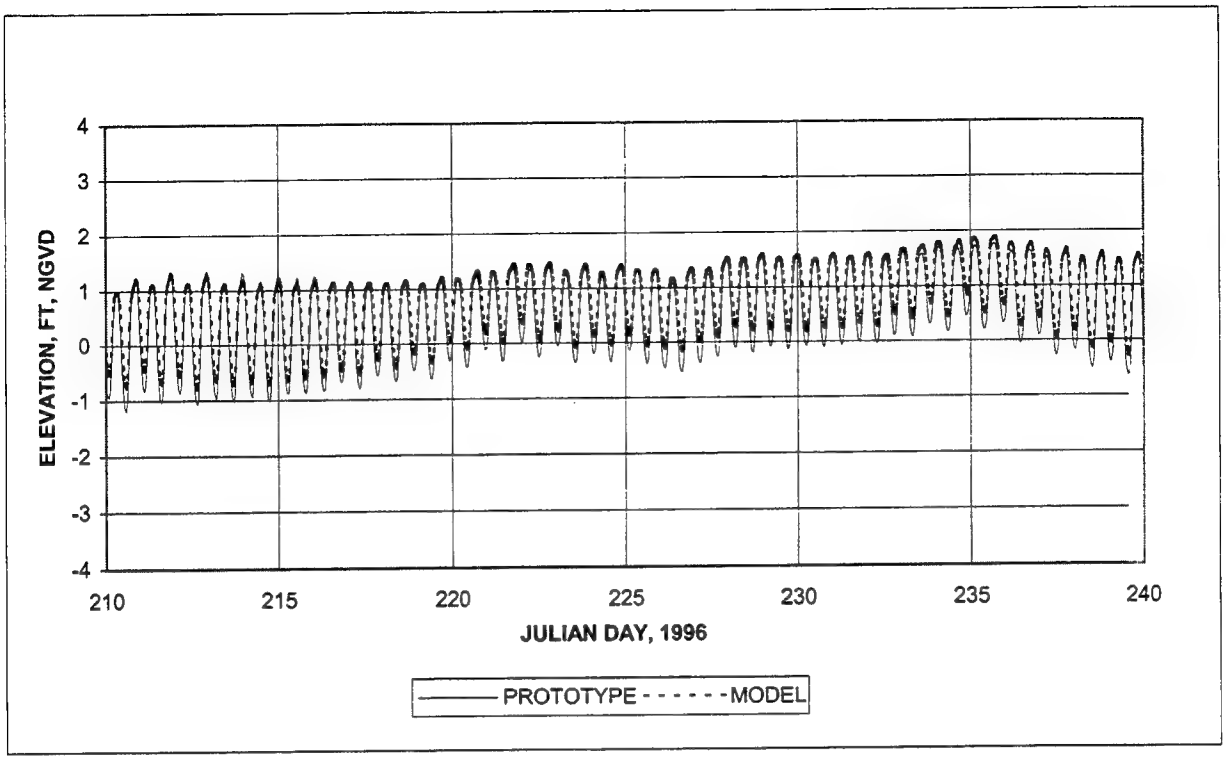

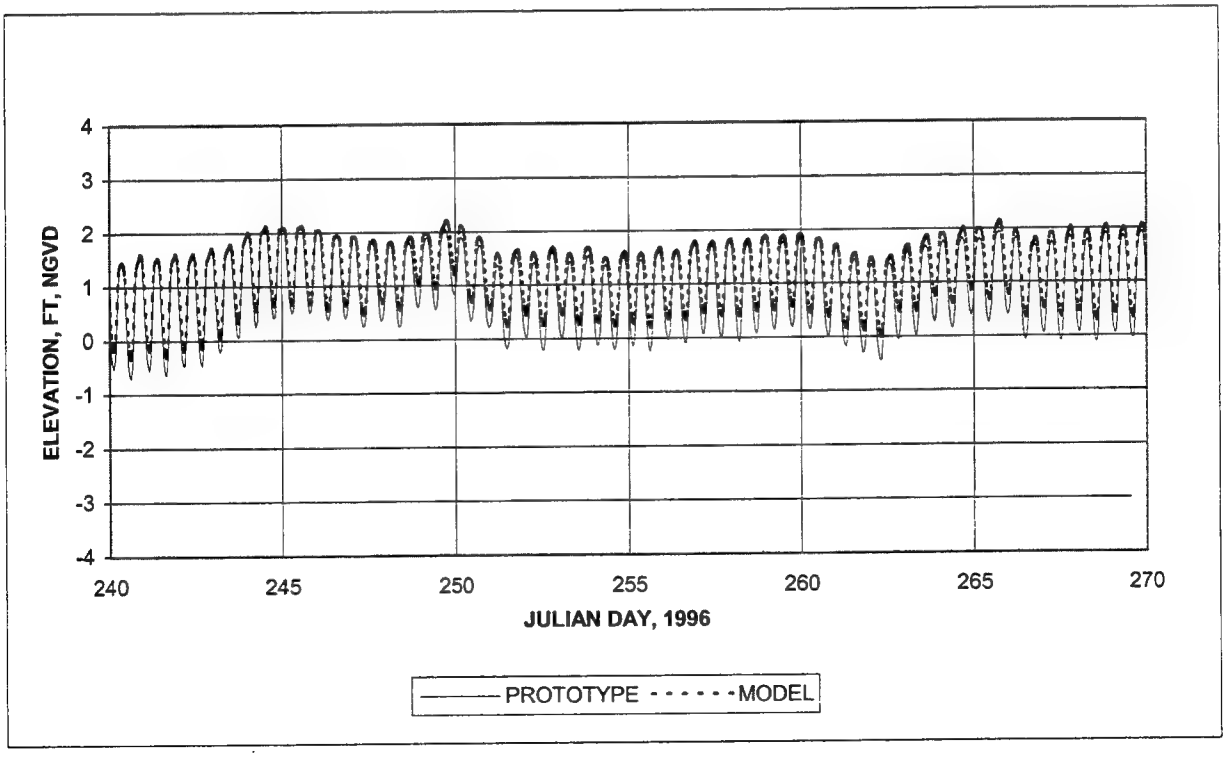

Figure 20. (Concluded)

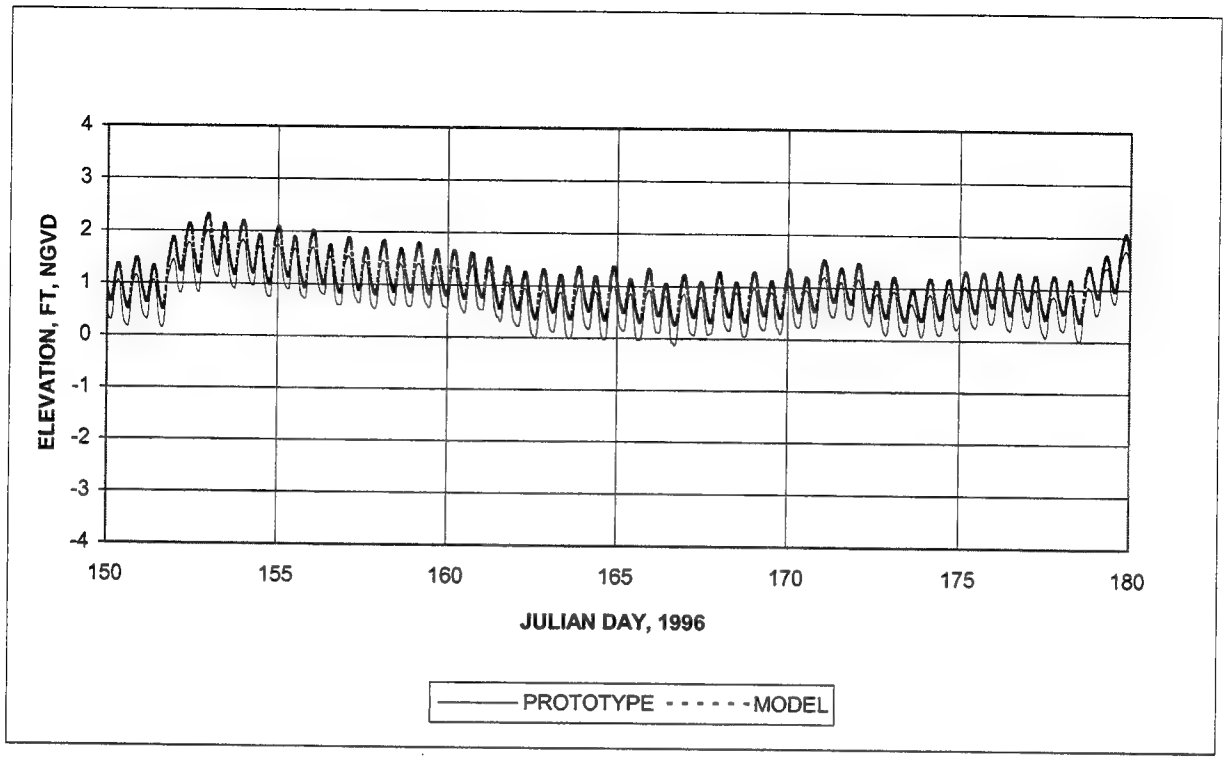

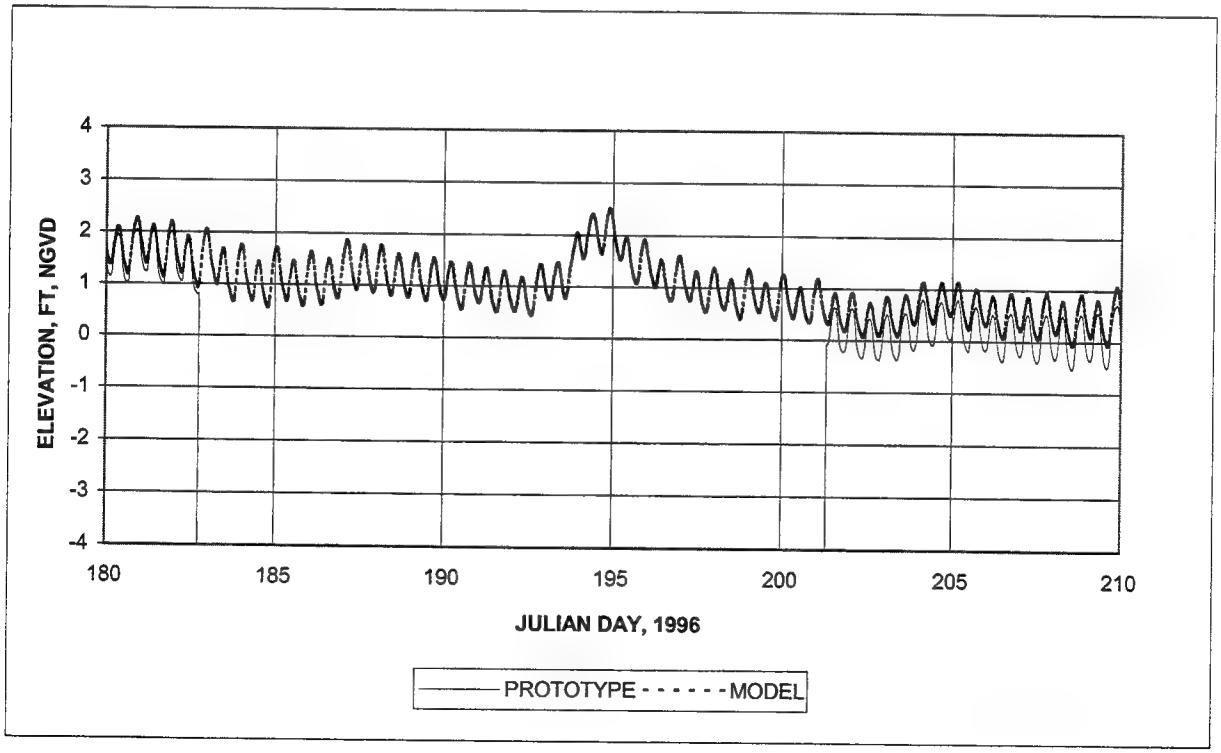

Figure 21. Water surface elevation at Buckman Bridge (Continued) (To convert elevation to meters, multiply by 0.3048)

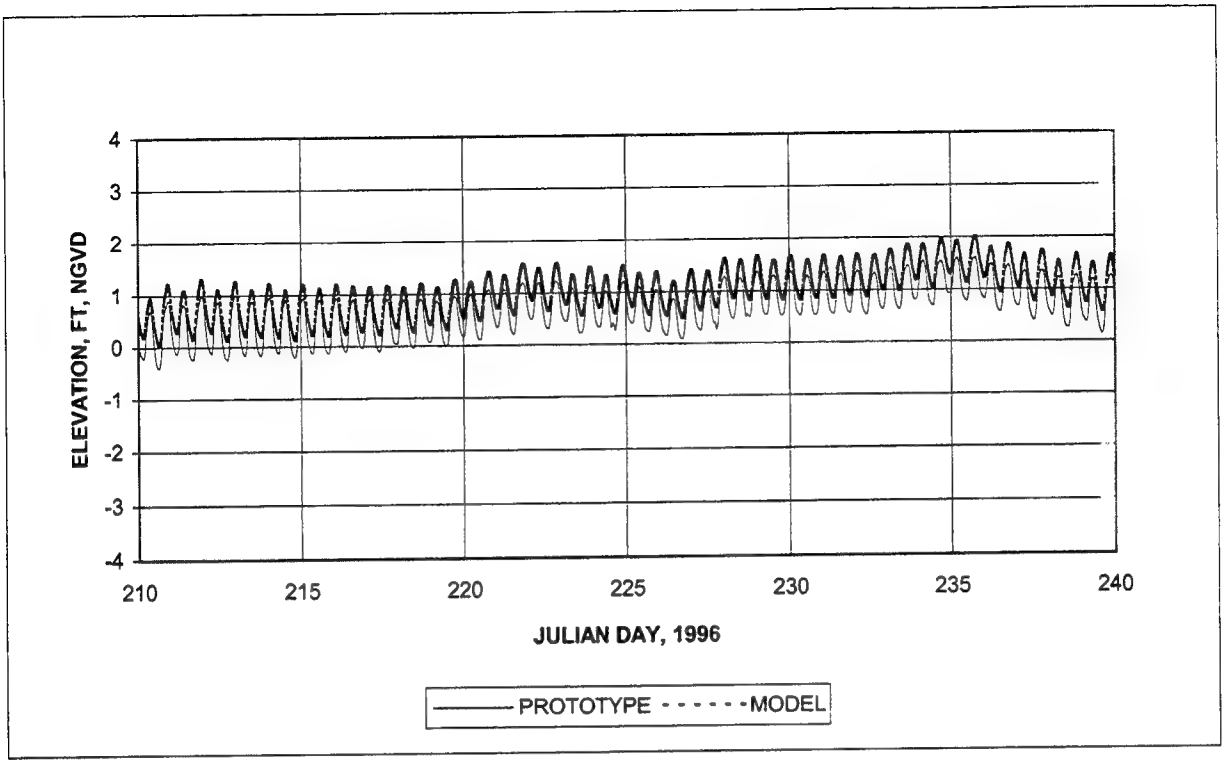

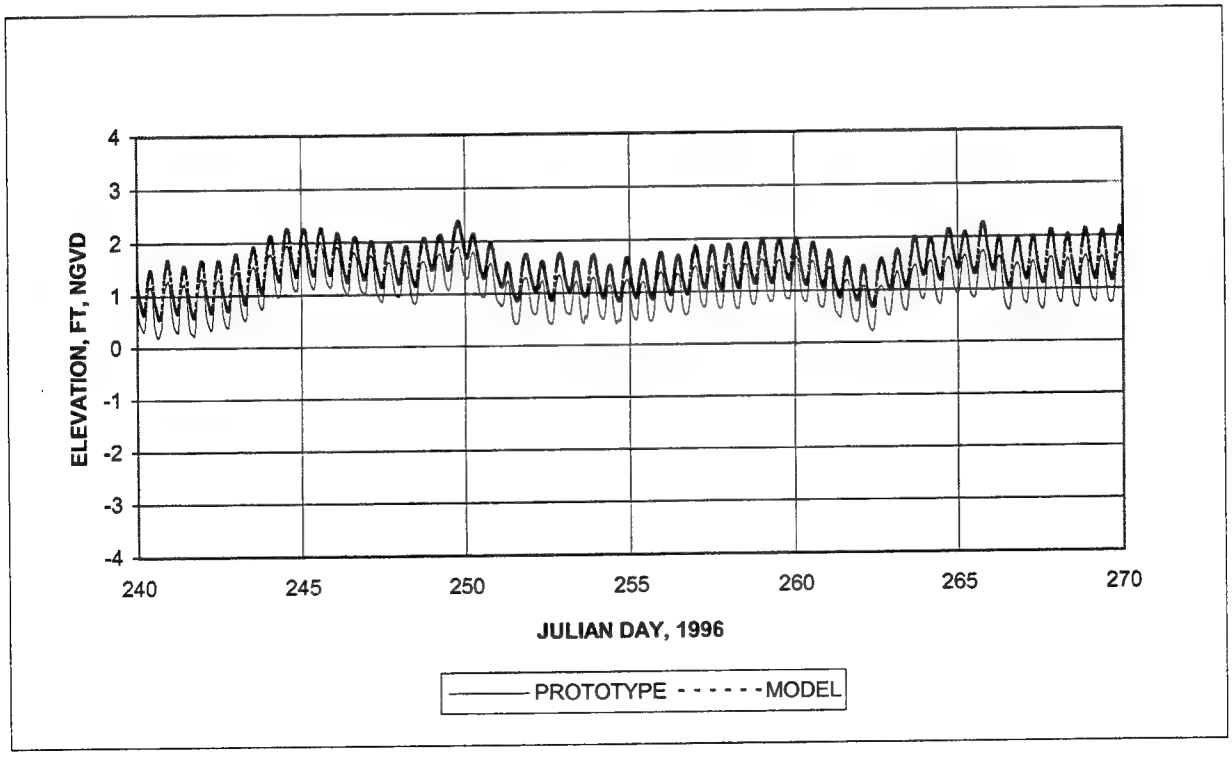

Figure 21. (Concluded)

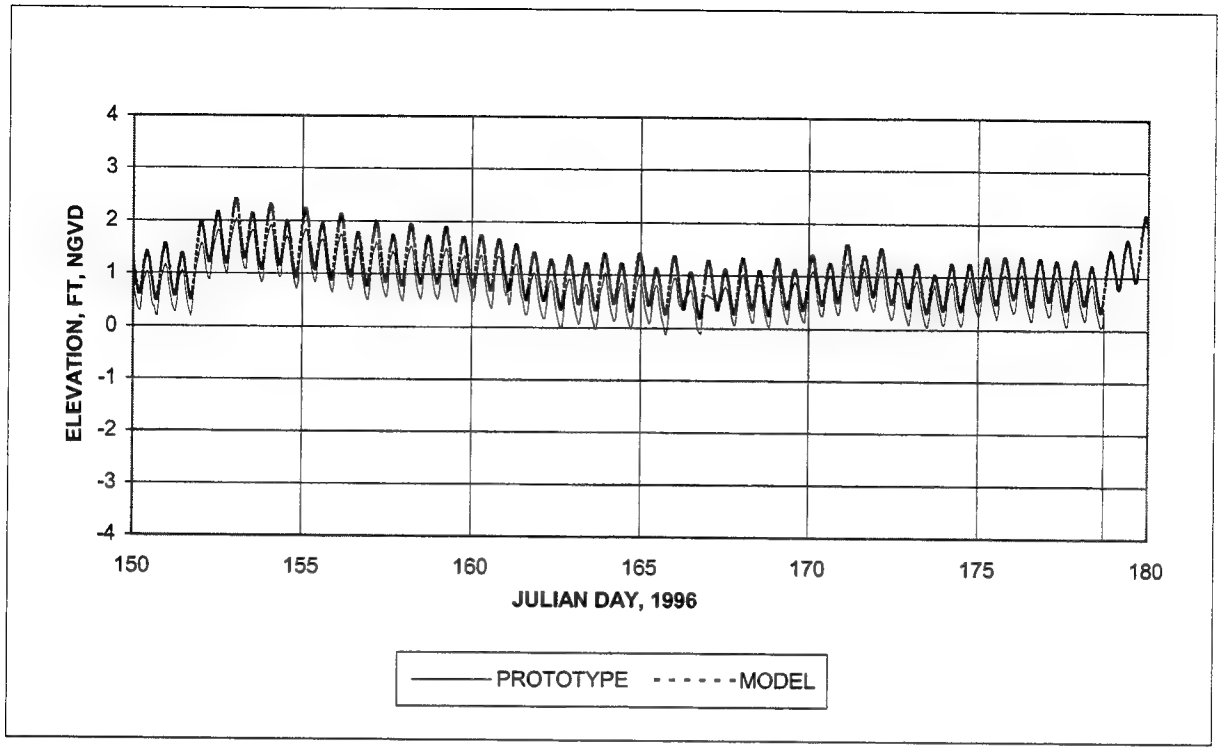

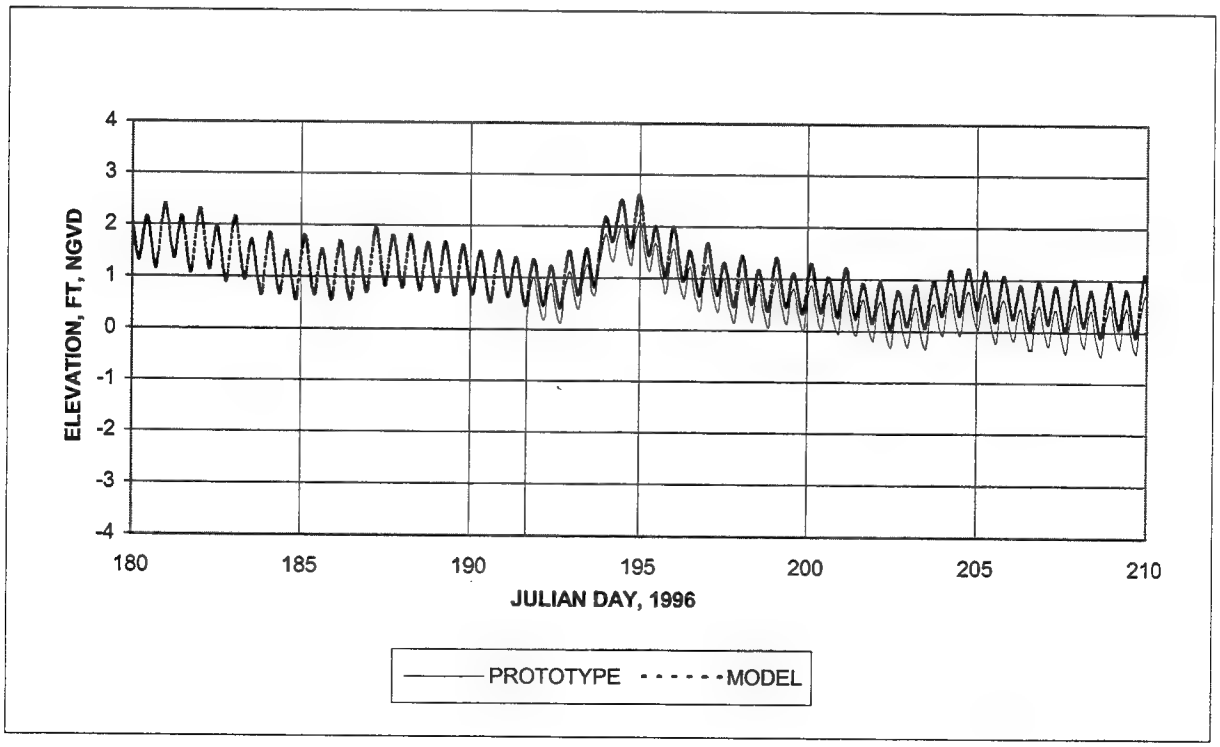

Figure 22. Water surface elevation at Shands Bridge (Continued) (To convert elevation to meters, multiply by 0.3048)

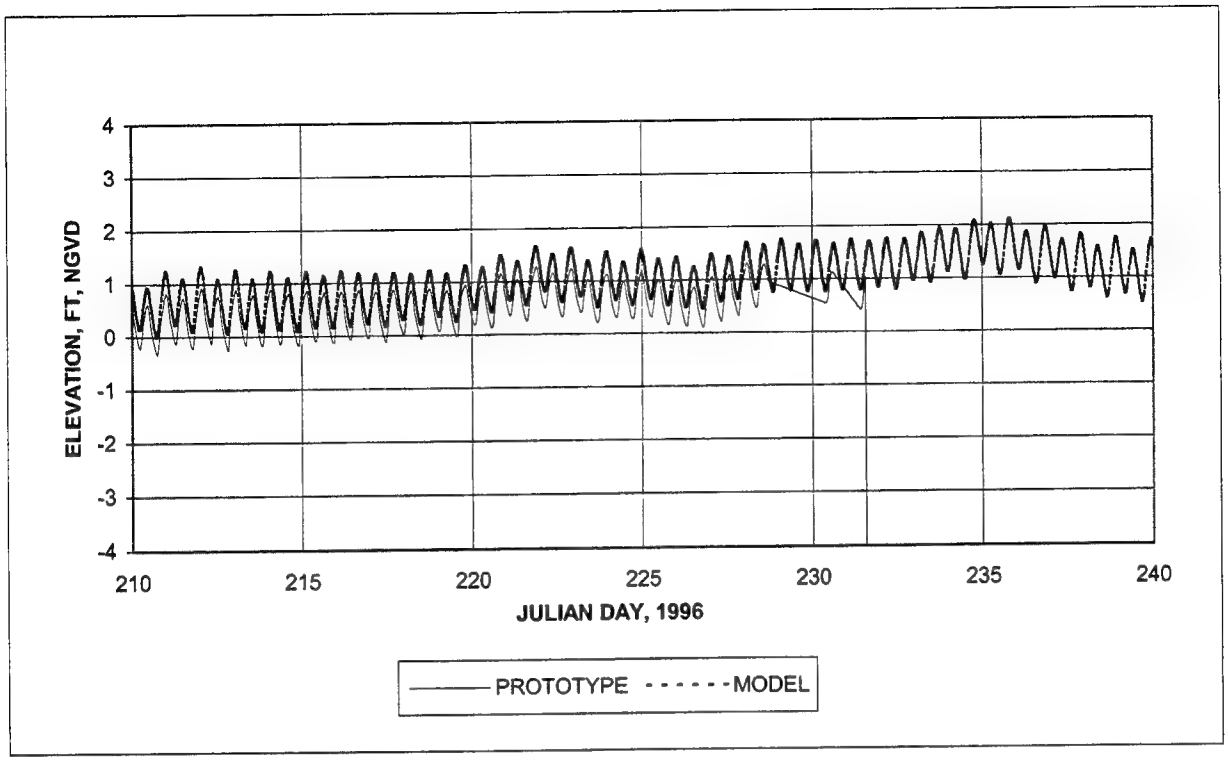

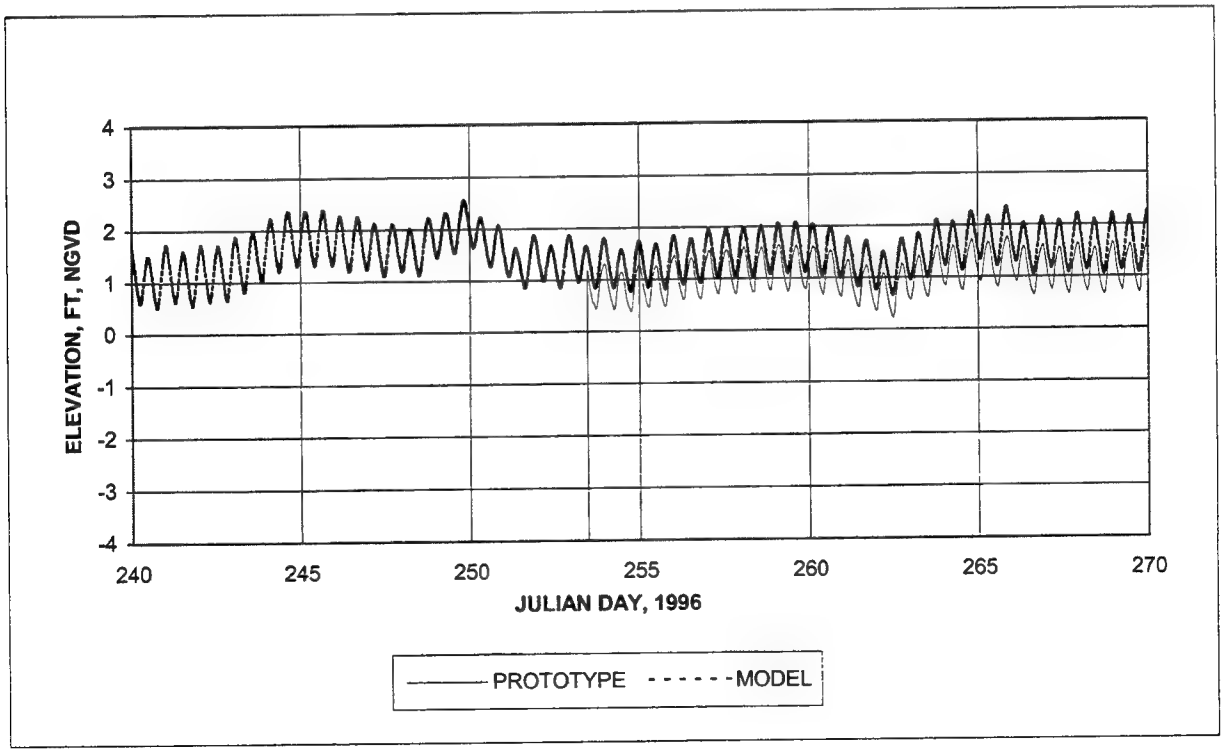

Figure 22. (Concluded)

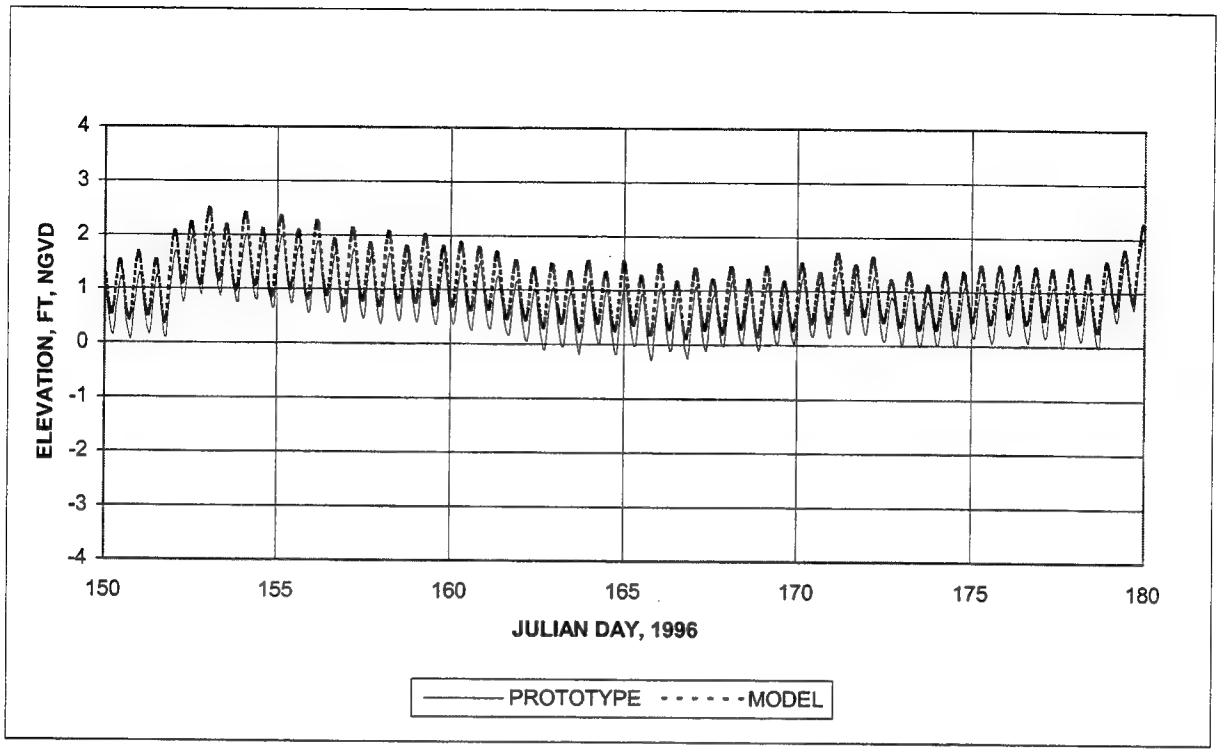

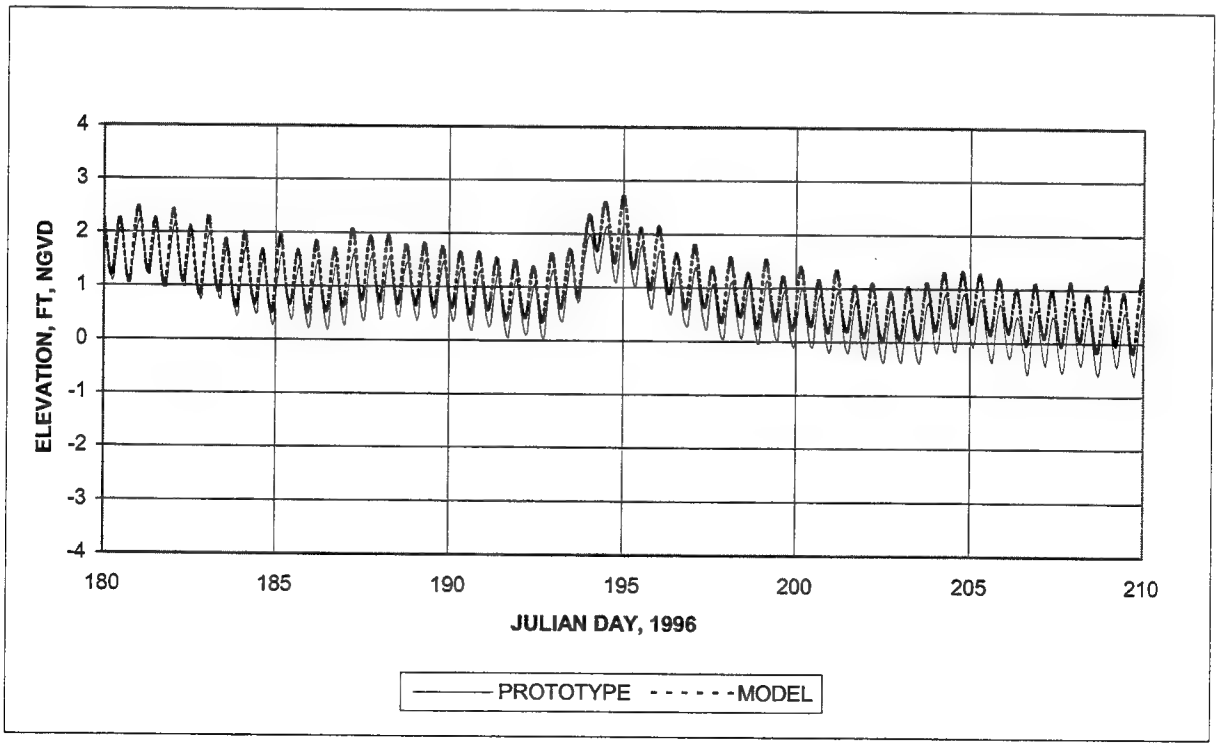

Figure 23. Water surface elevation at Racy Point (Continued) (To convert elevation to meters, multiply by 0.3048)

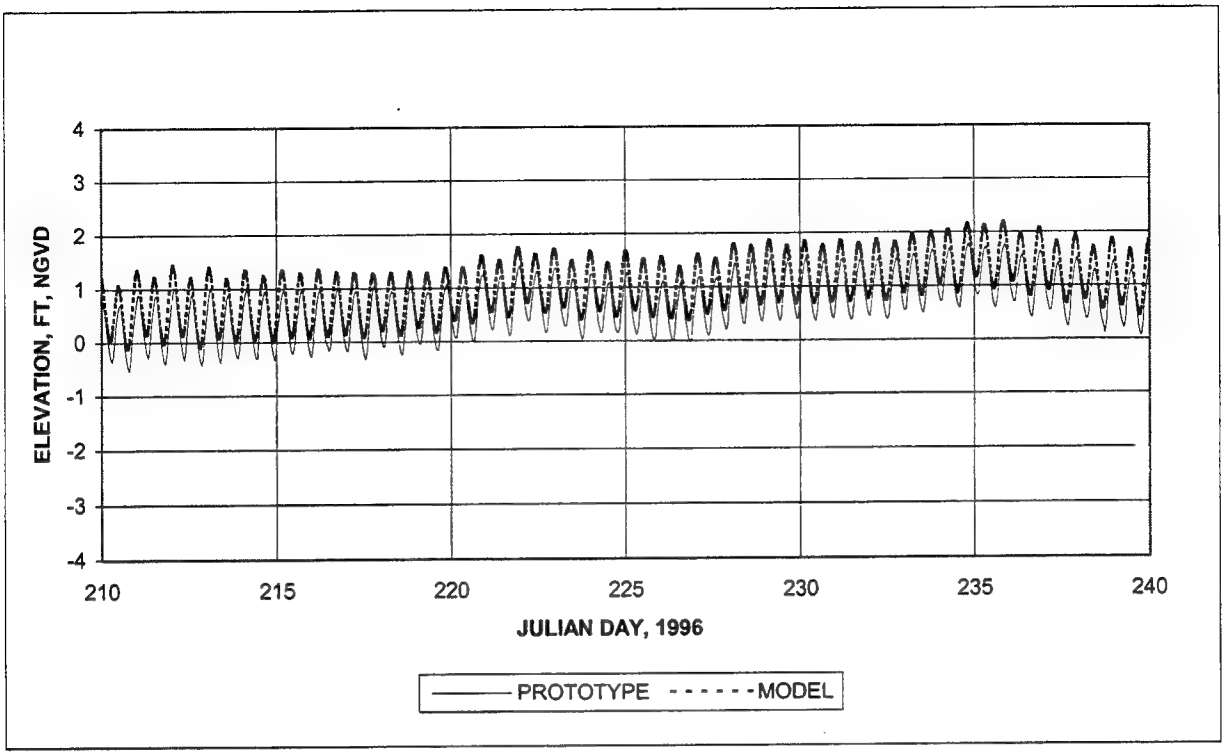

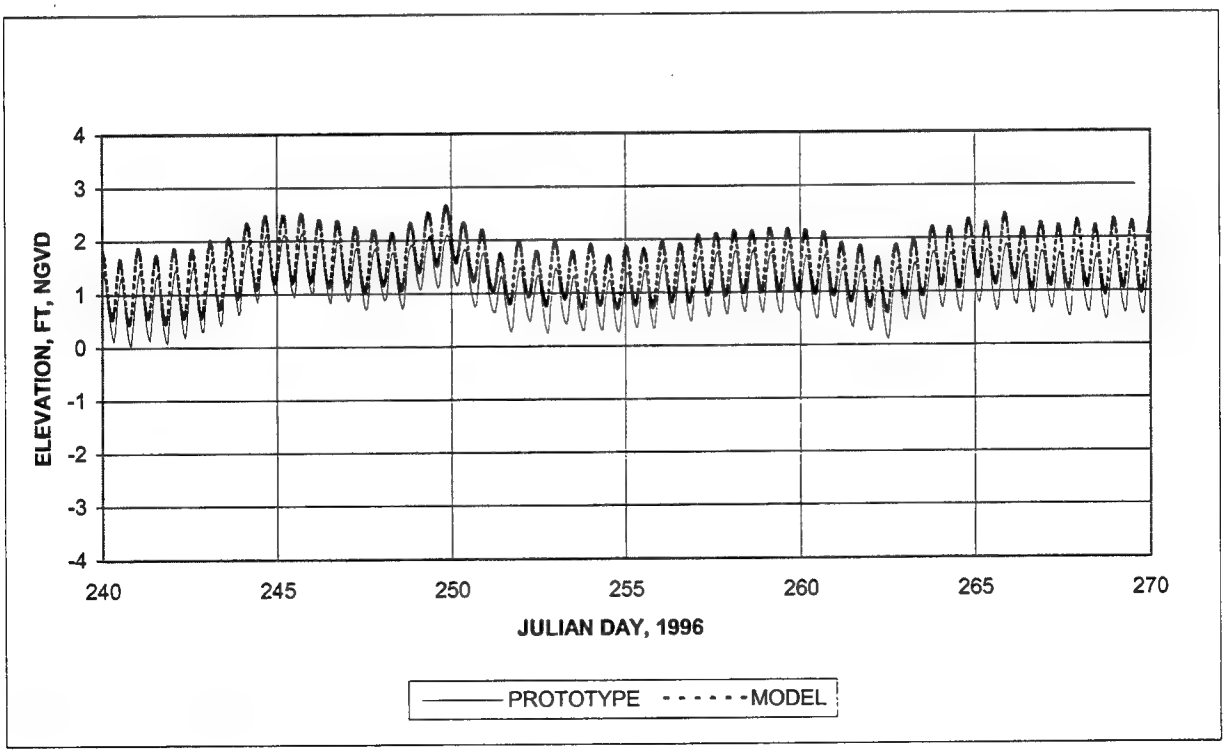

Figure 23. (Concluded)

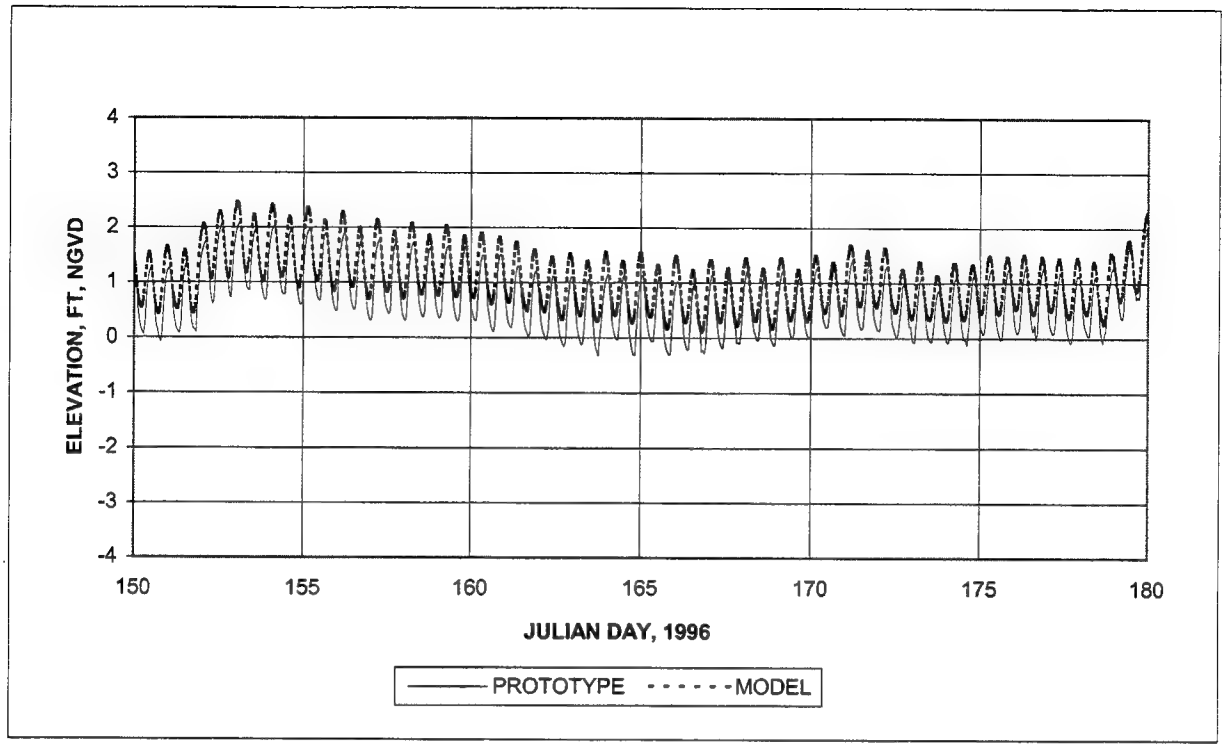

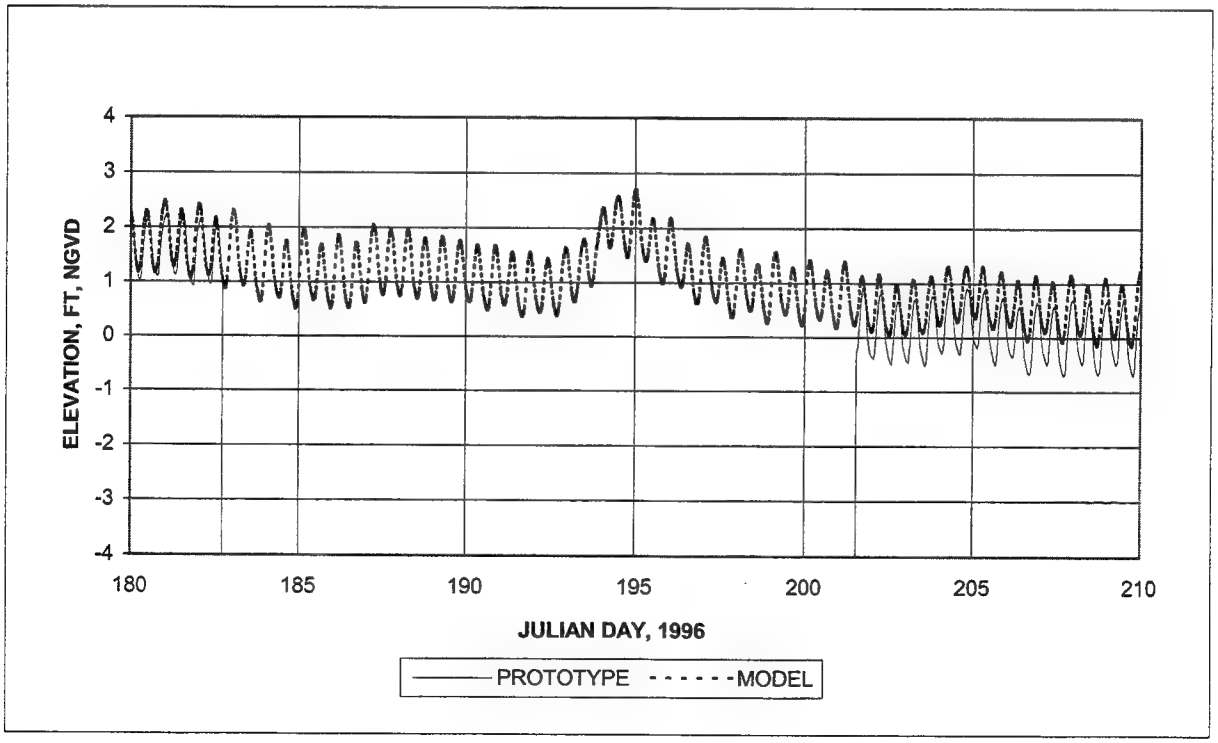

Figure 24. Water surface elevation at Palatka (Continued) (To convert elevation to meters, multiply by 0.3048)

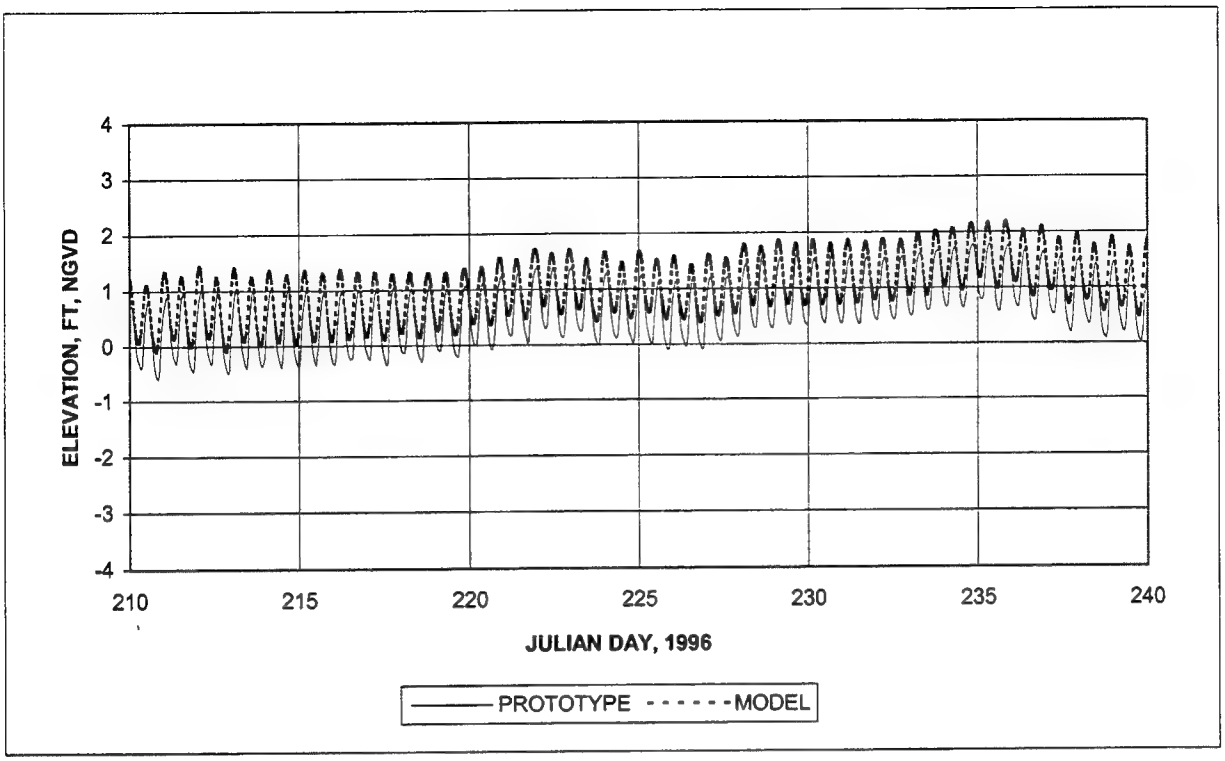

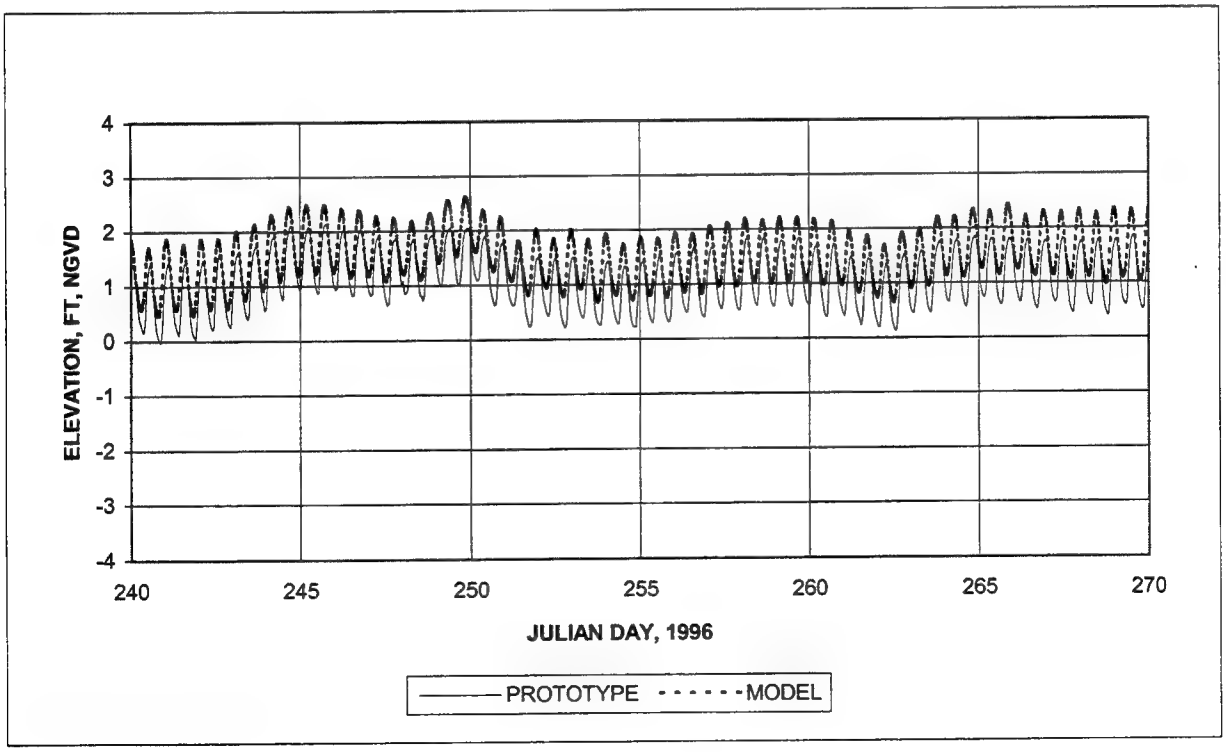

Figure 24. (Concluded)

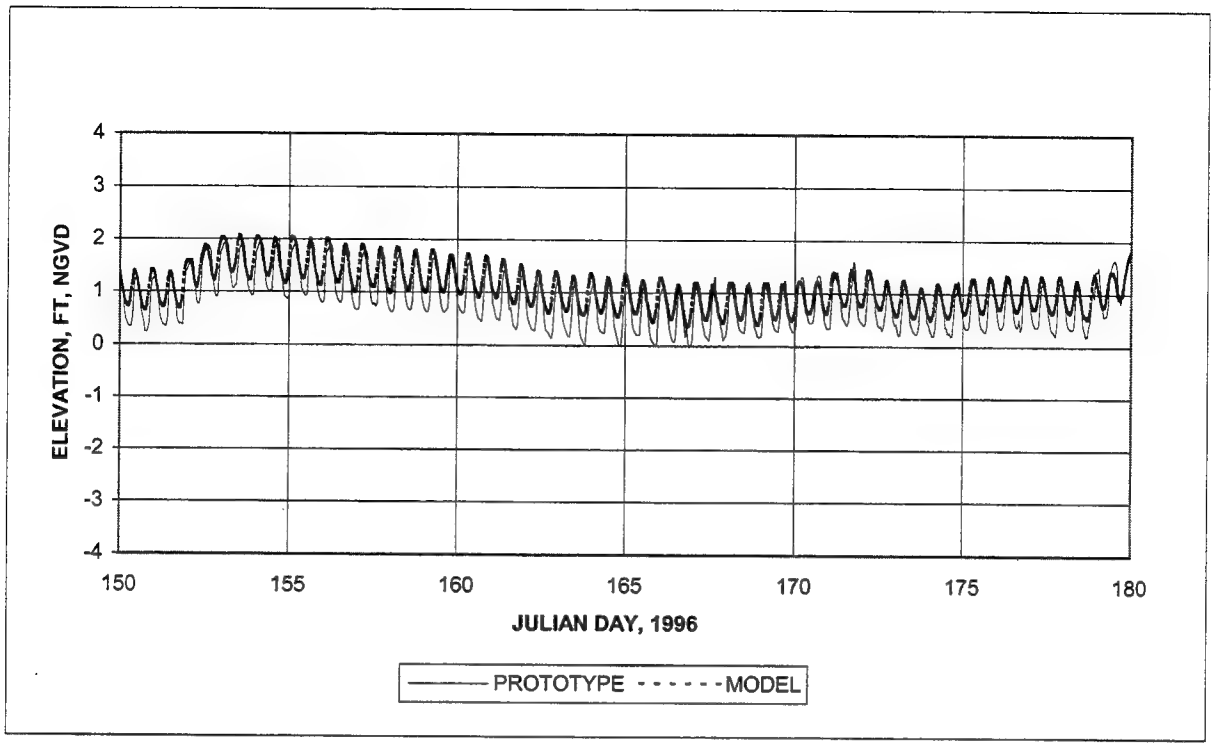

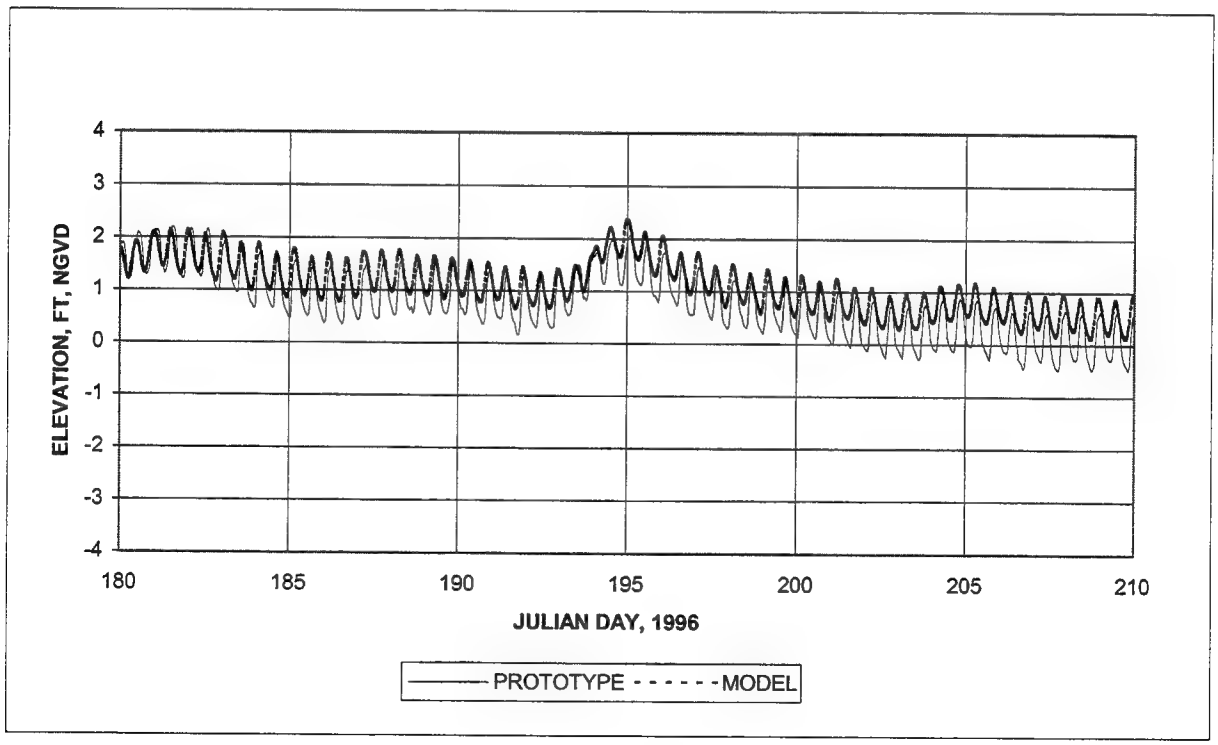

Figure 25. Water surface elevation at Buffalo Bluff (Continued) (To convert elevation to meters, multiply by 0.3048)

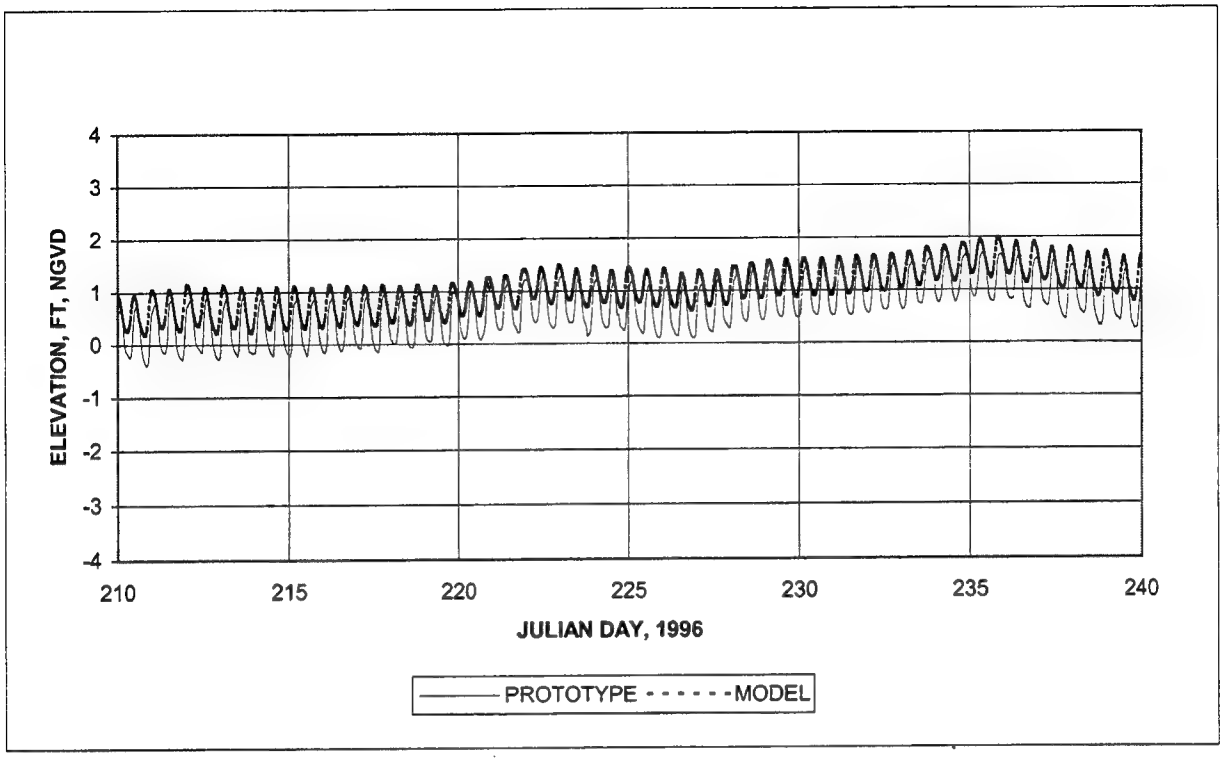

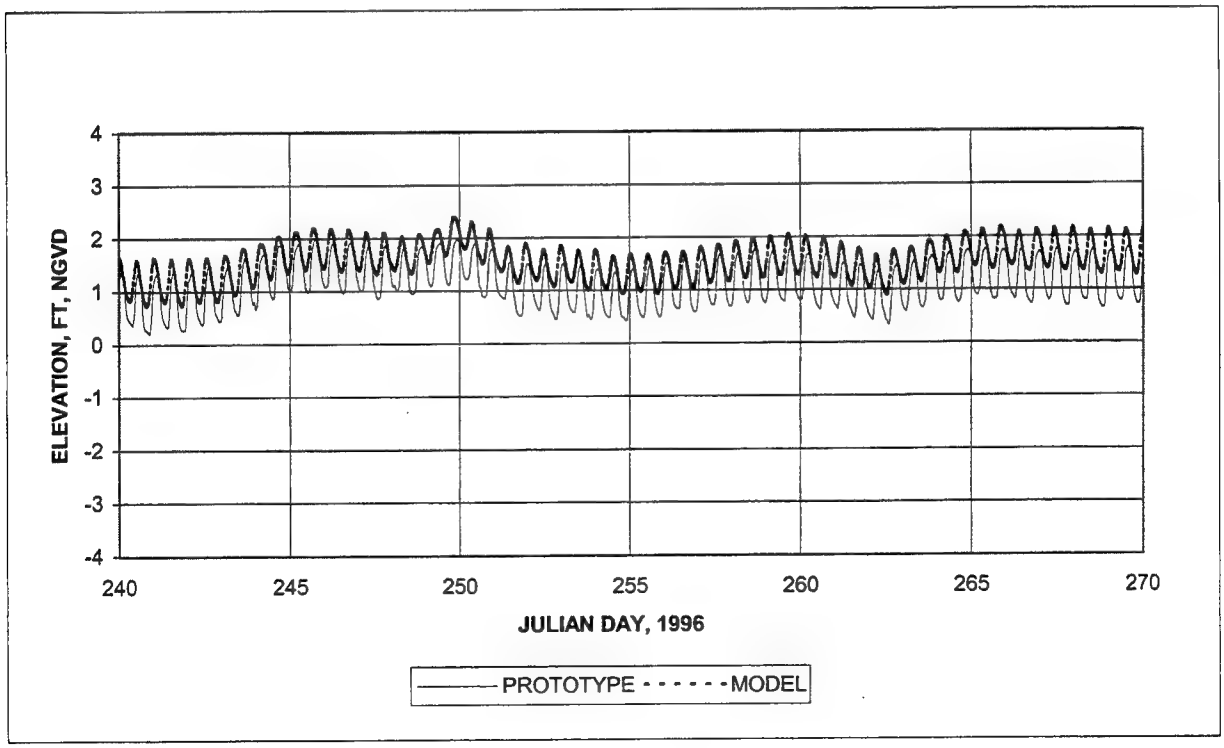

Figure 25. (Concluded)

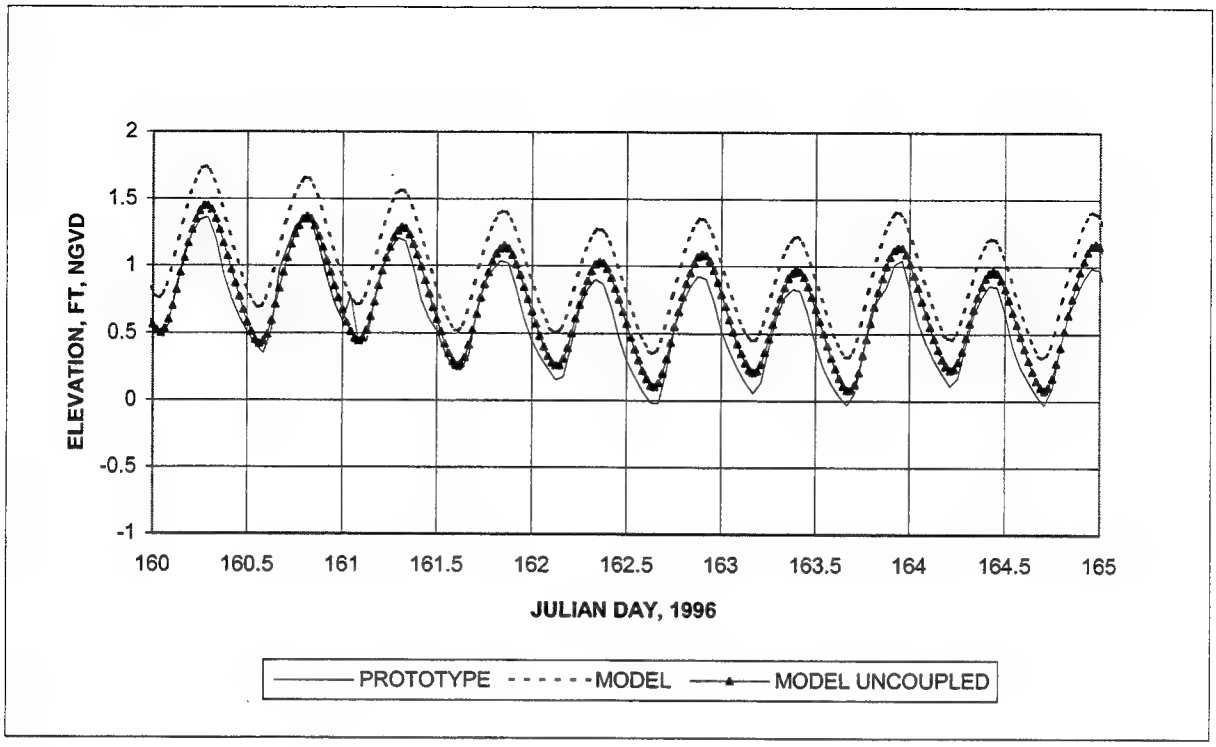

Figure 26. Effect of uncoupling hydrodynamic and salinity computations on water surface elevation at Shands Bridge (To convert elevation to meters, multiply by 0.3048)

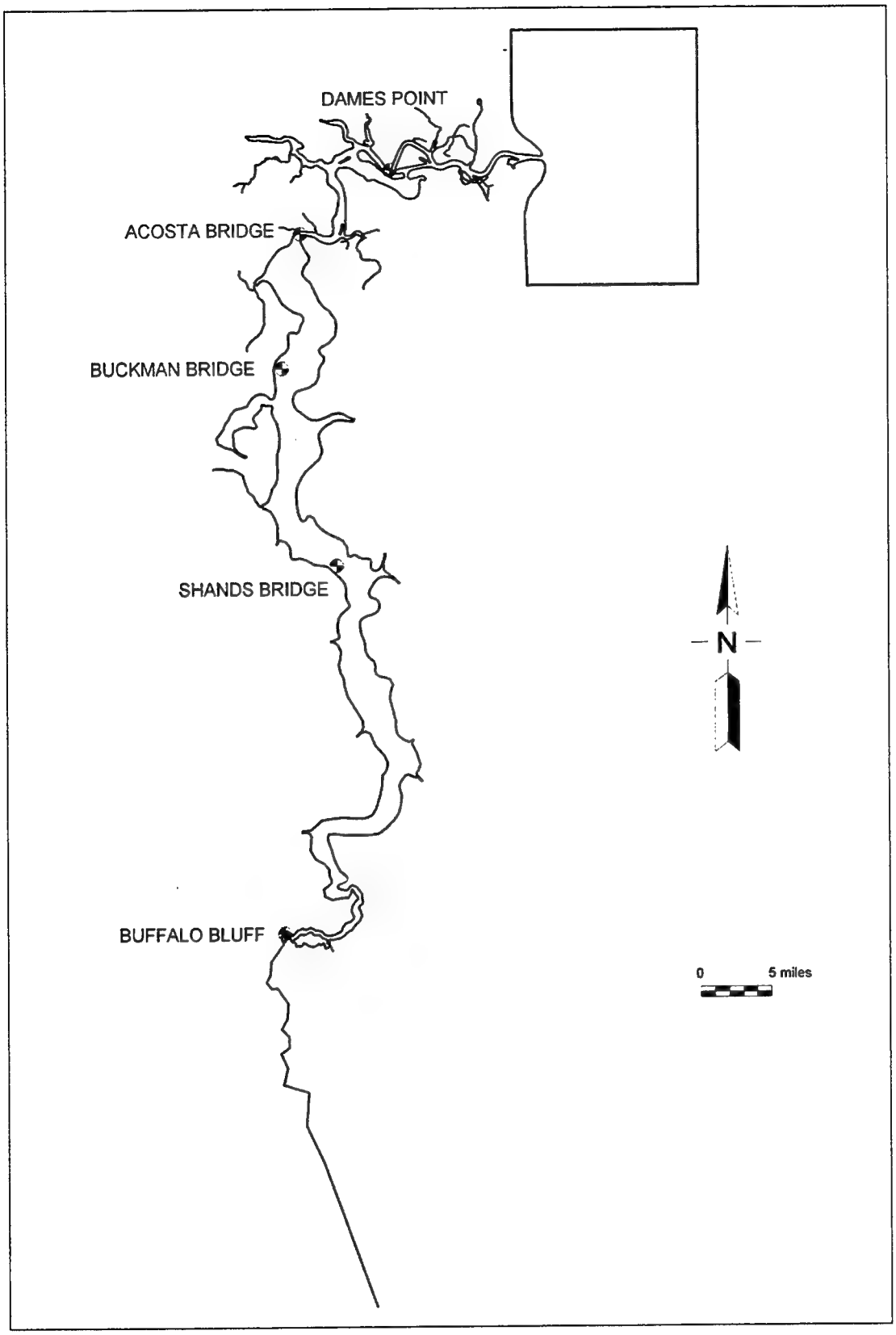

Figure 27. LSJRE salinity stations

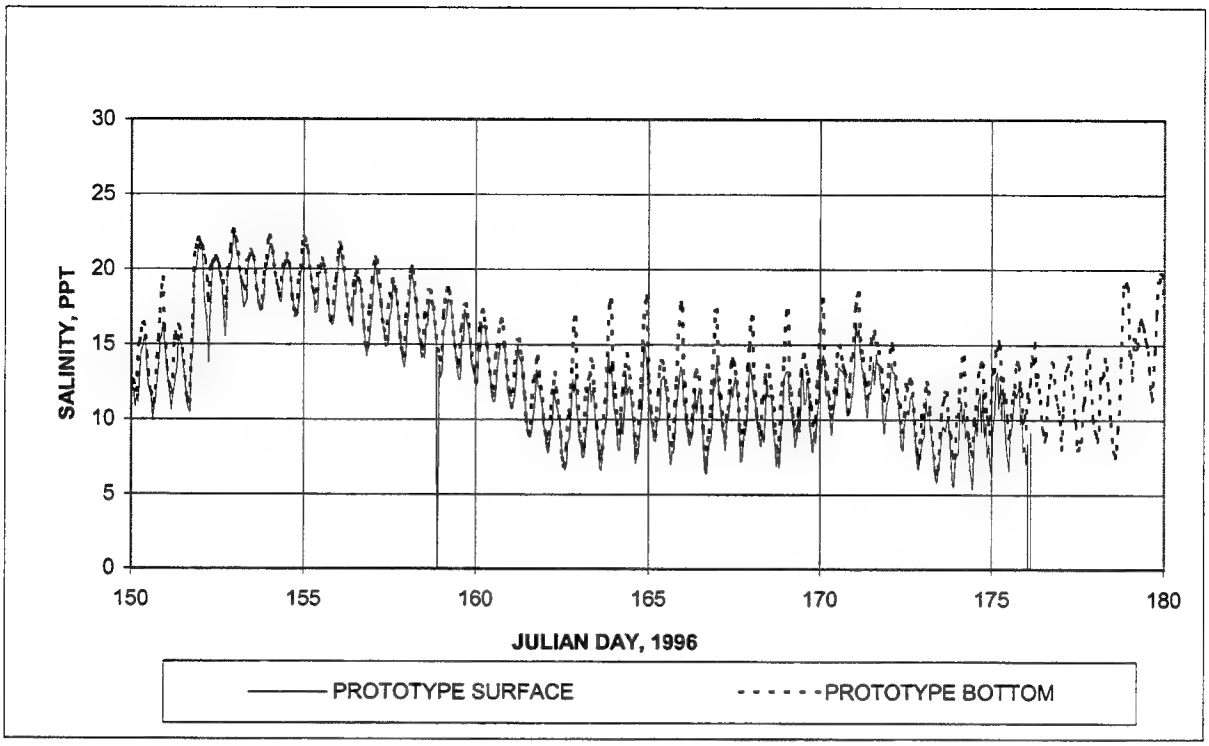

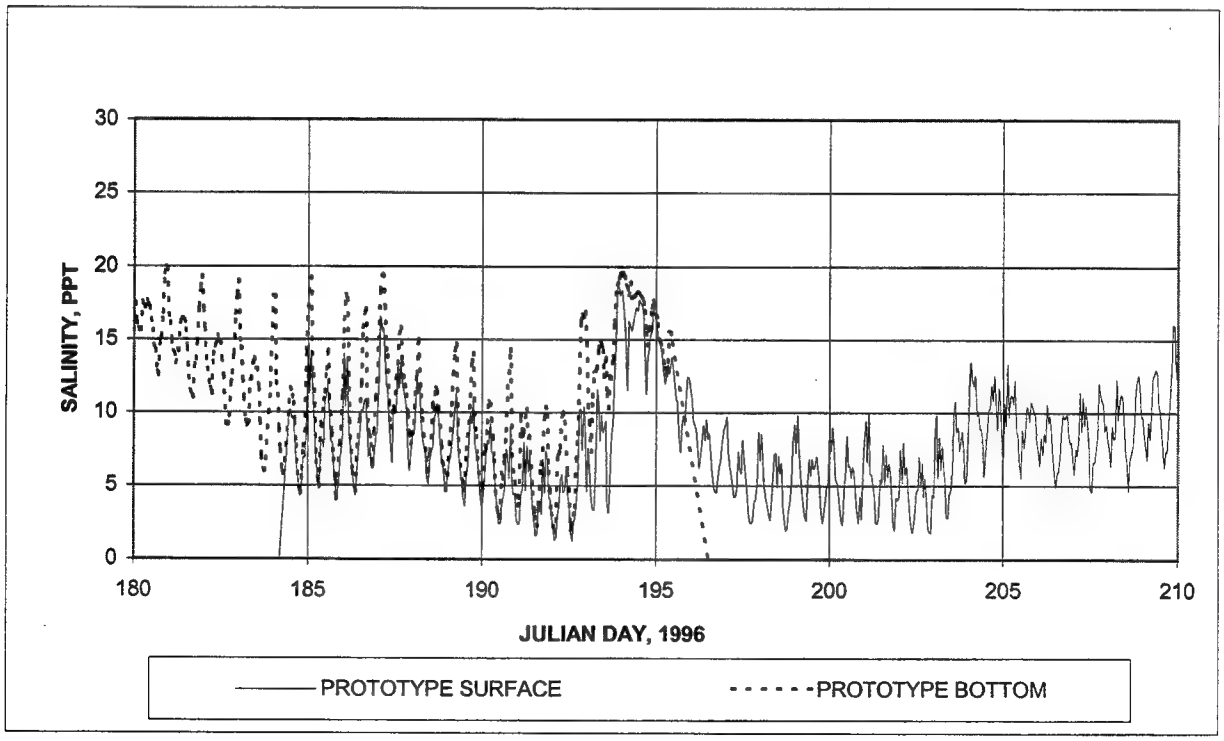

Figure 28. Prototype salinity at Dames Point (Continued)

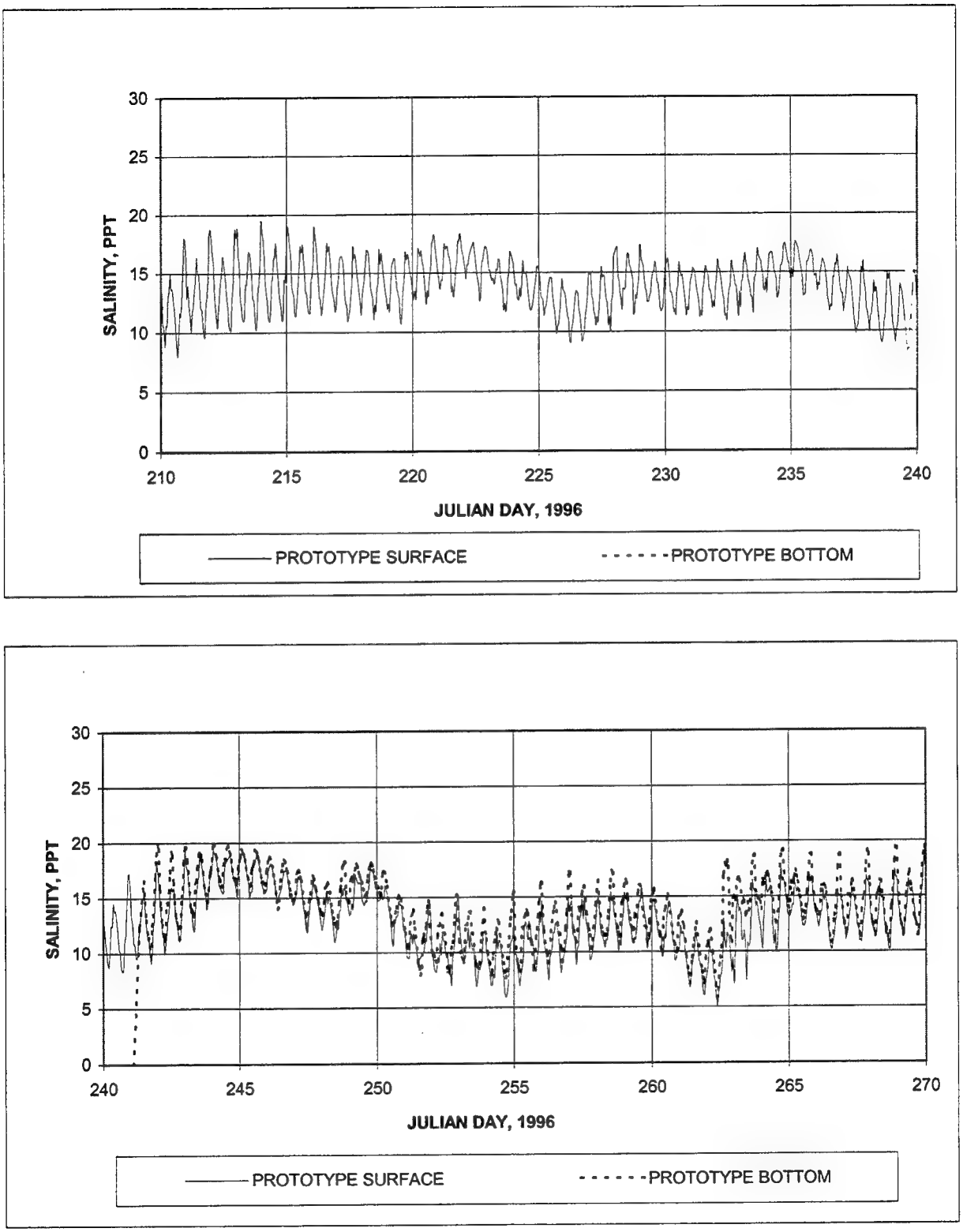

Figure 28. (Concluded)

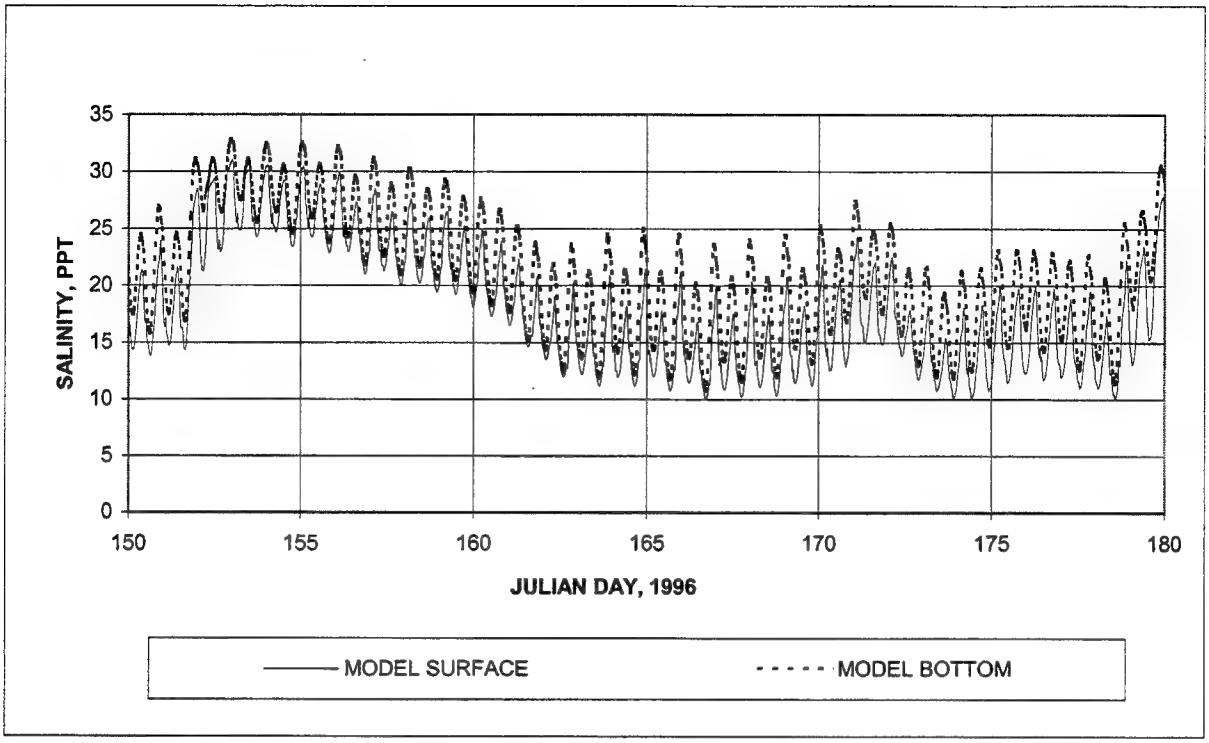

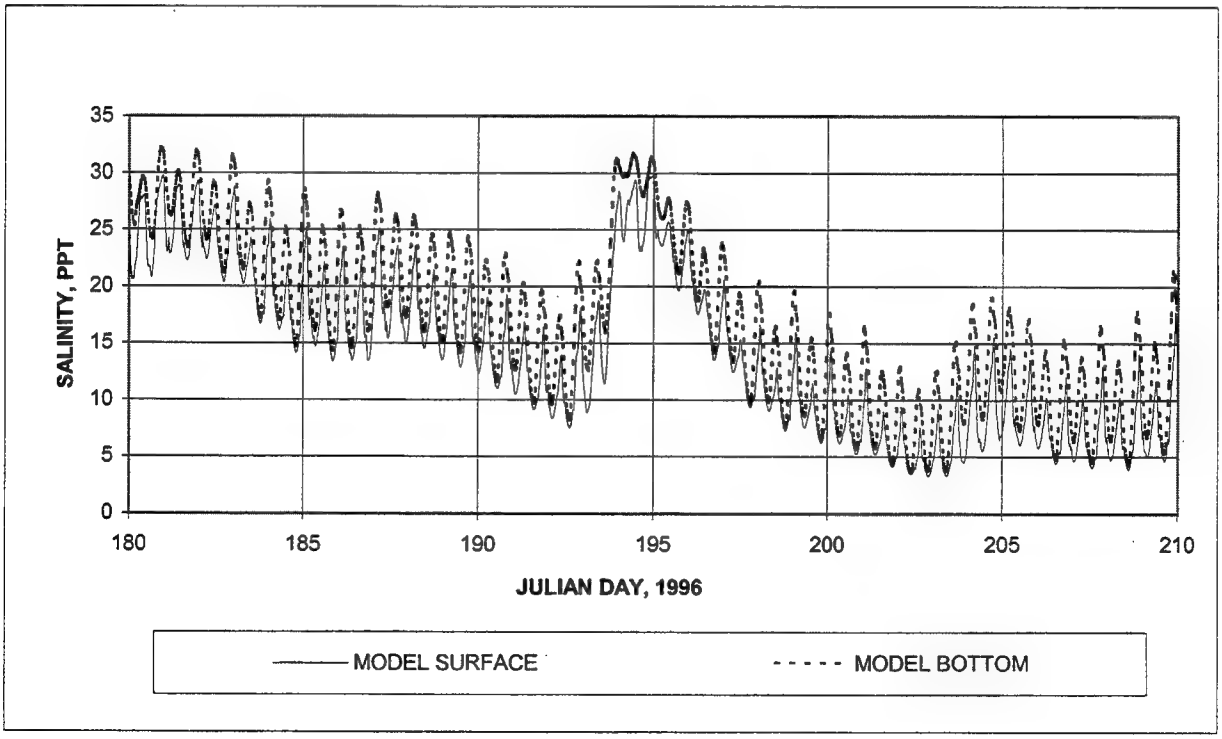

Figure 29. Model salinity at Dames Point (Continued)

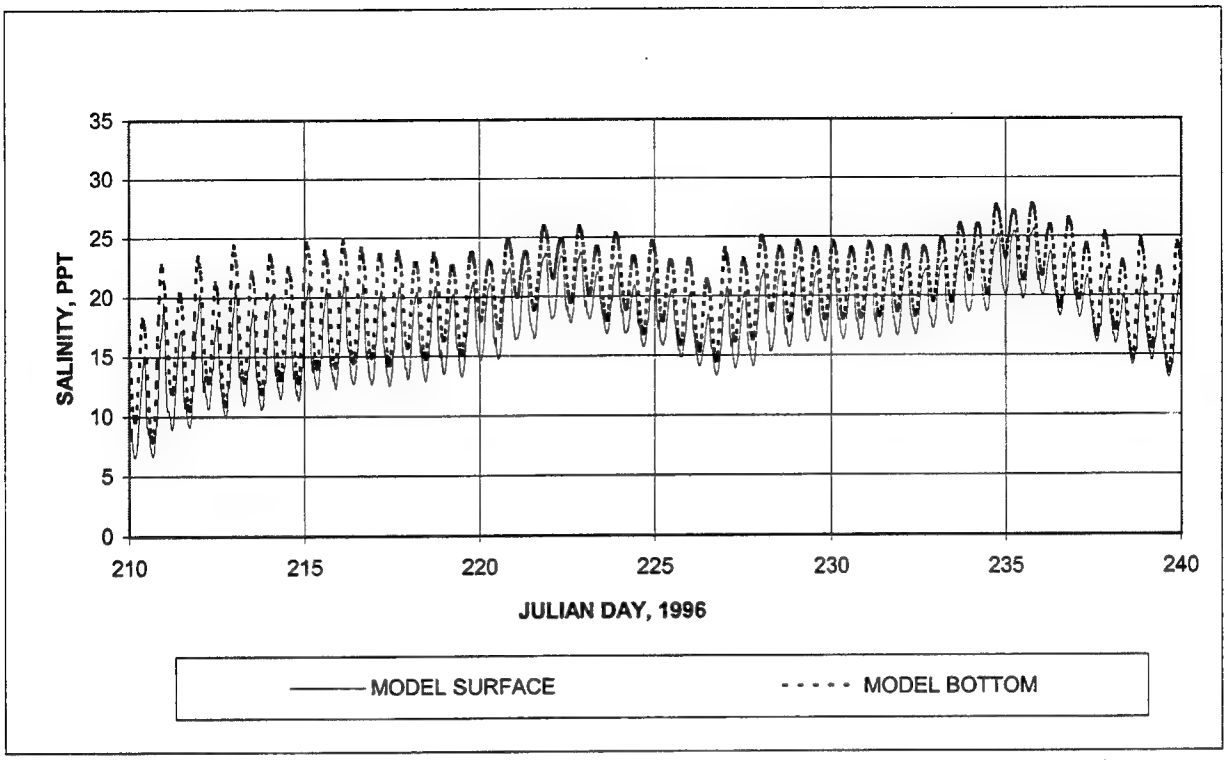

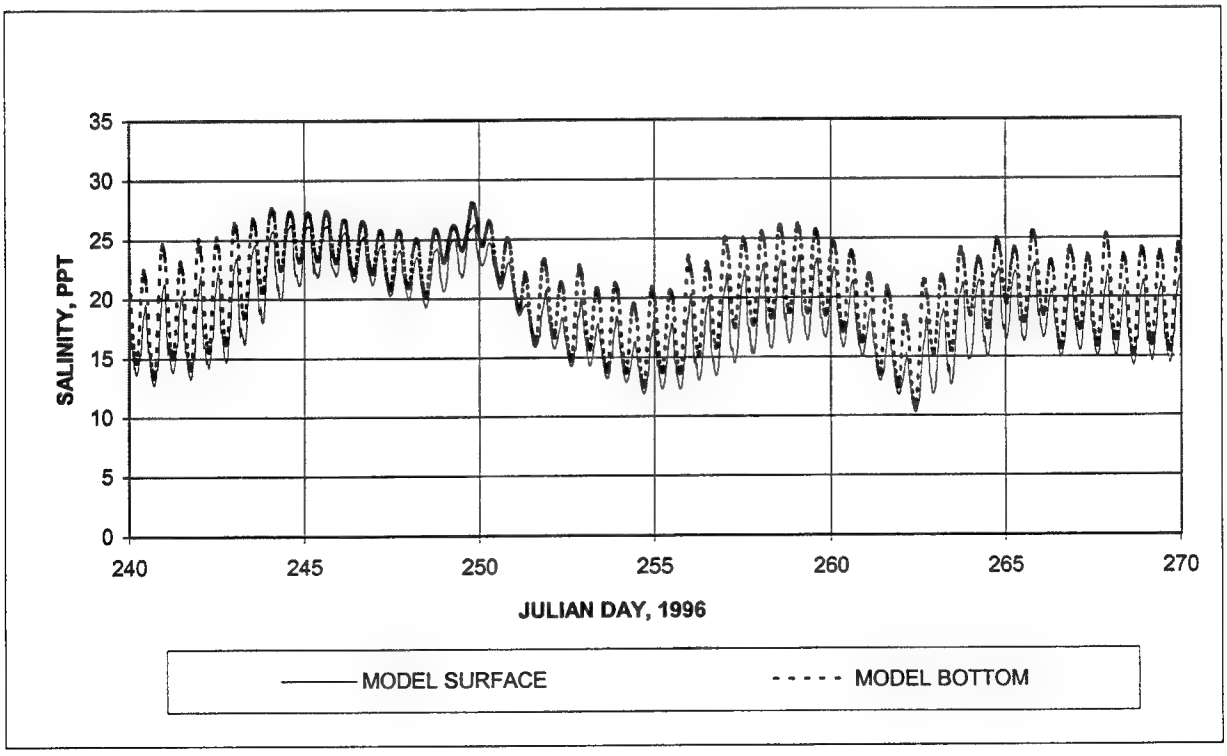

Figure 29. (Concluded)

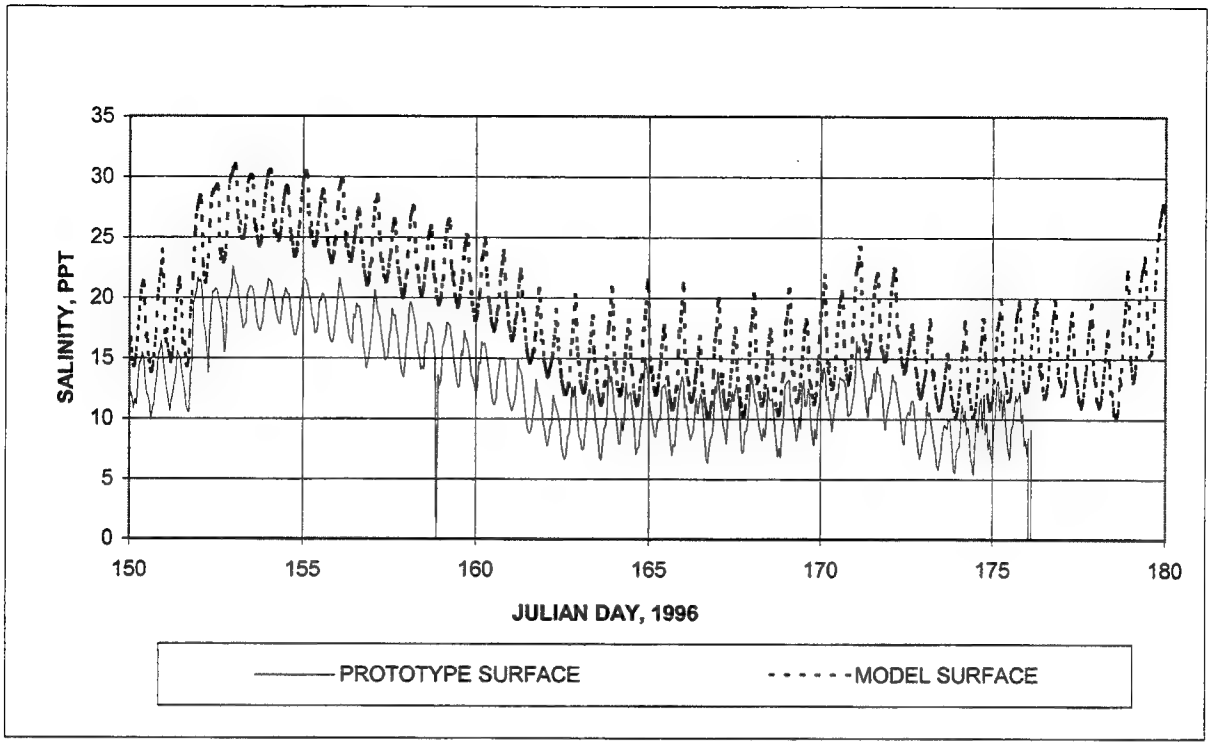

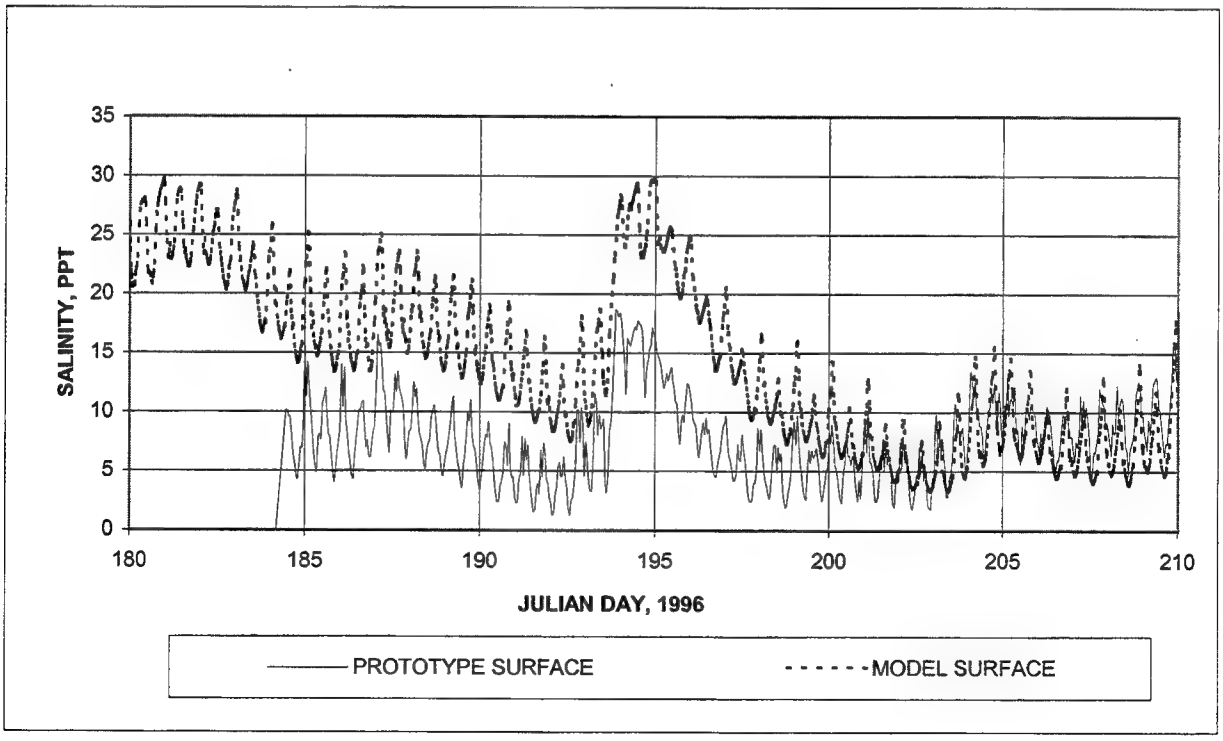

Figure 30. Surface salinity at Dames Point (Continued)

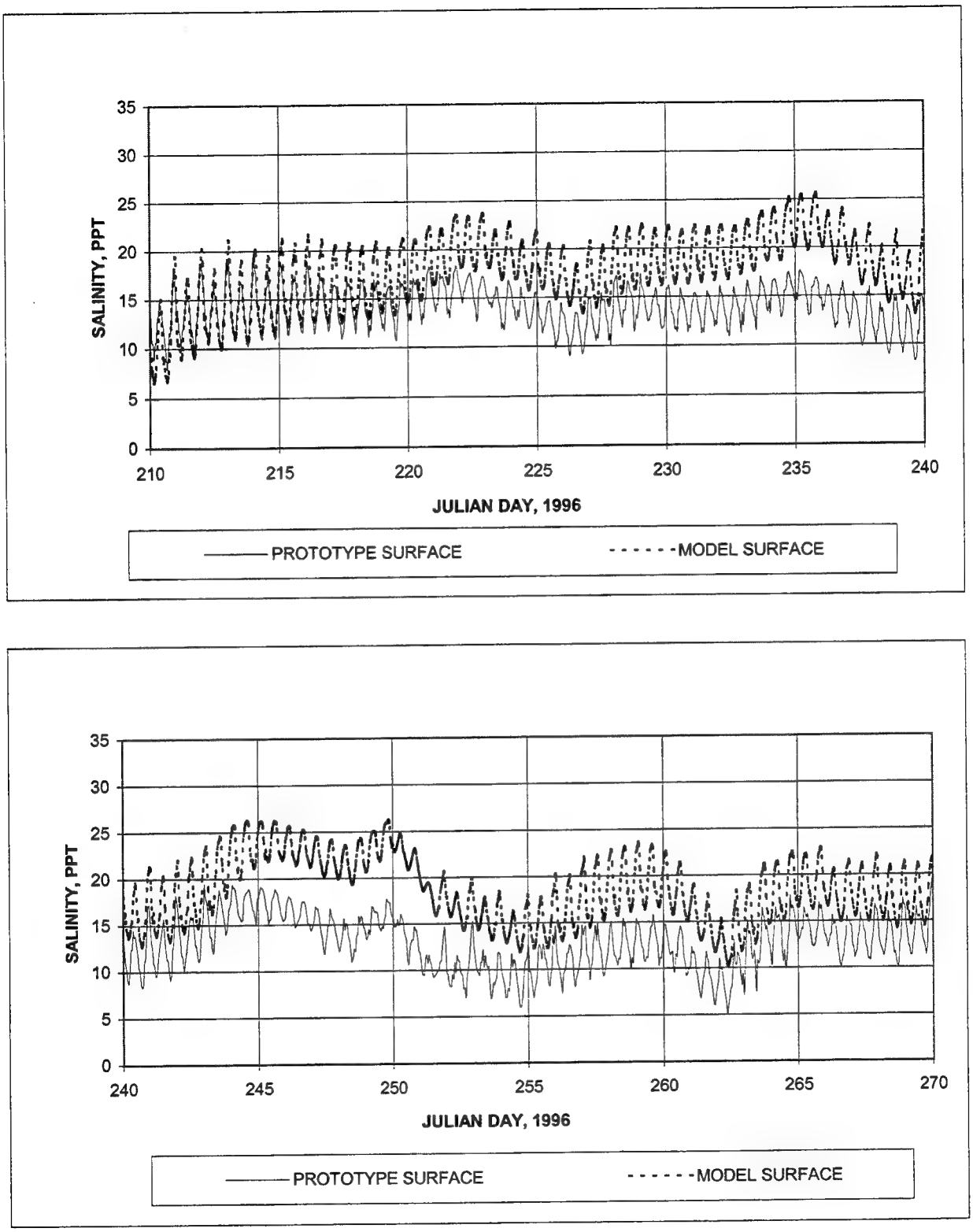

Figure 30. (Concluded)

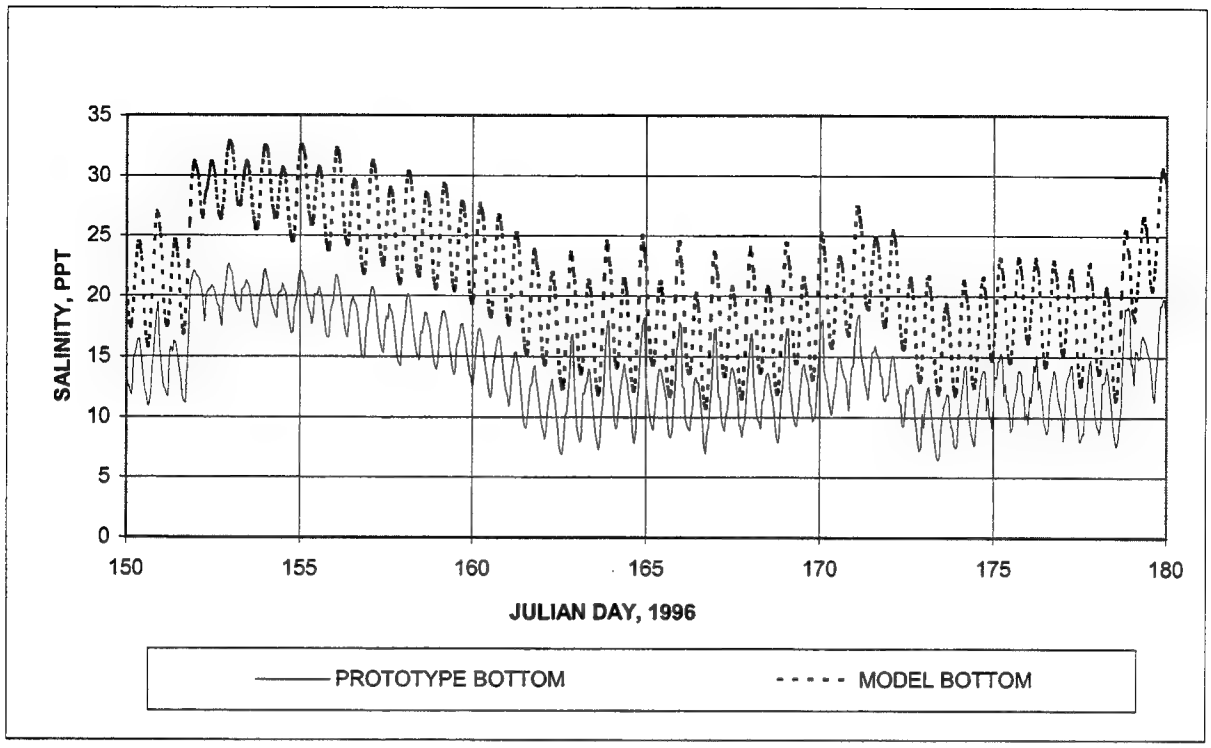

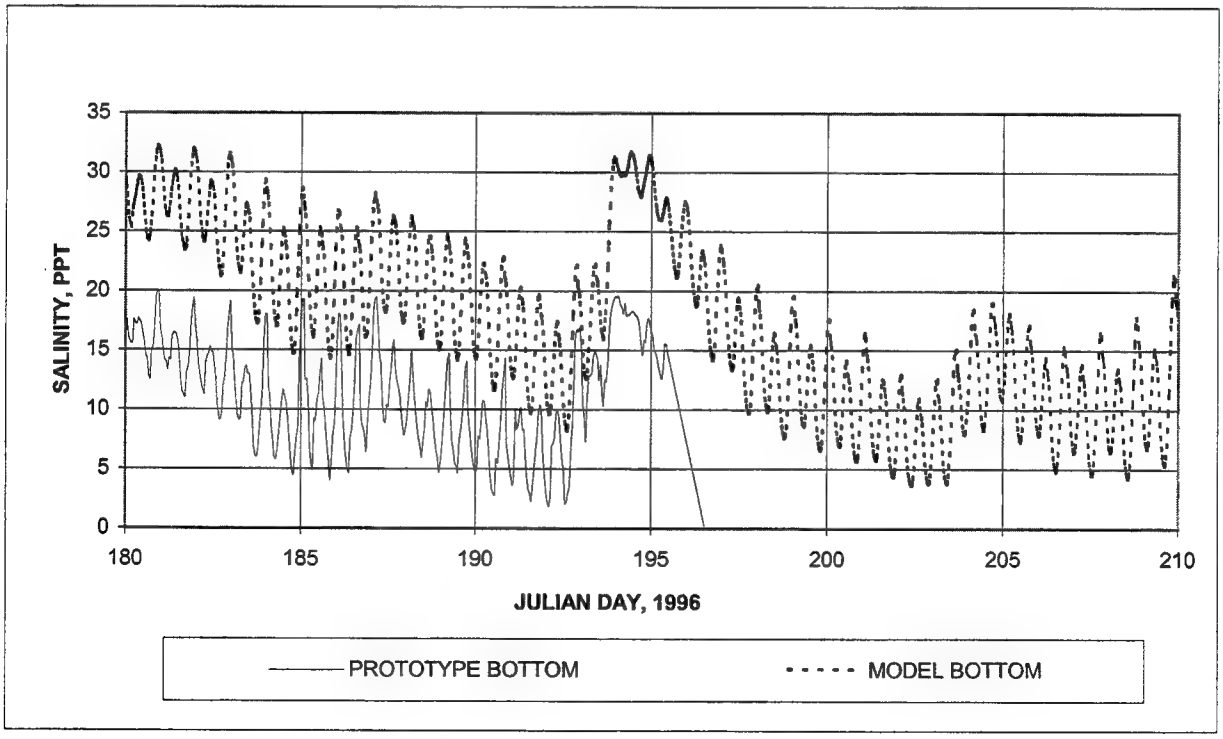

Figure 31. Bottom salinity at Dames Point (Continued)

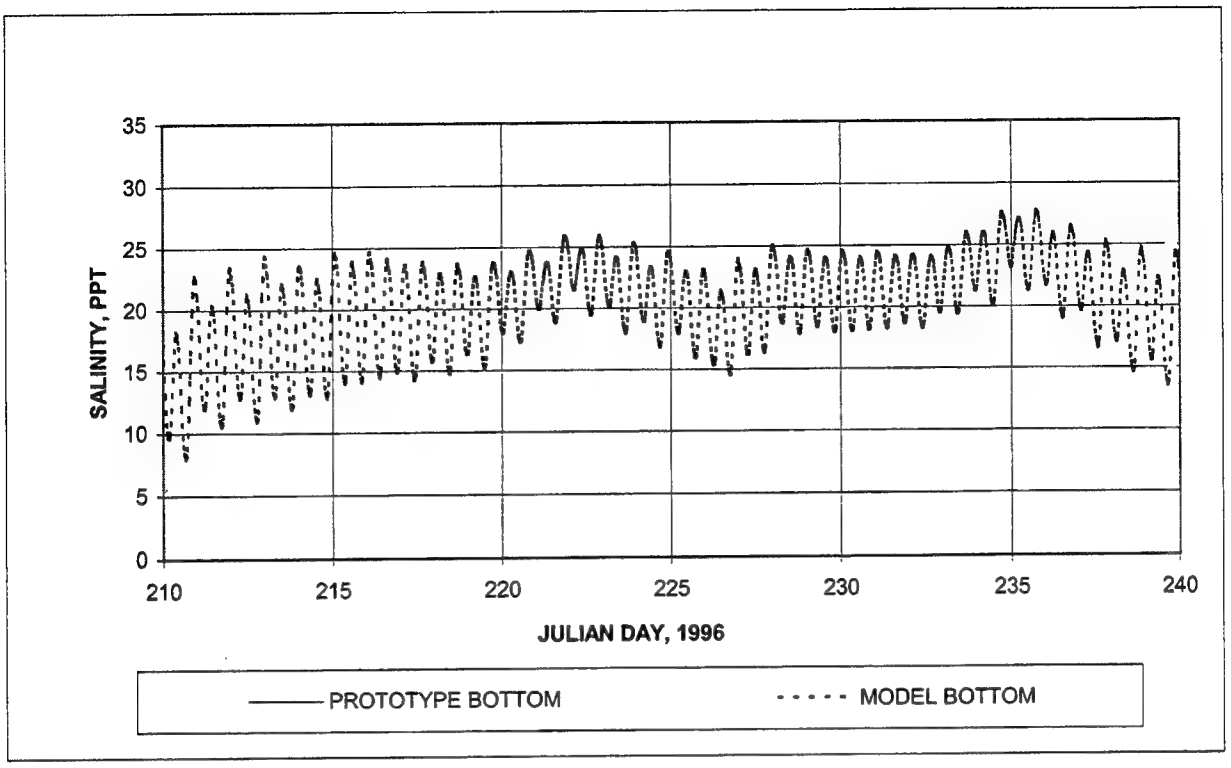

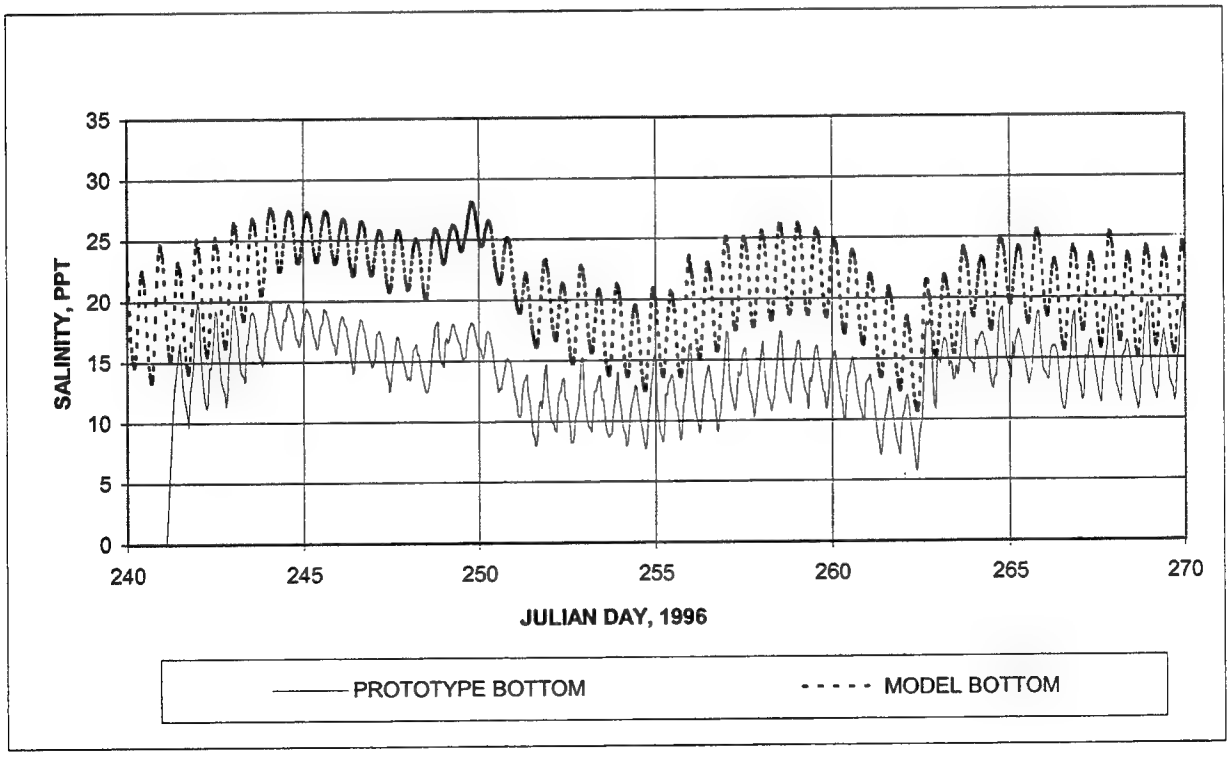

Figure 31. (Concluded)

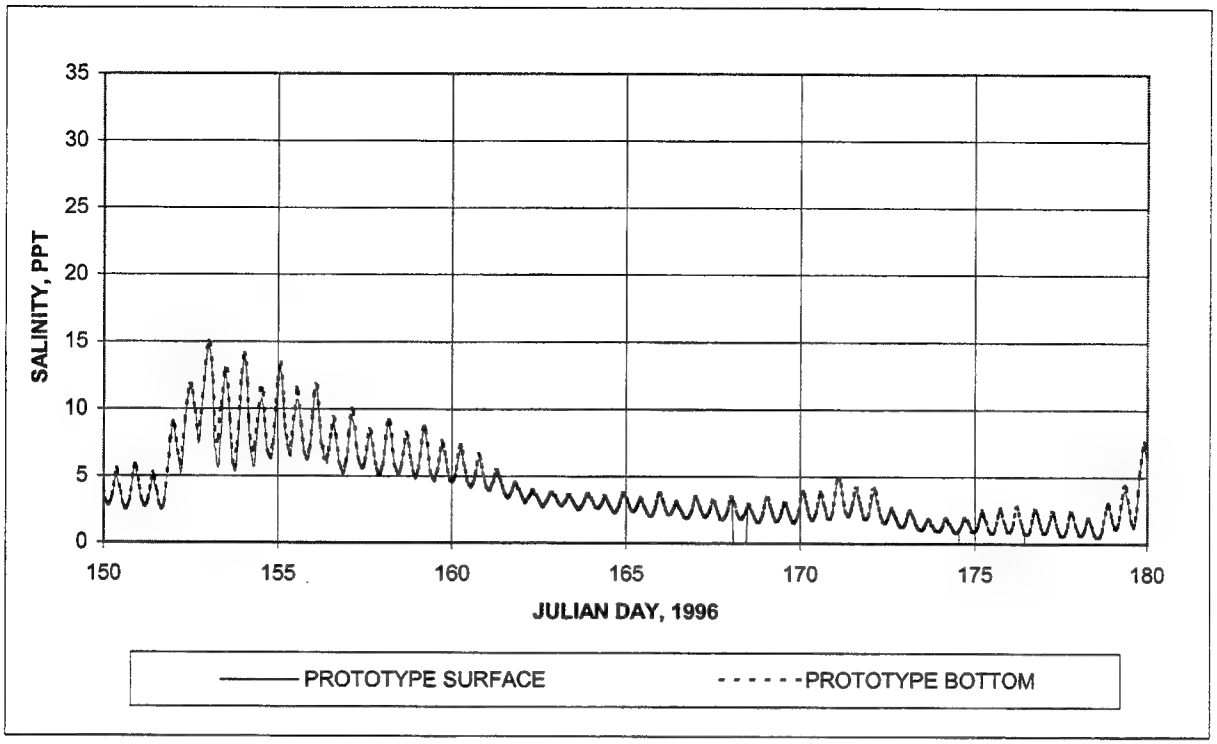

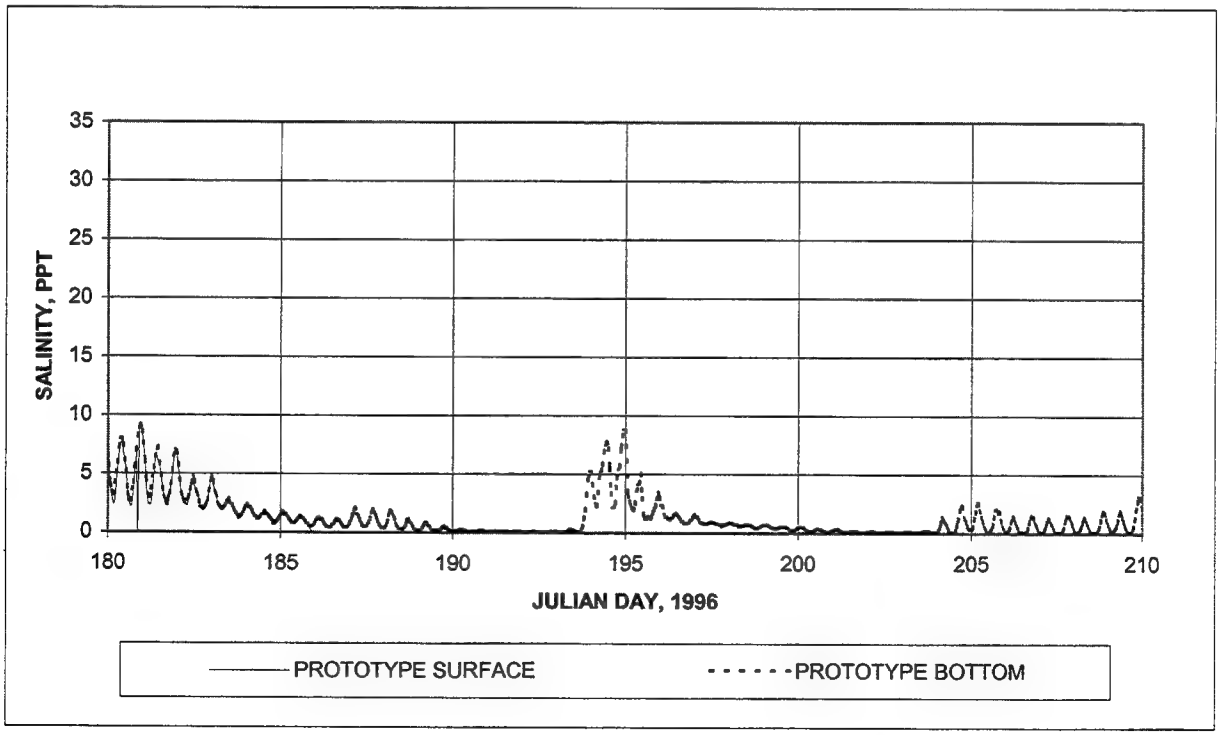

Figure 32. Prototype salinity at Acosta Bridge (Continued)

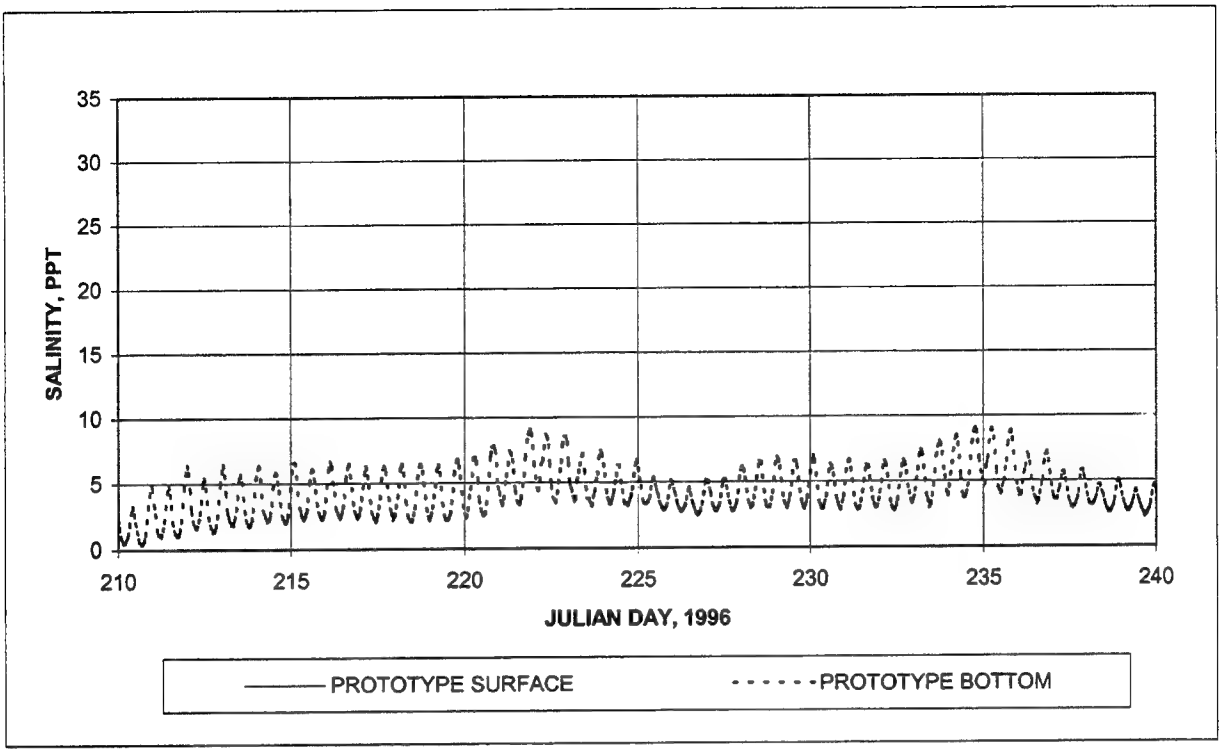

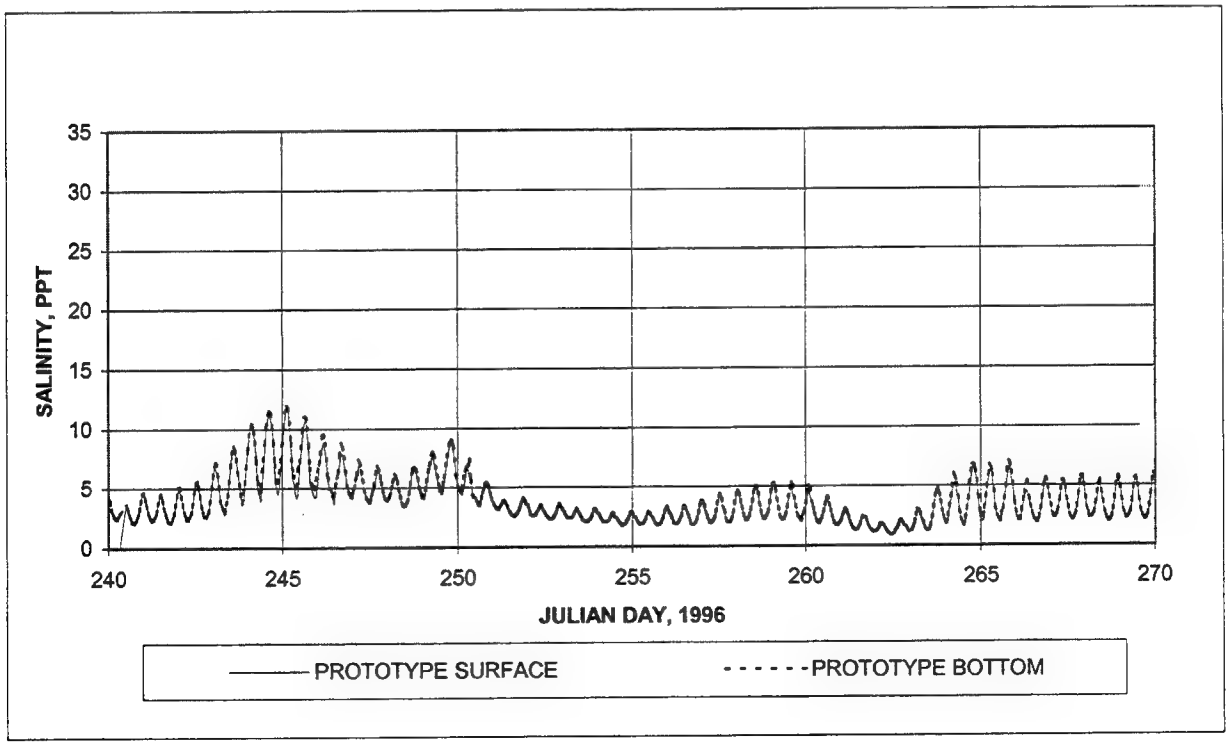

Figure 32. (Concluded)

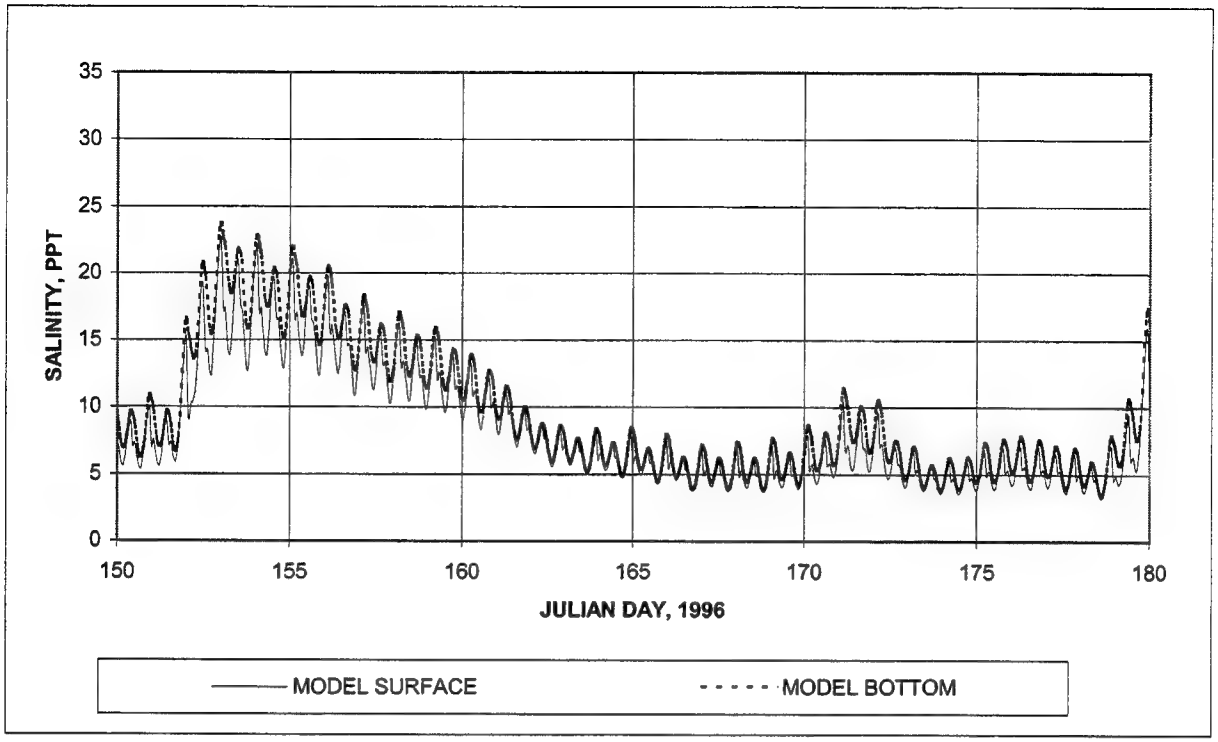

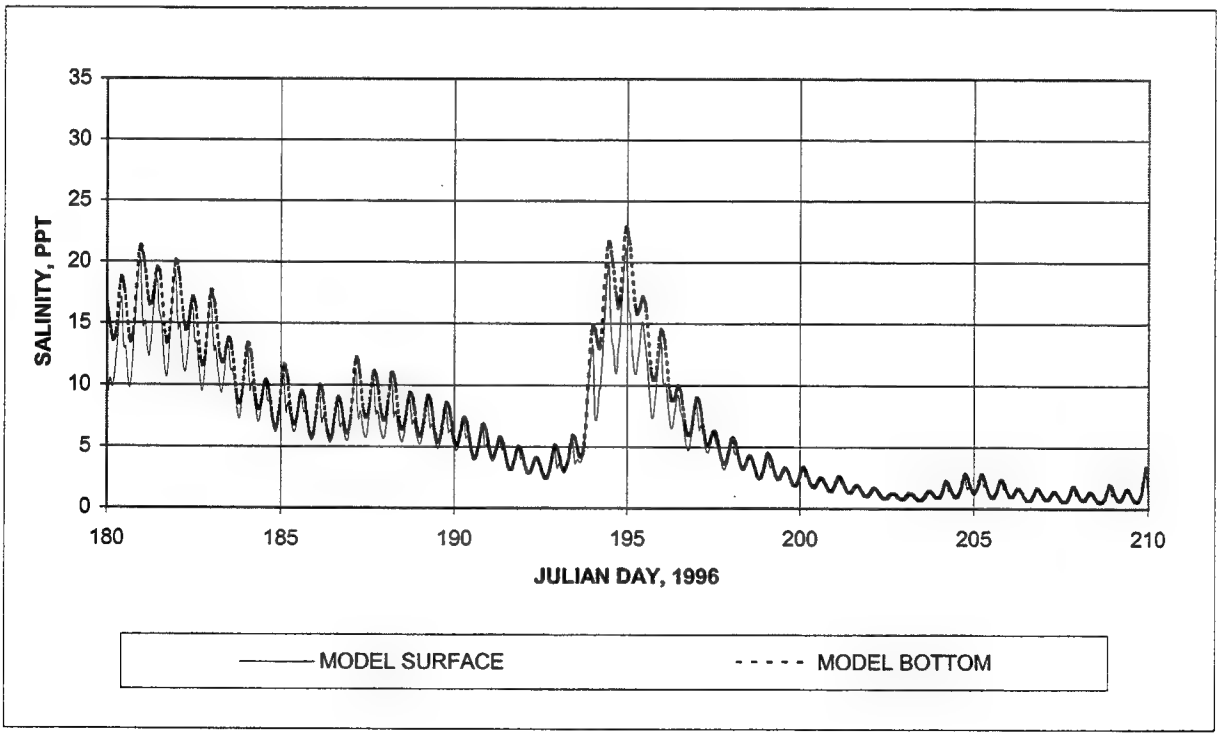

Figure 33. Model salinity at Acosta Bridge (Continued)

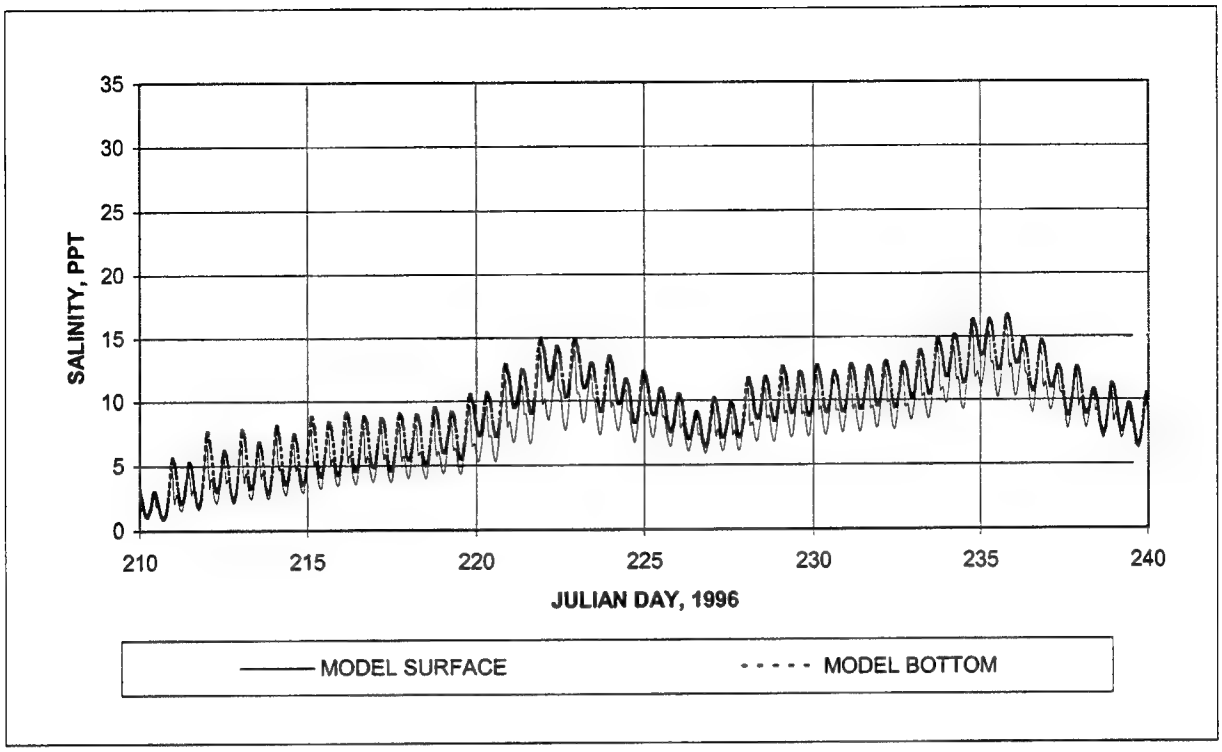

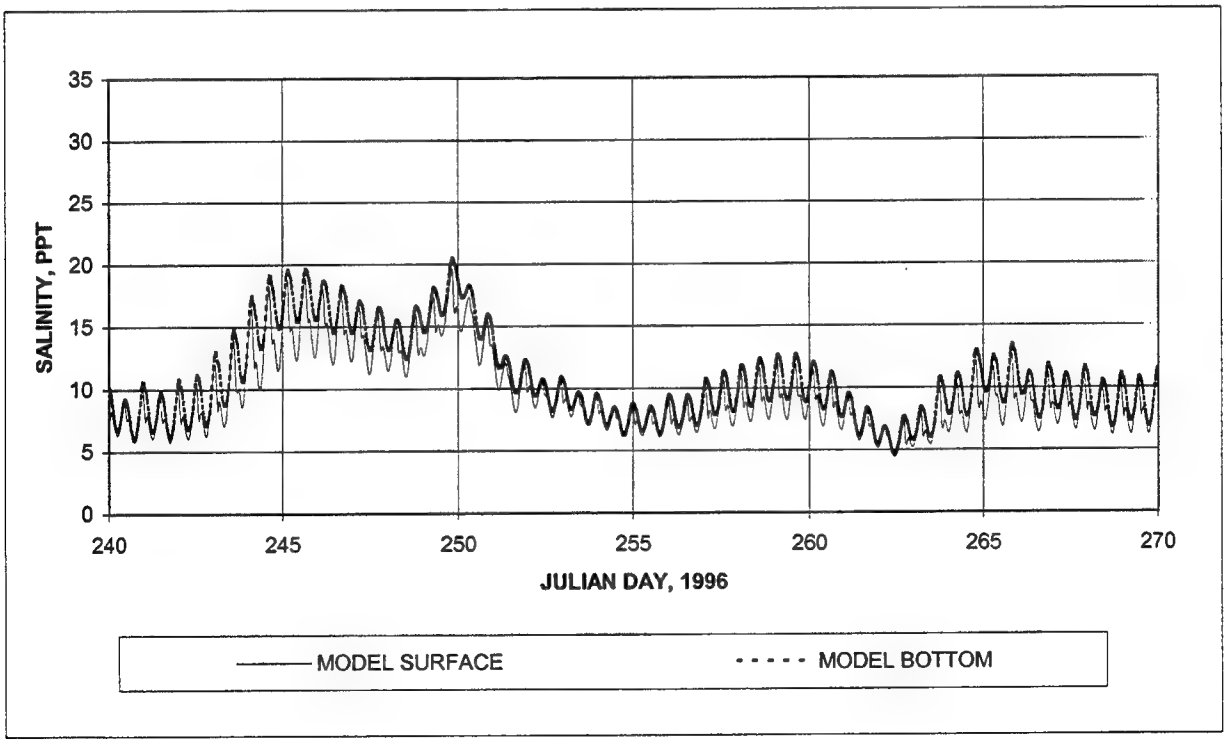

Figure 33. (Concluded)

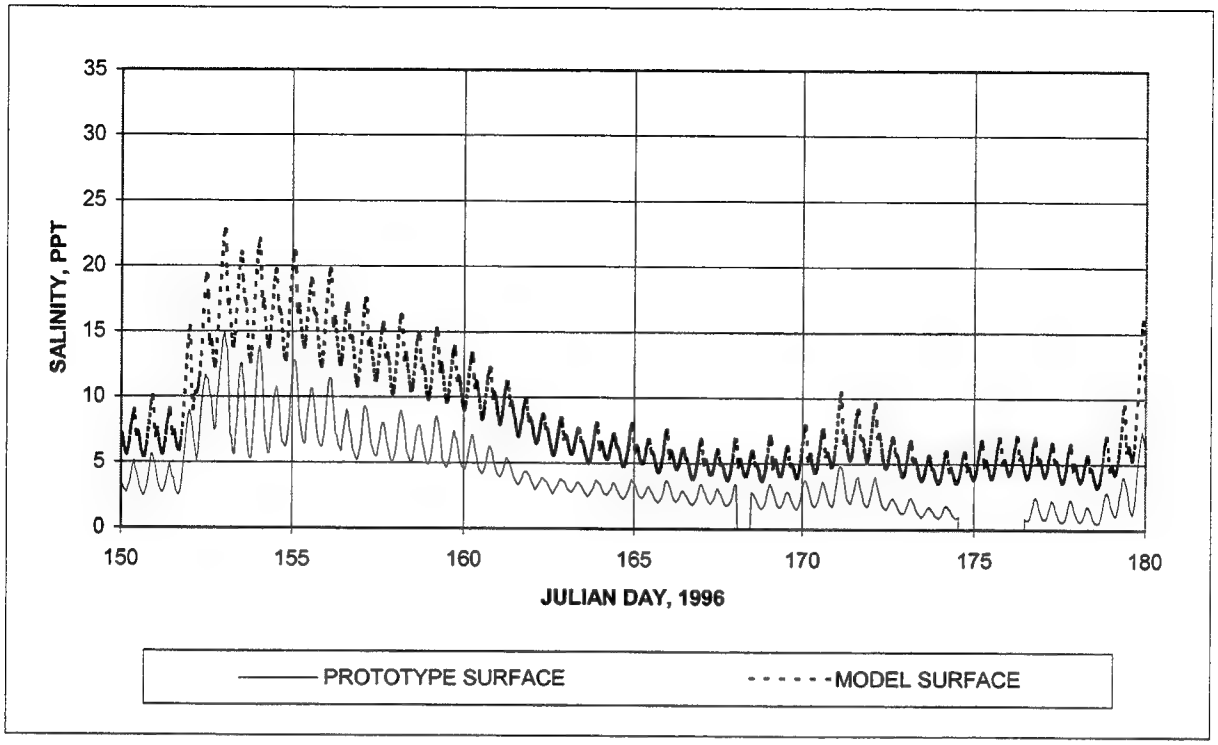

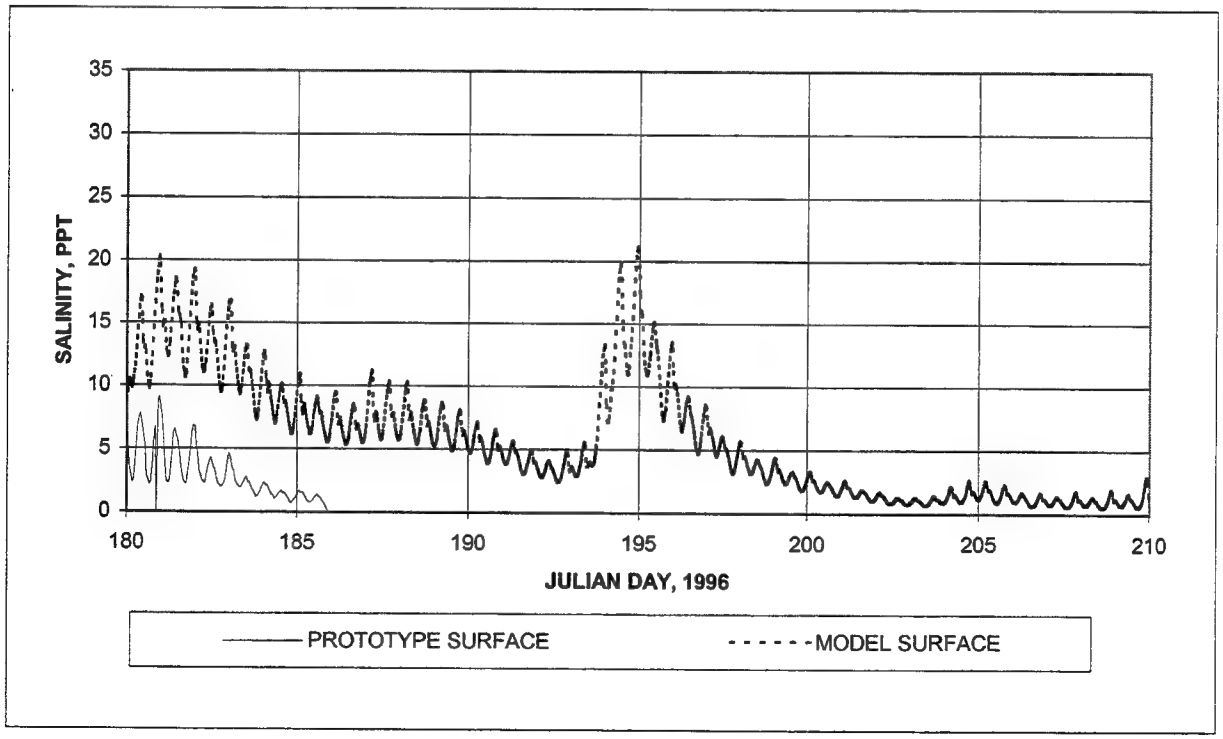

Figure 34. Surface salinity at Acosta Bridge (Continued)

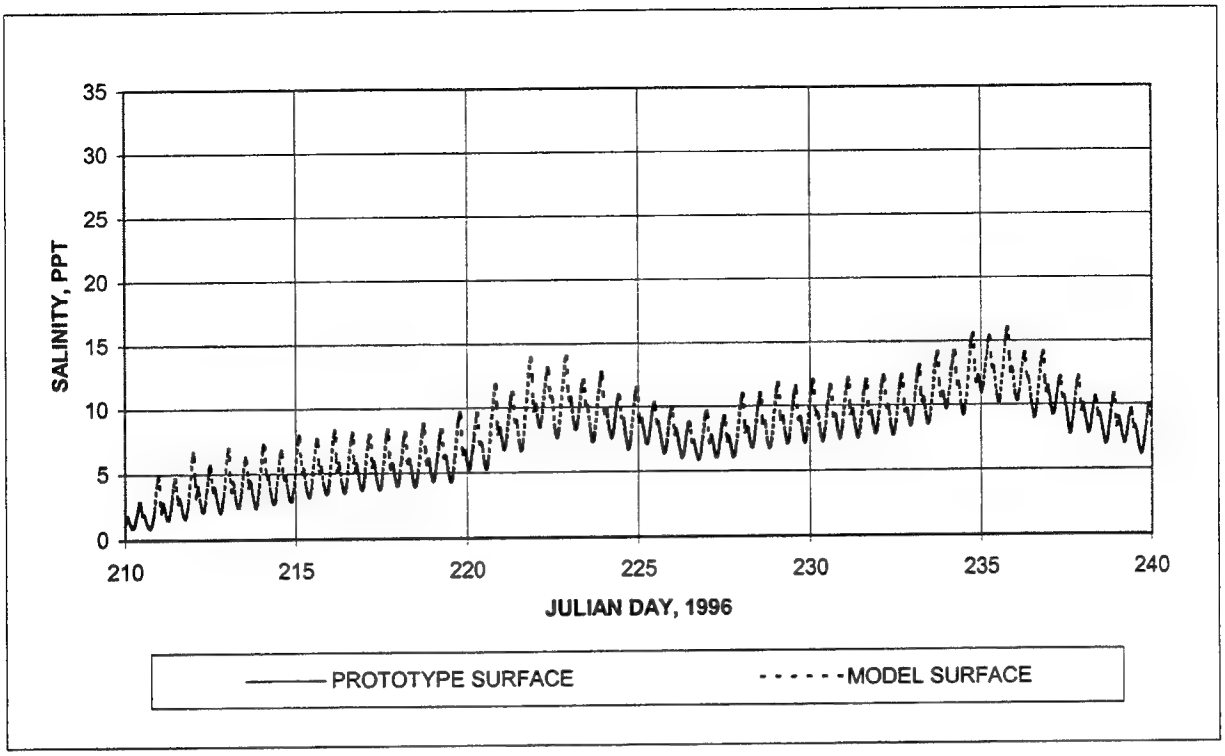

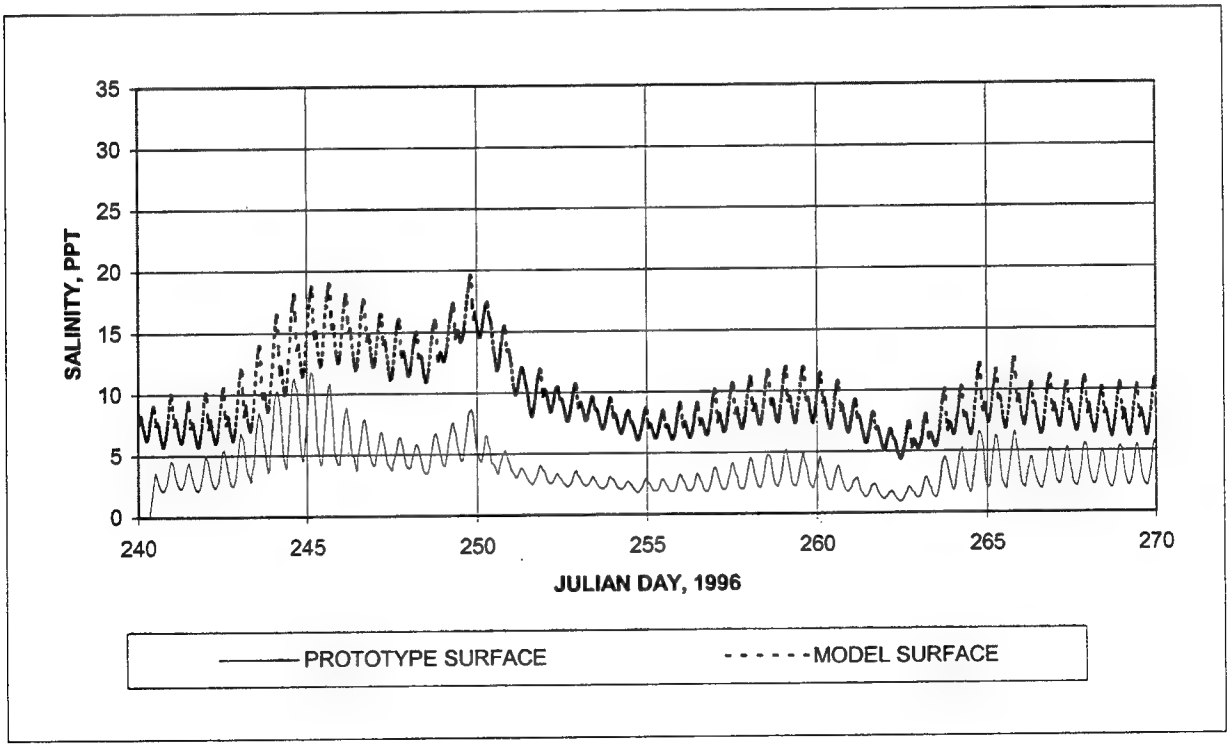

Figure 34. (Concluded)

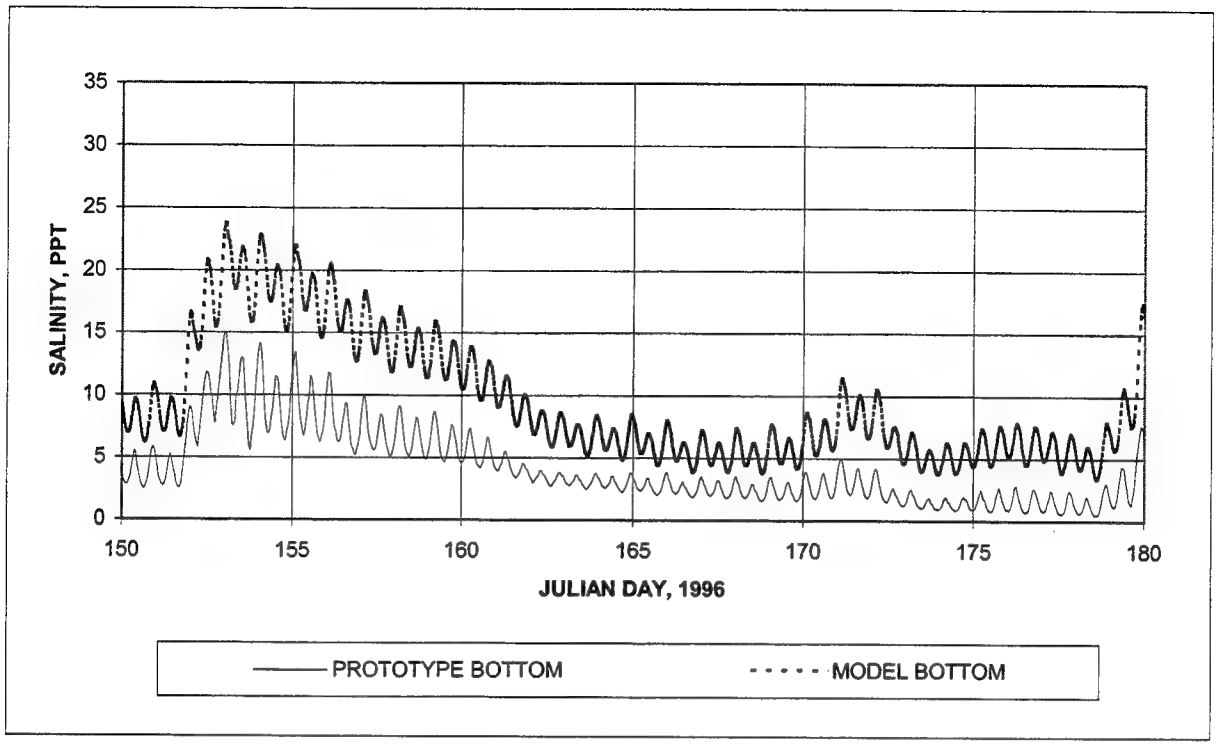

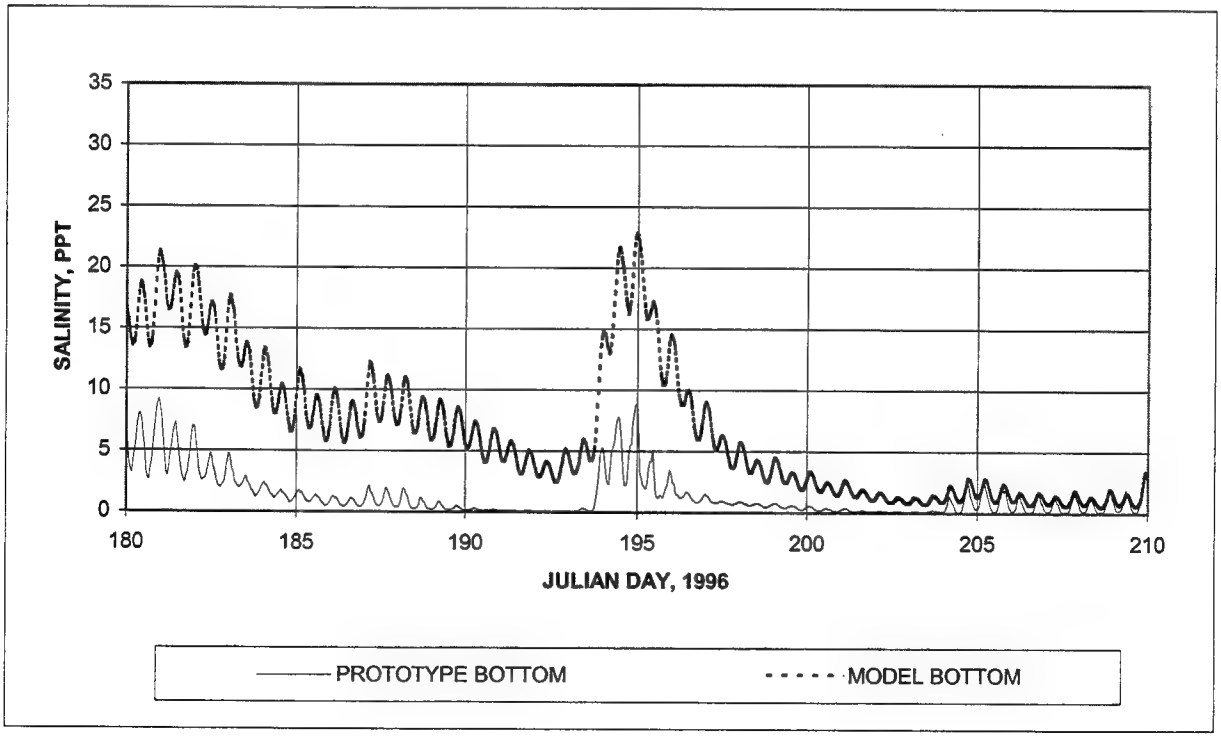

Figure 35. Bottom Salinity at Acosta Bridge (Continued)

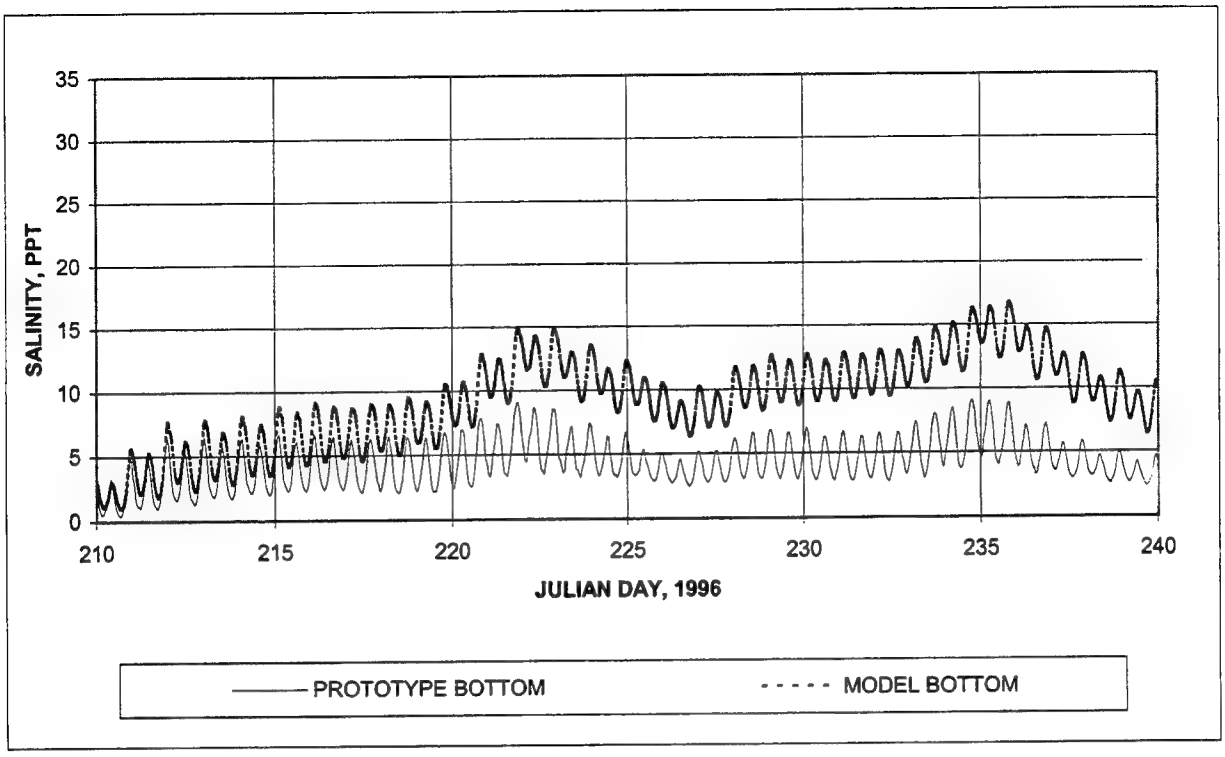

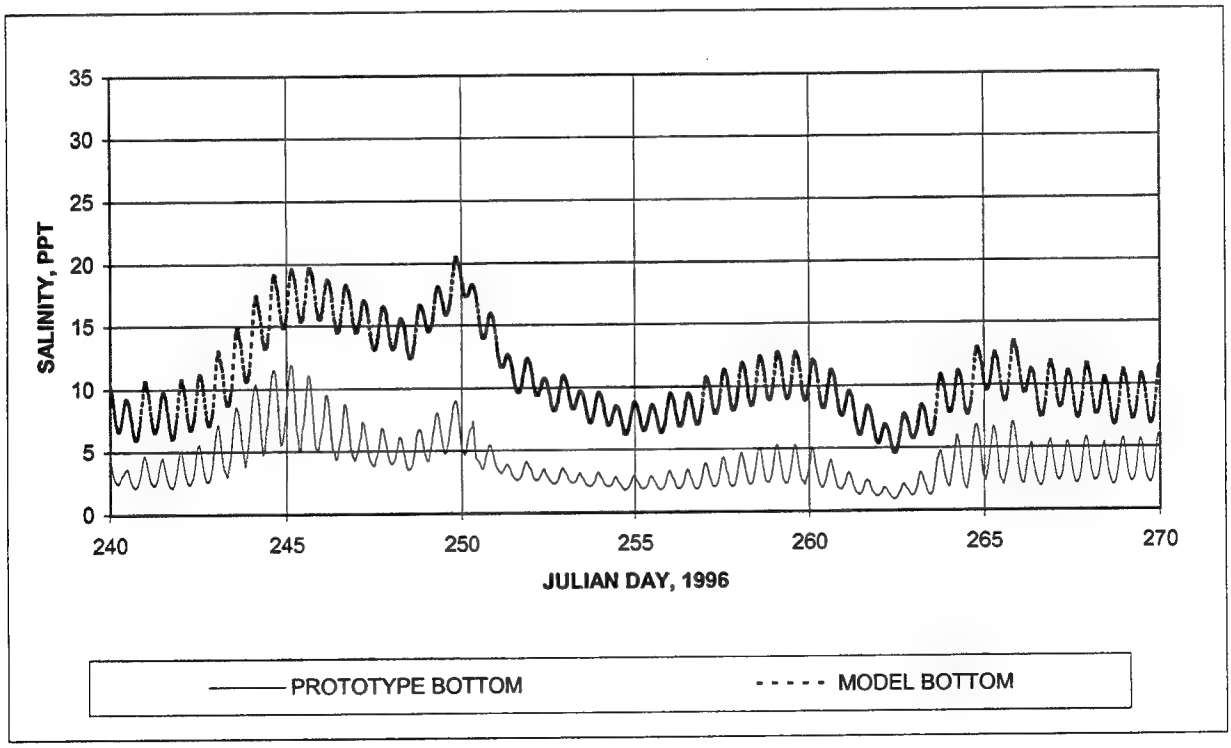

Figure 35. (Concluded)

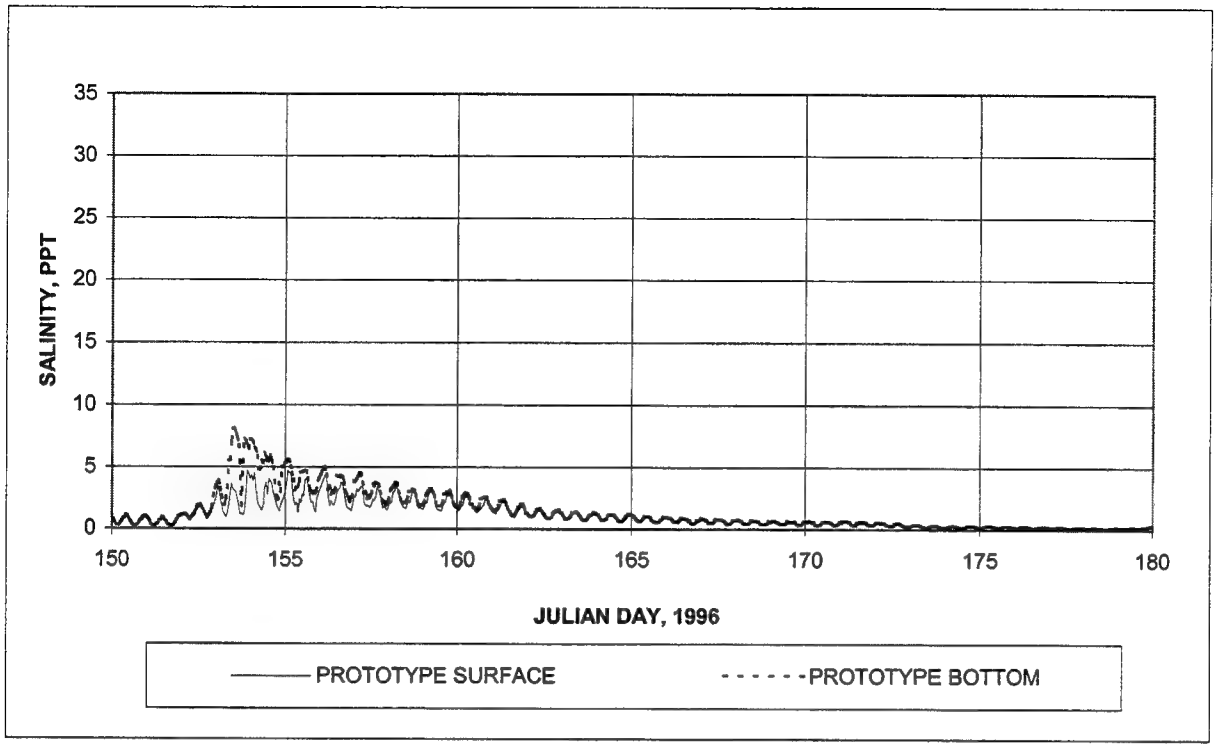

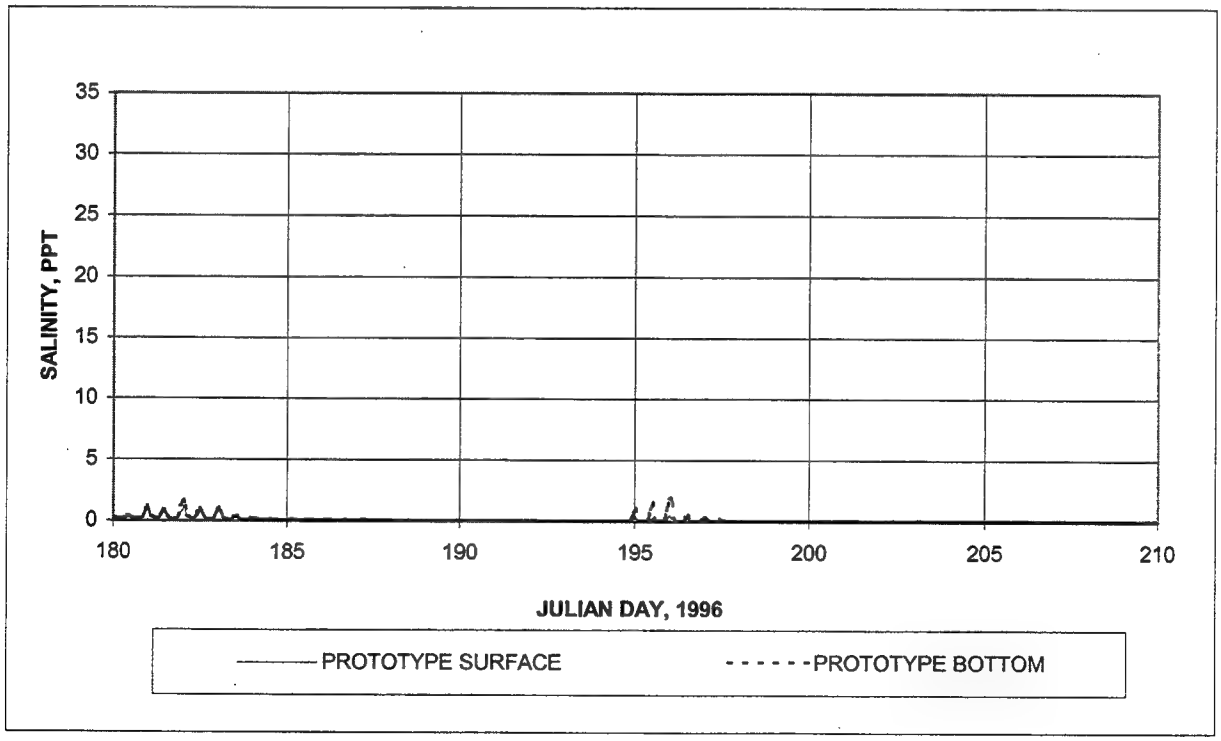

Figure 36. Prototype salinity at Buckman Bridge (Continued)

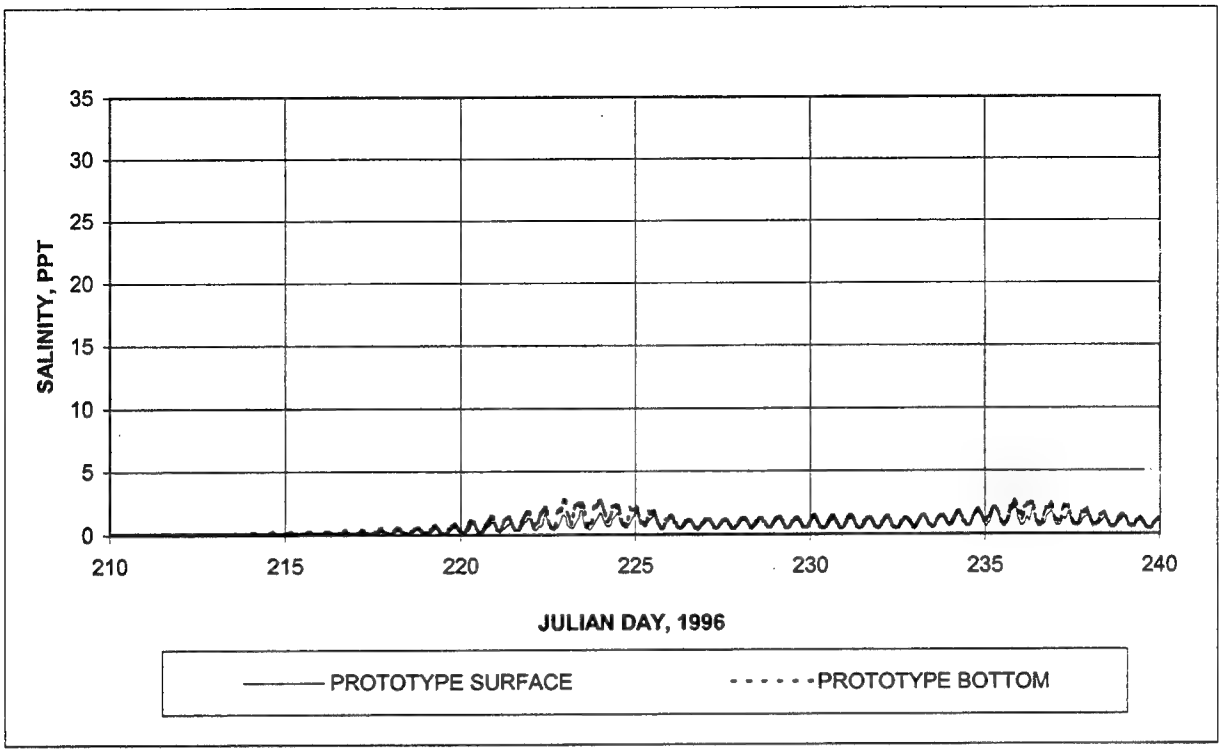

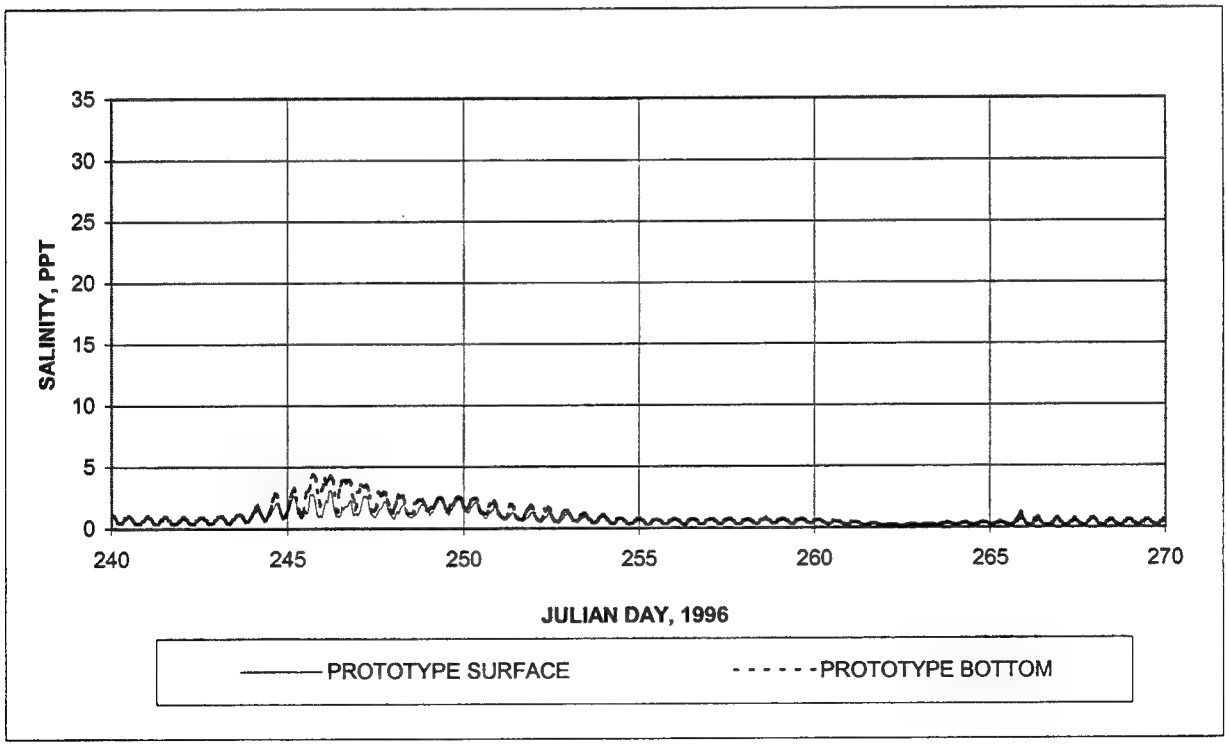

Figure 36. (Concluded)

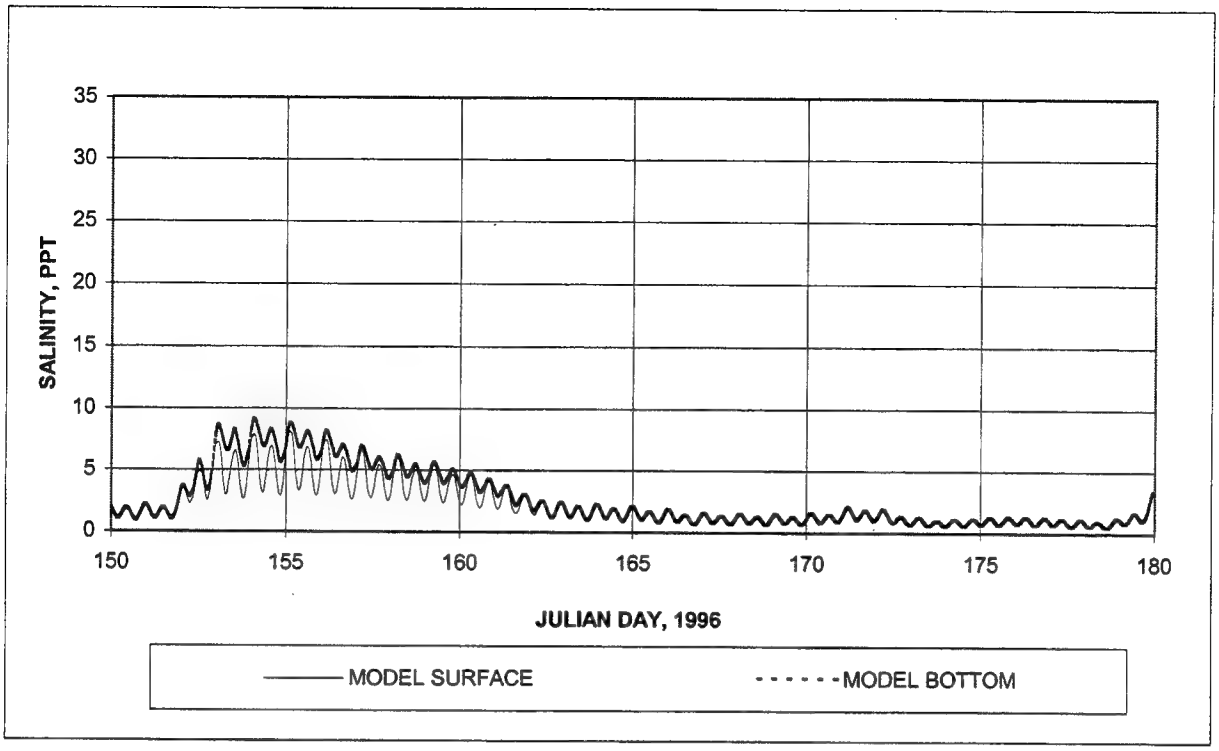

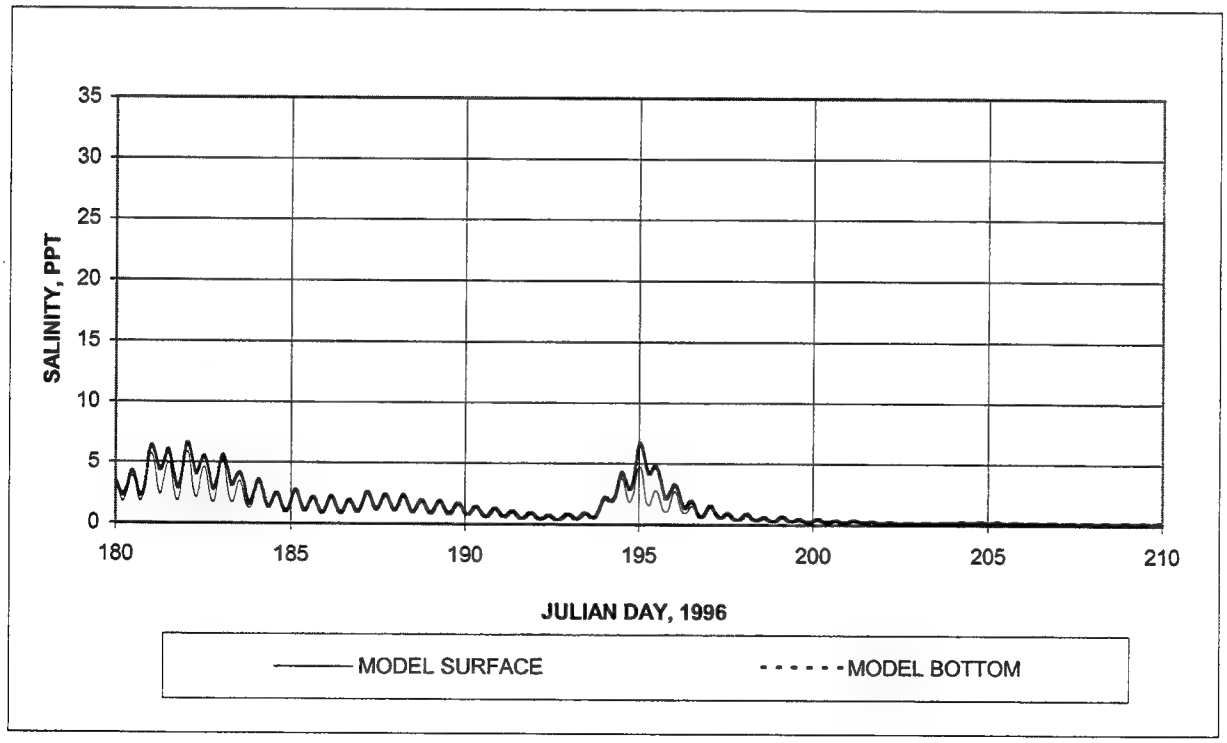

Figure 37. Model salinity at Buckman Bridge (Continued)

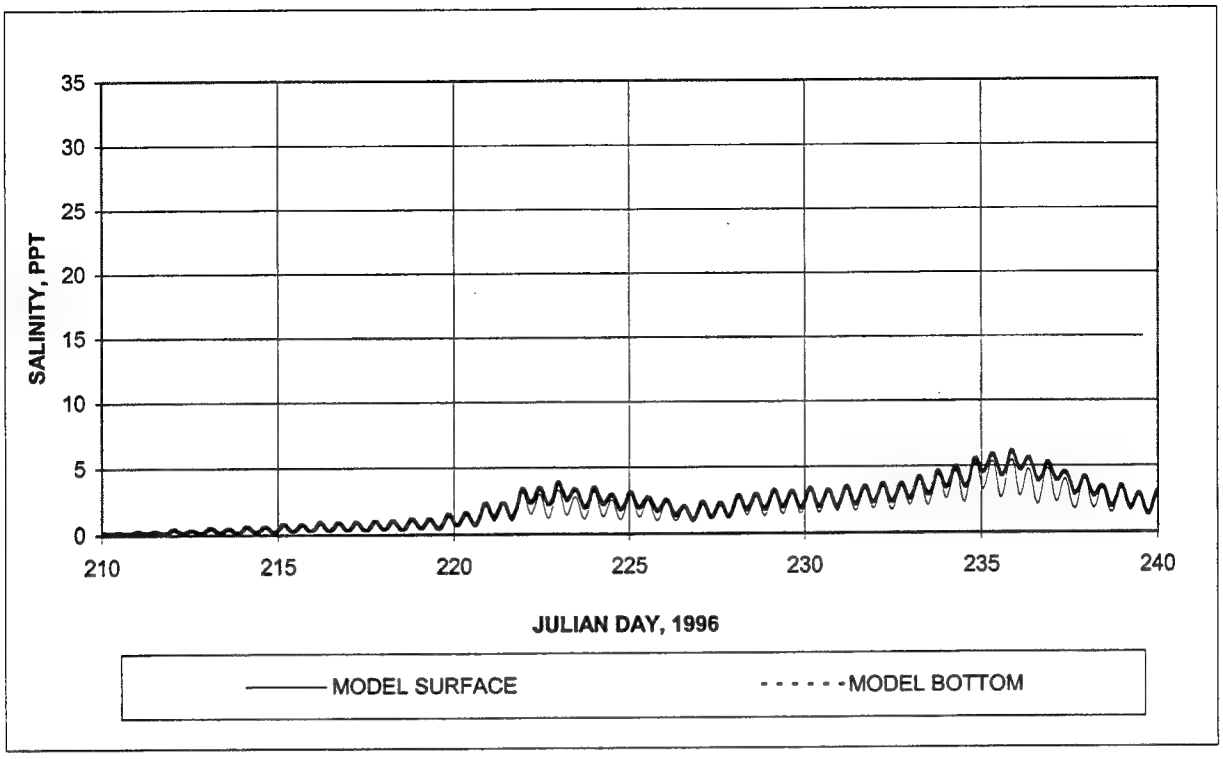

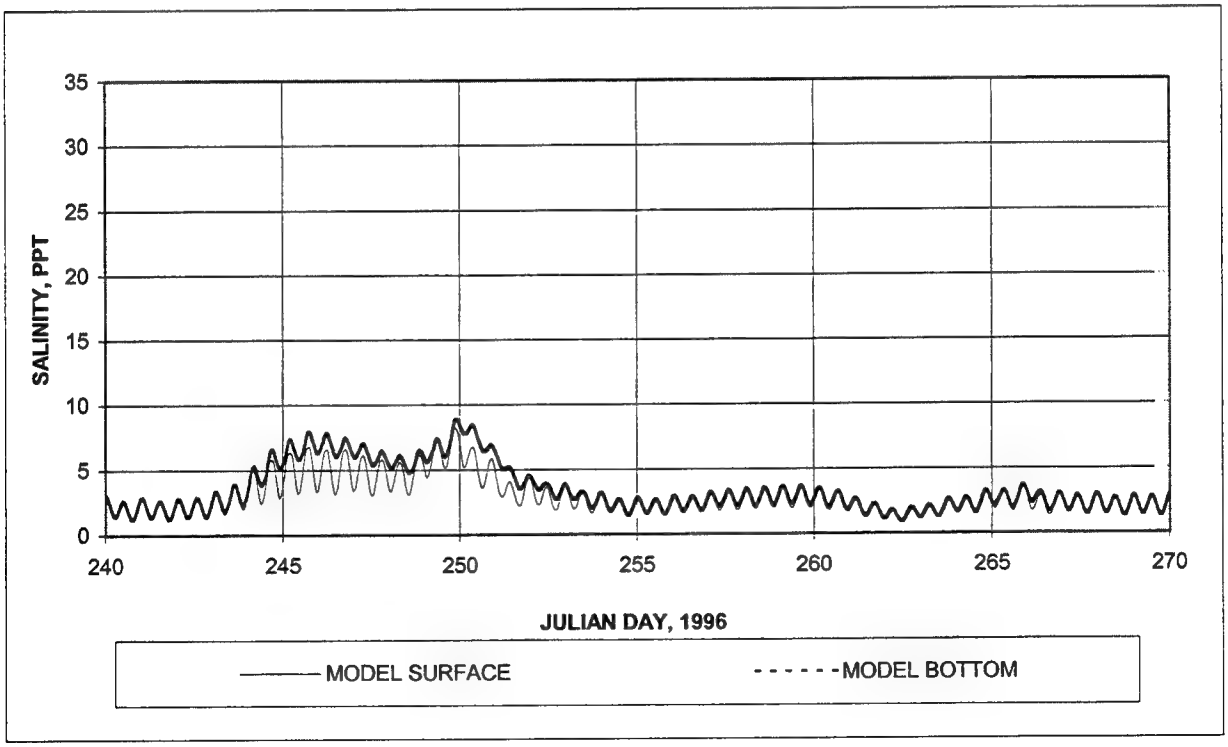

Figure 37. (Concluded)

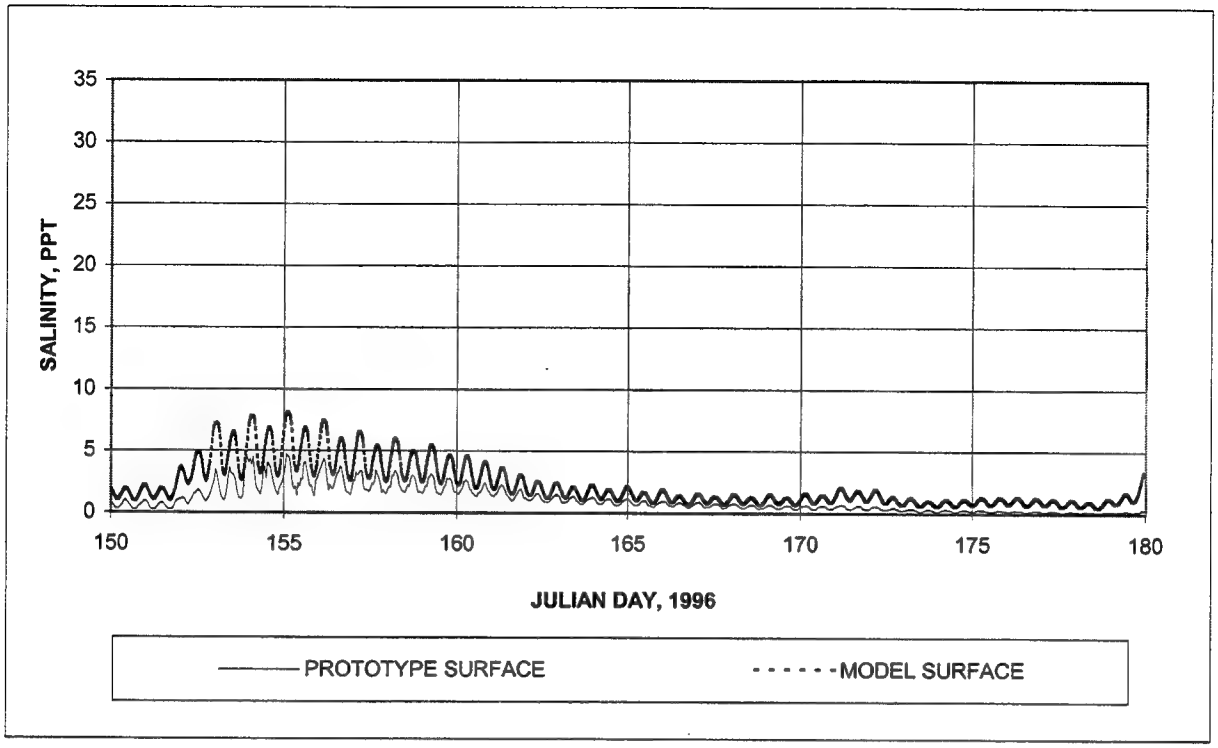

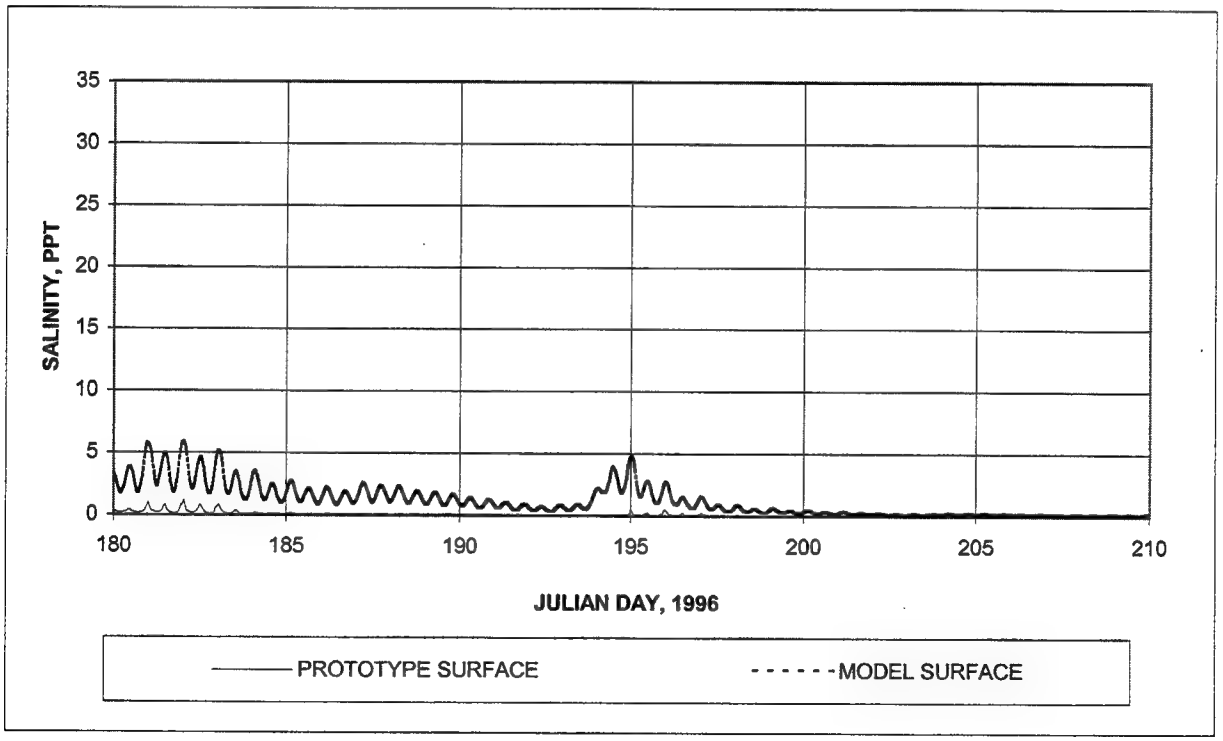

Figure 38. Surface salinity at Buckman Bridge (Continued)

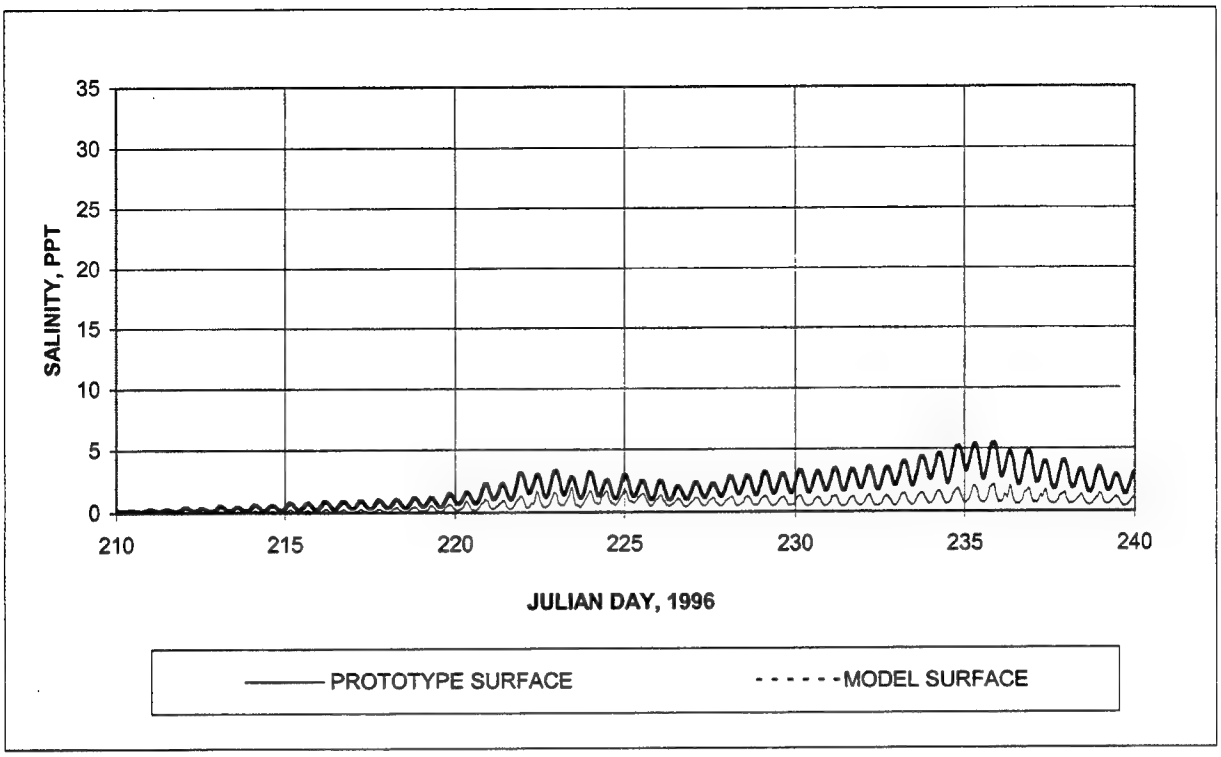

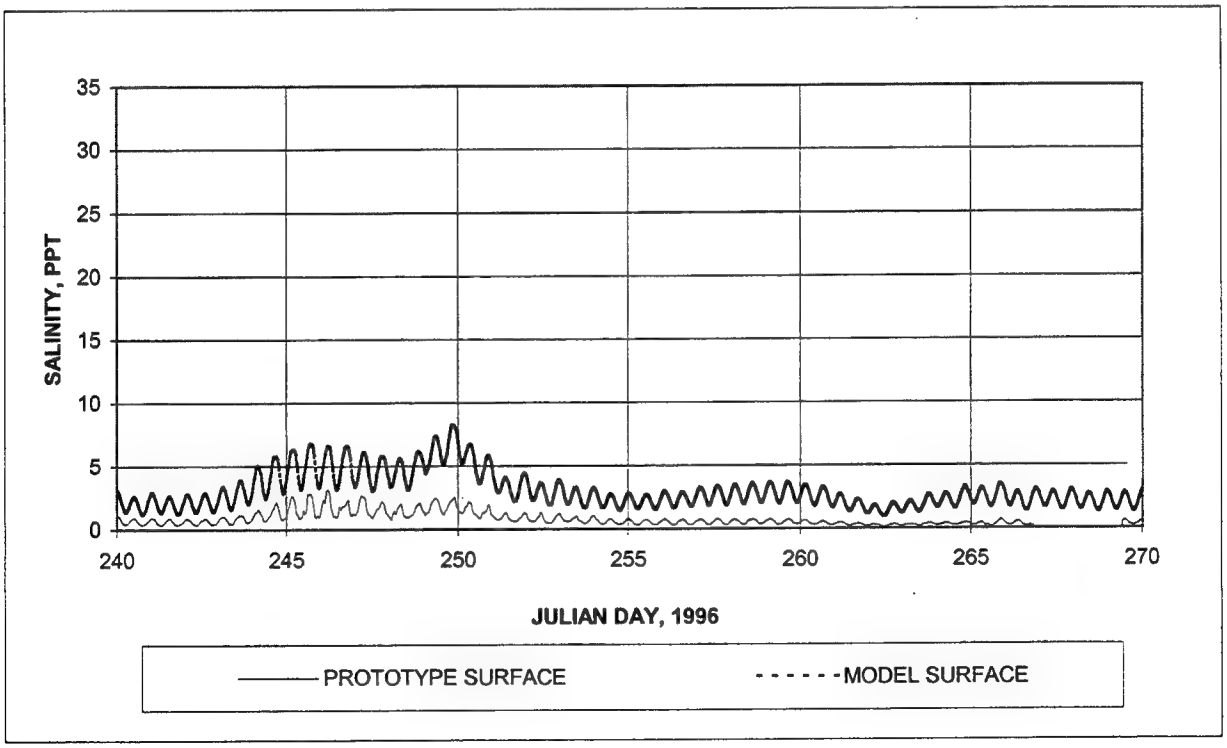

Figure 38. (Concluded)

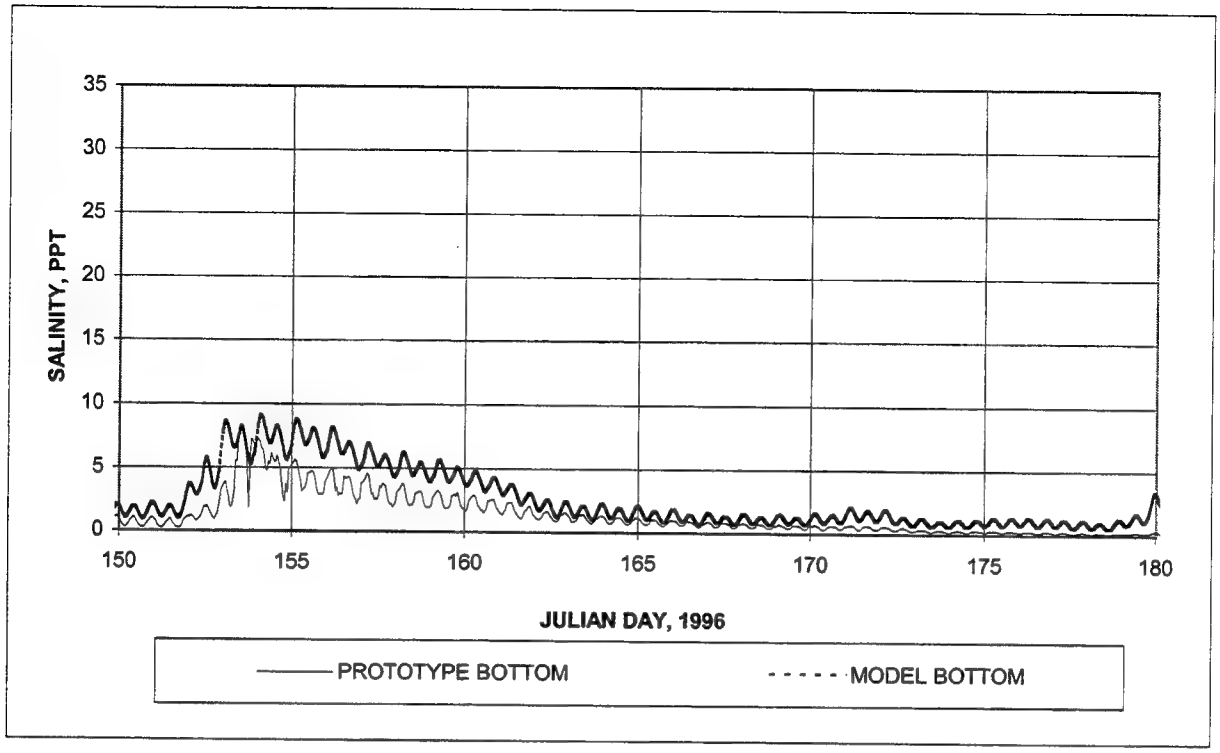

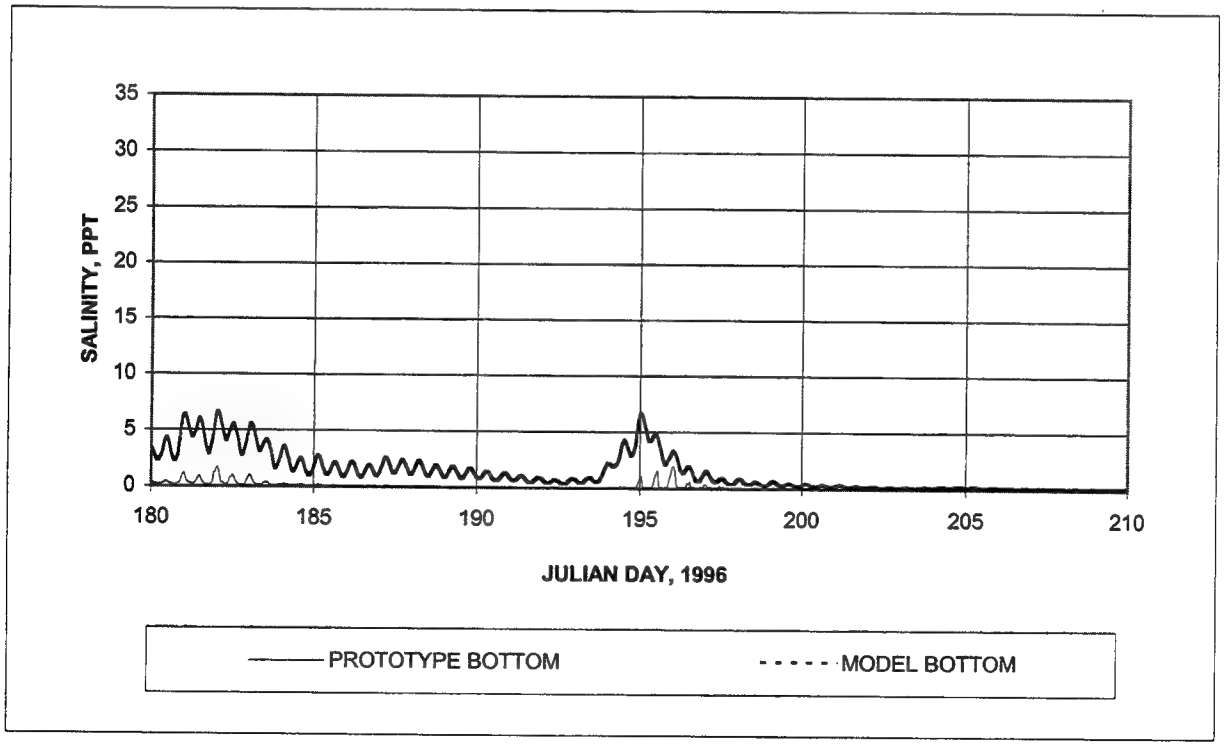

Figure 39. Bottom salinity at Buckman Bridge (Continued)

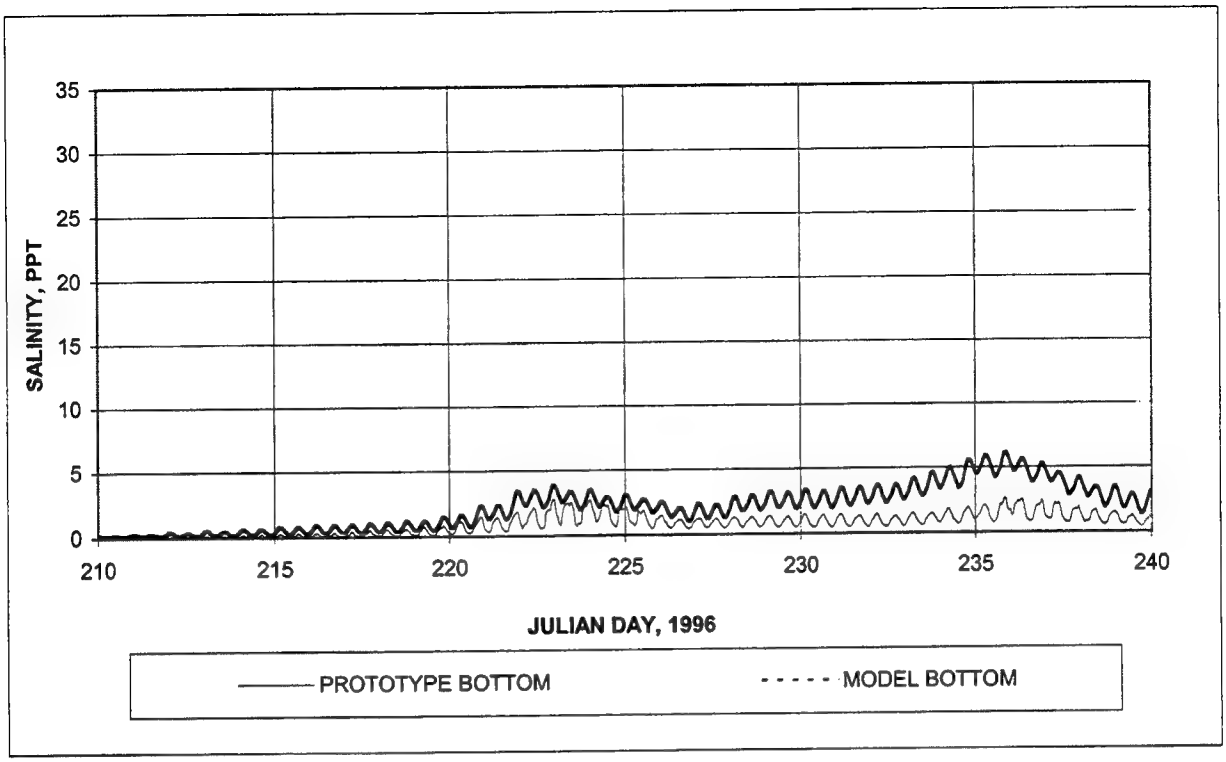

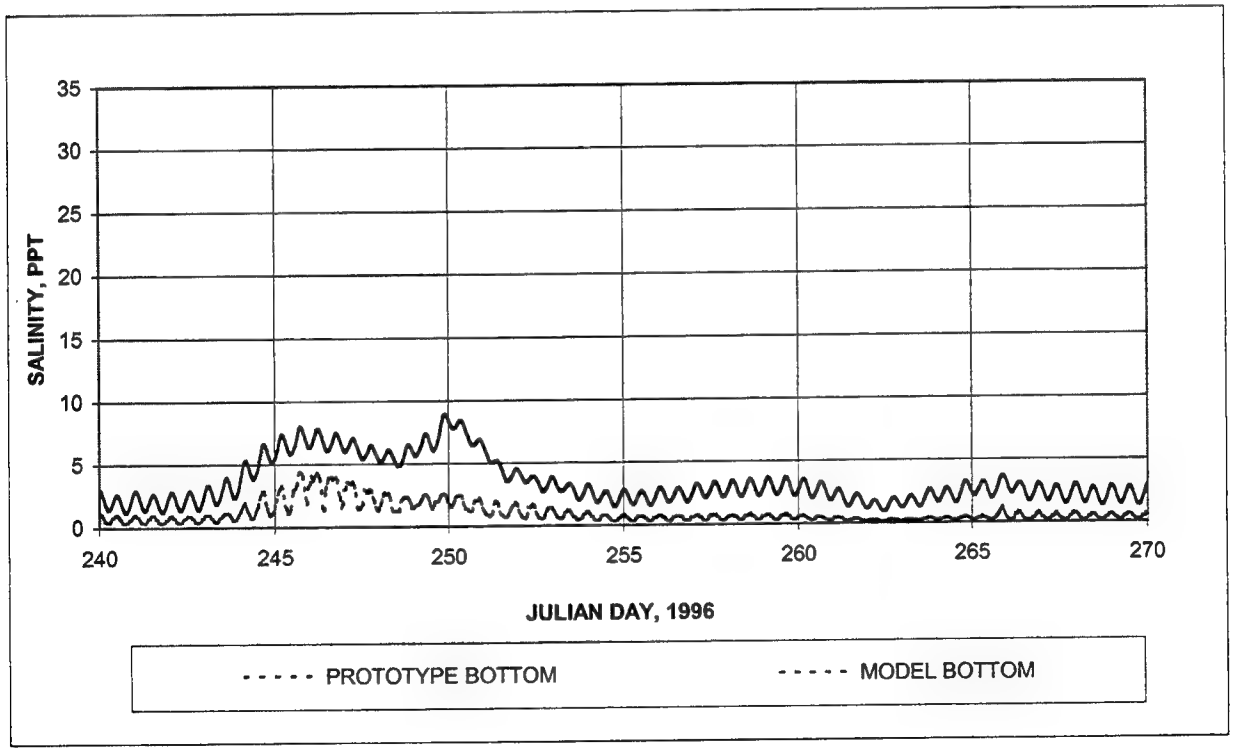

Figure 39. (Concluded)

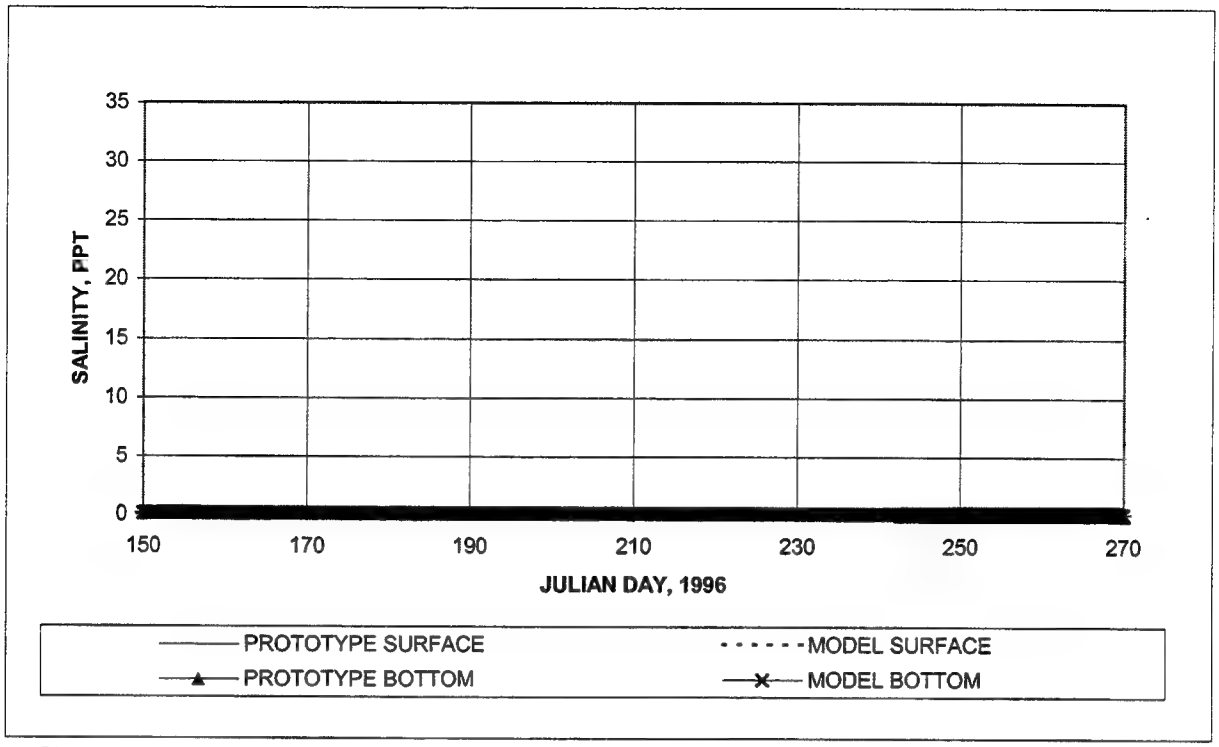

a. Shands Bridge

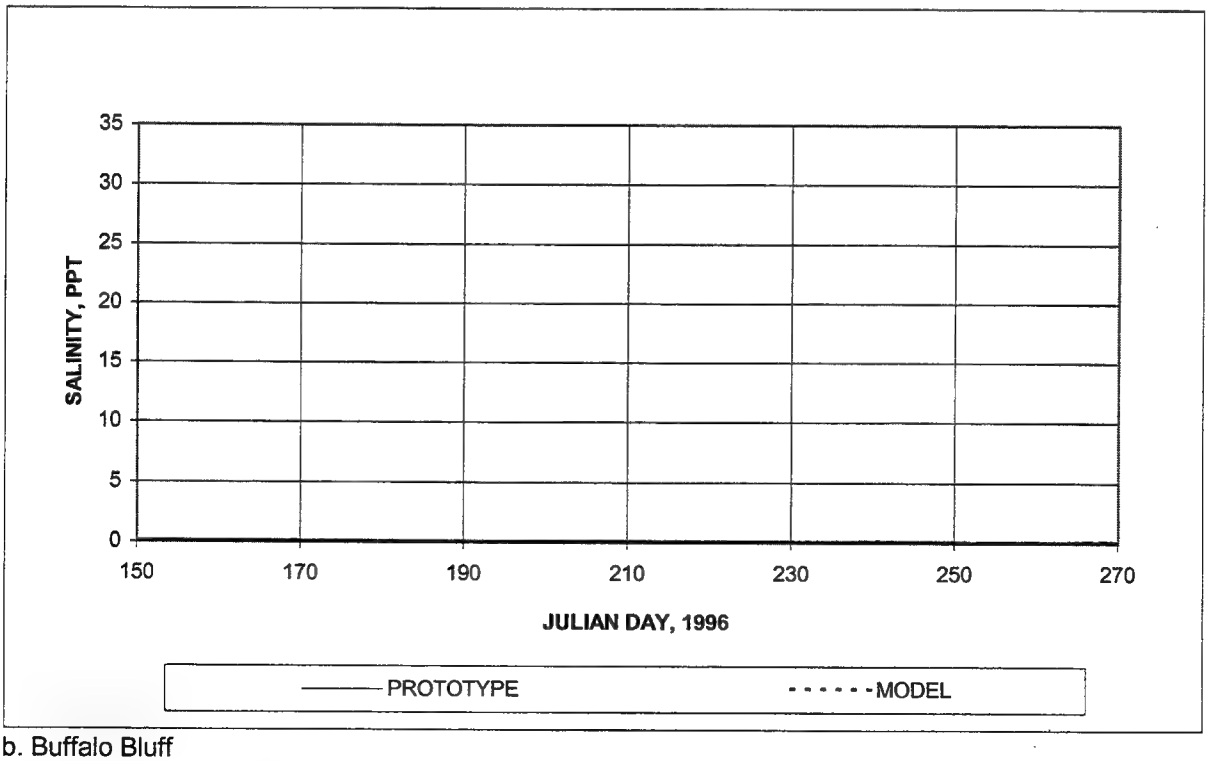

b. Buffalo Bluff

Figure 40. Salinity at Shands Bridge and Buffalo Bluff

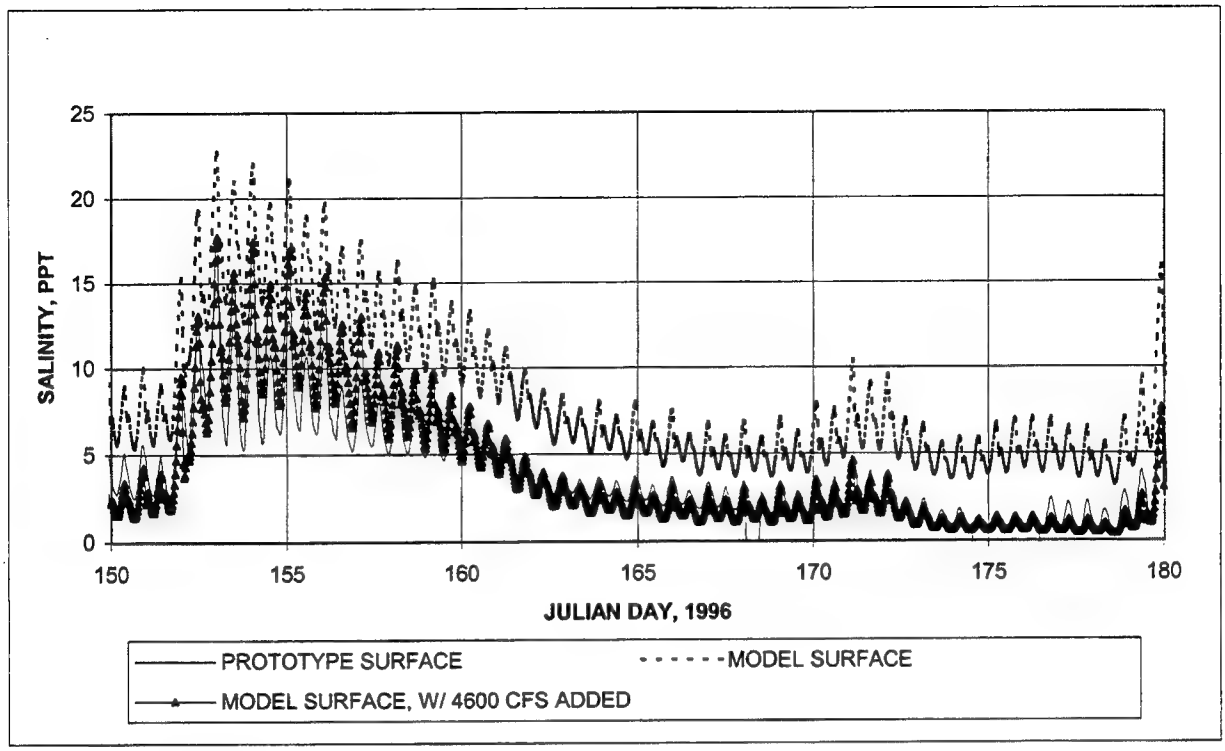

Figure 41. Model reaction to 4,600 cfs of extra inflow evenly distributed throughout the model (Acosta Bridge)

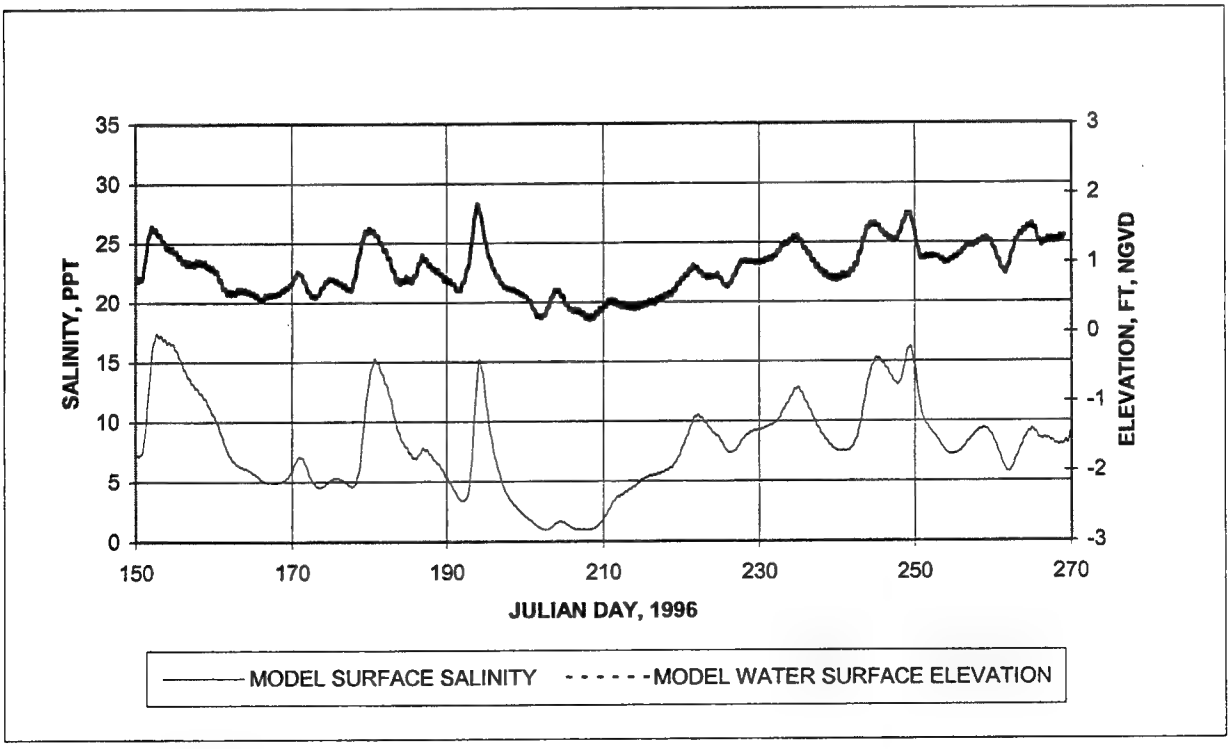

Figure 42. Relationship between daily averages of salinity and water surface elevation (Acosta Bridge)

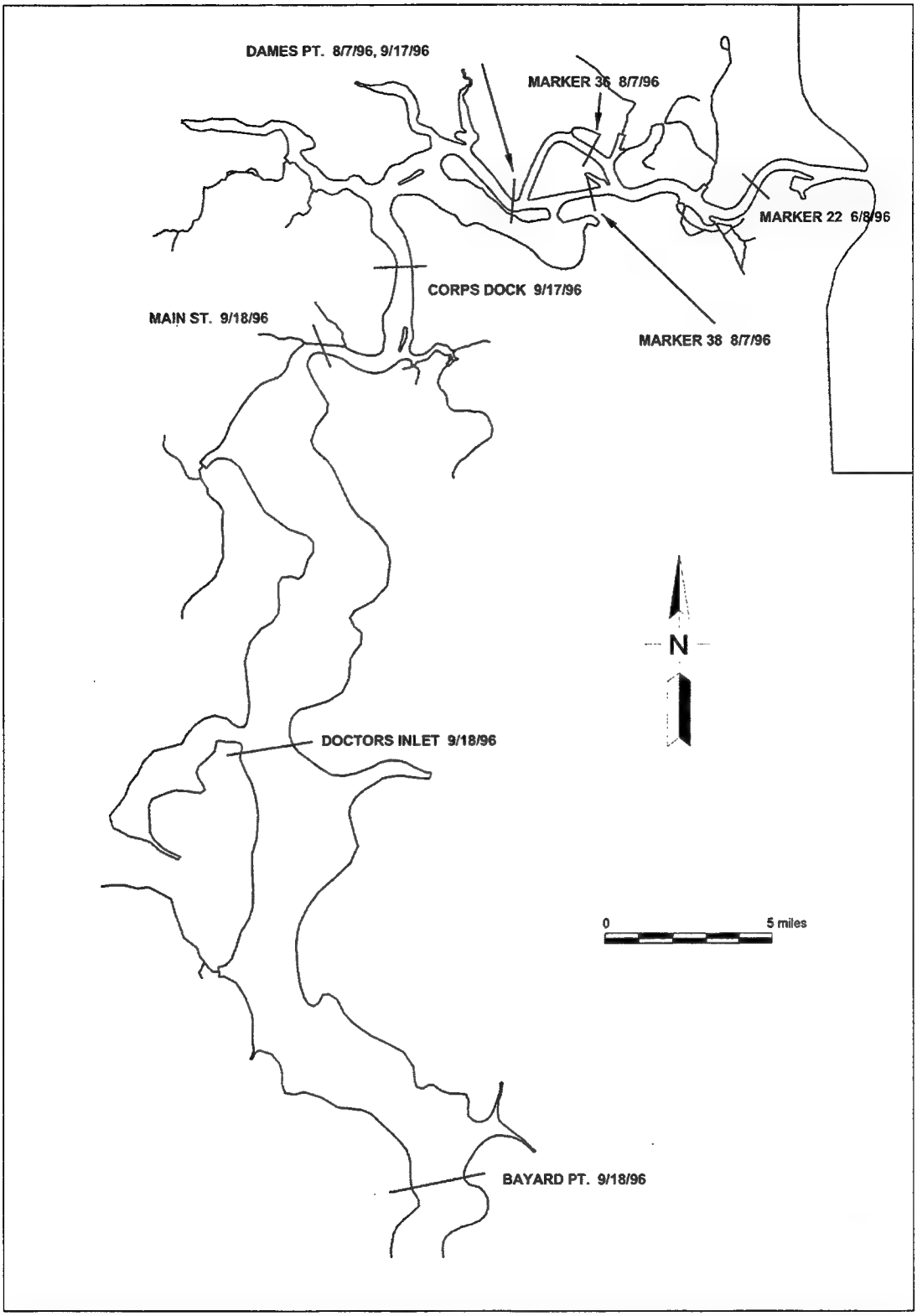

Figure 43. Location of water discharge measurements

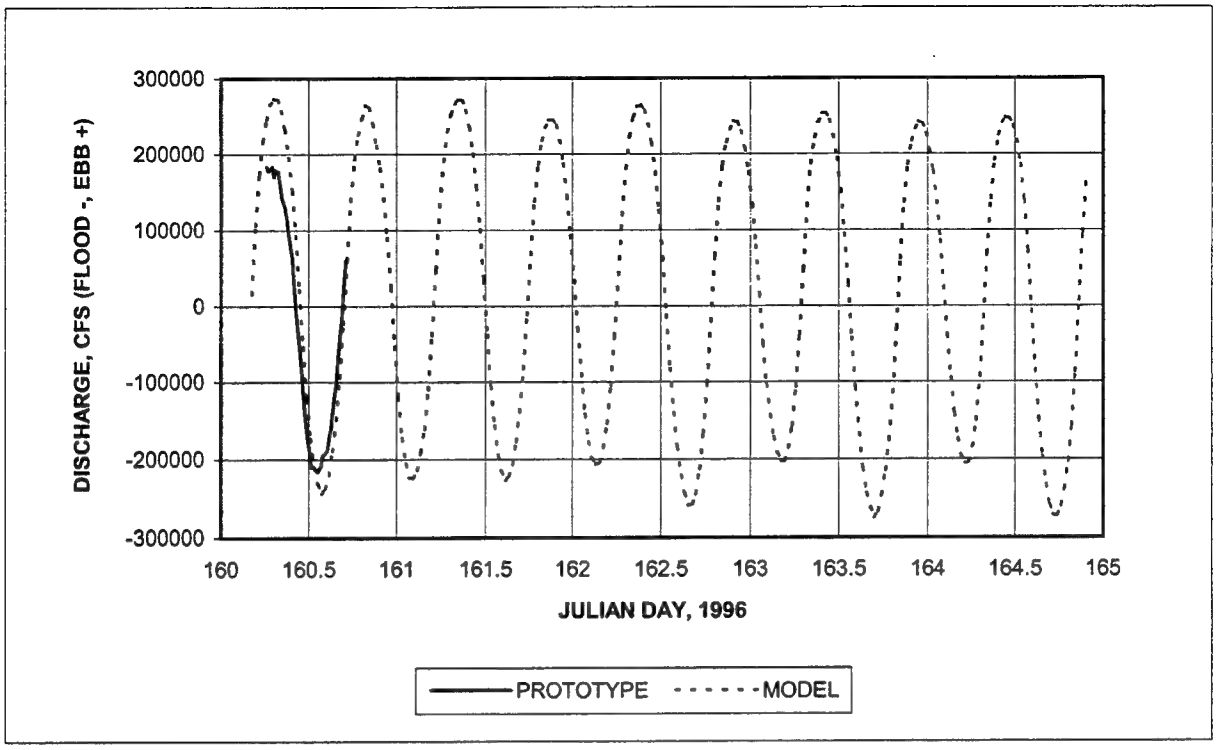

Figure 44. Water discharge at Mayport (Marker 22) (To convert dicharge to cubic meters per second, multiply by 0.02832)

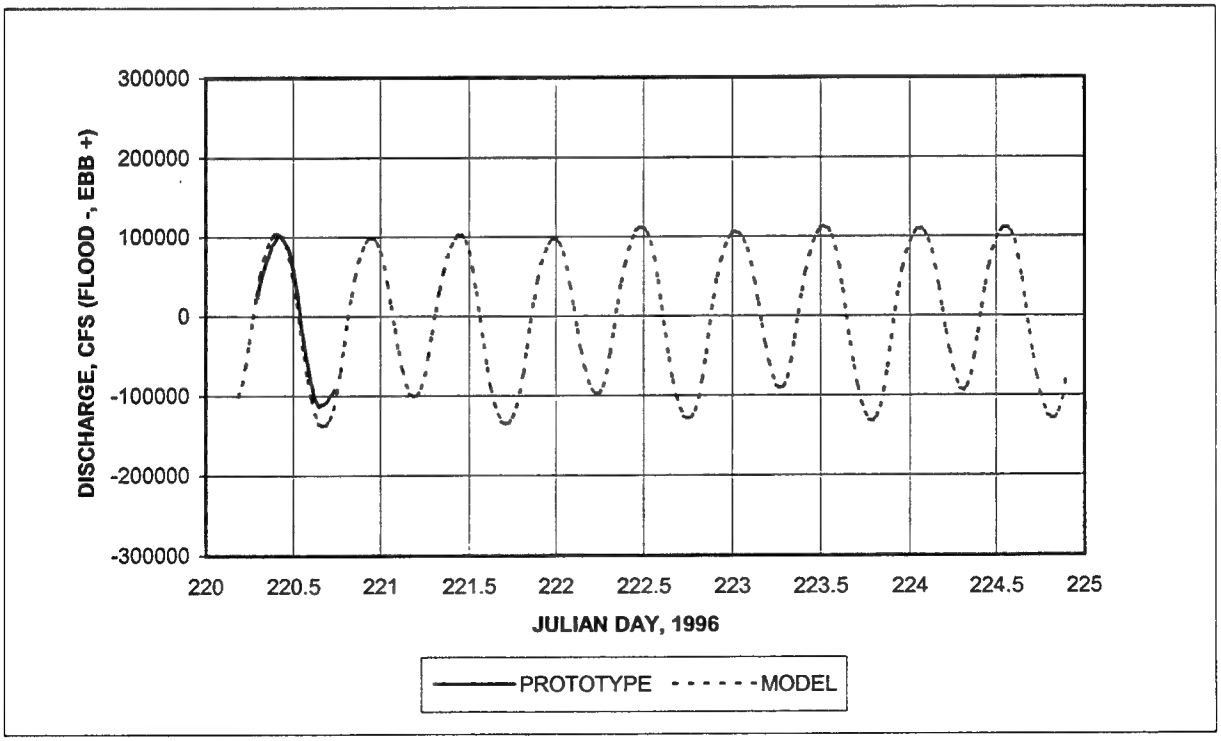

Figure 45. Water discharge at Fulton-Dame Point Cutoff Range (Marker 38) (To convert discharge to cubic meters per second, multiply by 0.02832)

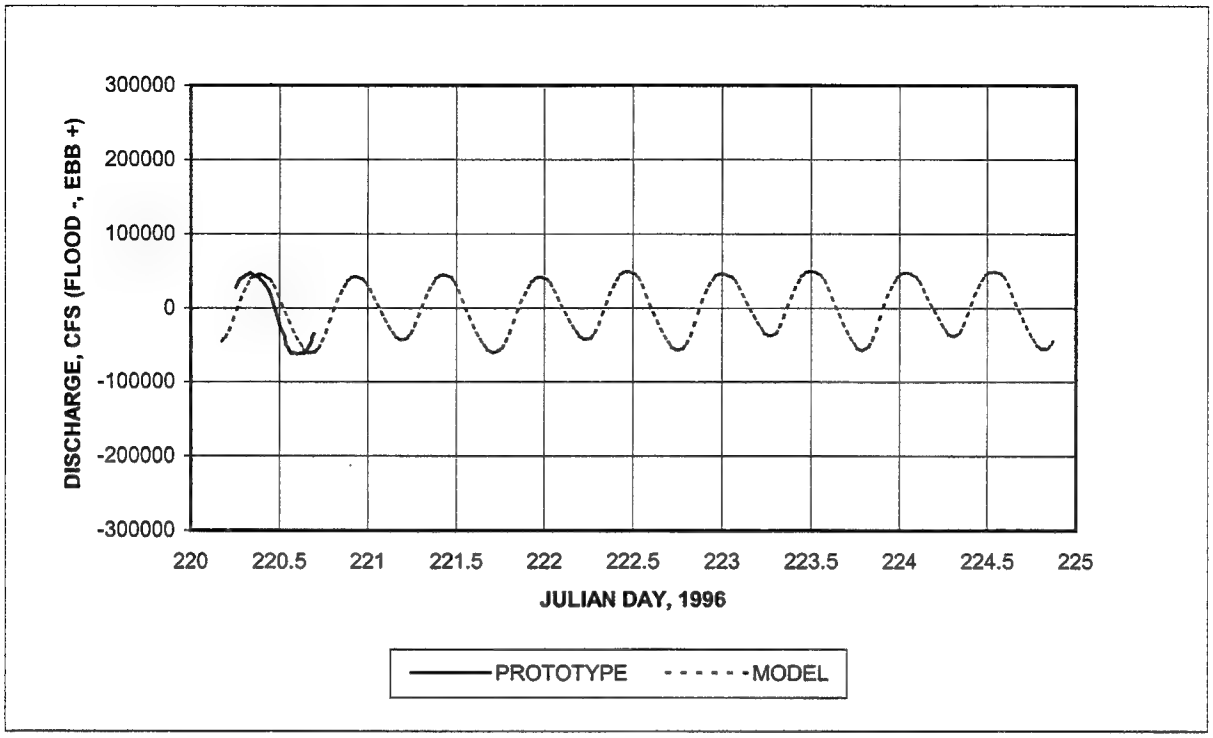

Figure 46. Water discharge at Blount Island Channel (Marker 36) (To convert discharge to cubic meters per second, multiply by 0.02832)

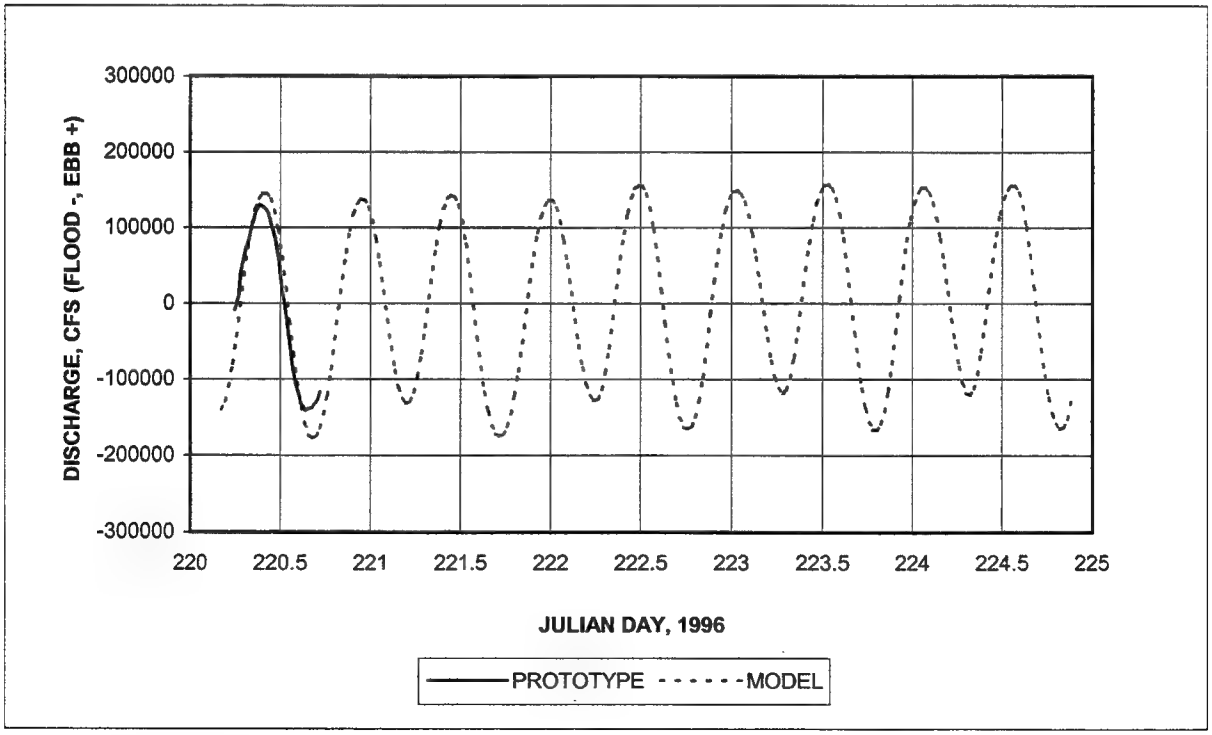

Figure 47. Water discharge at Dames Point (To convert discharge to cubic meters per second, multiply by 0.02832)

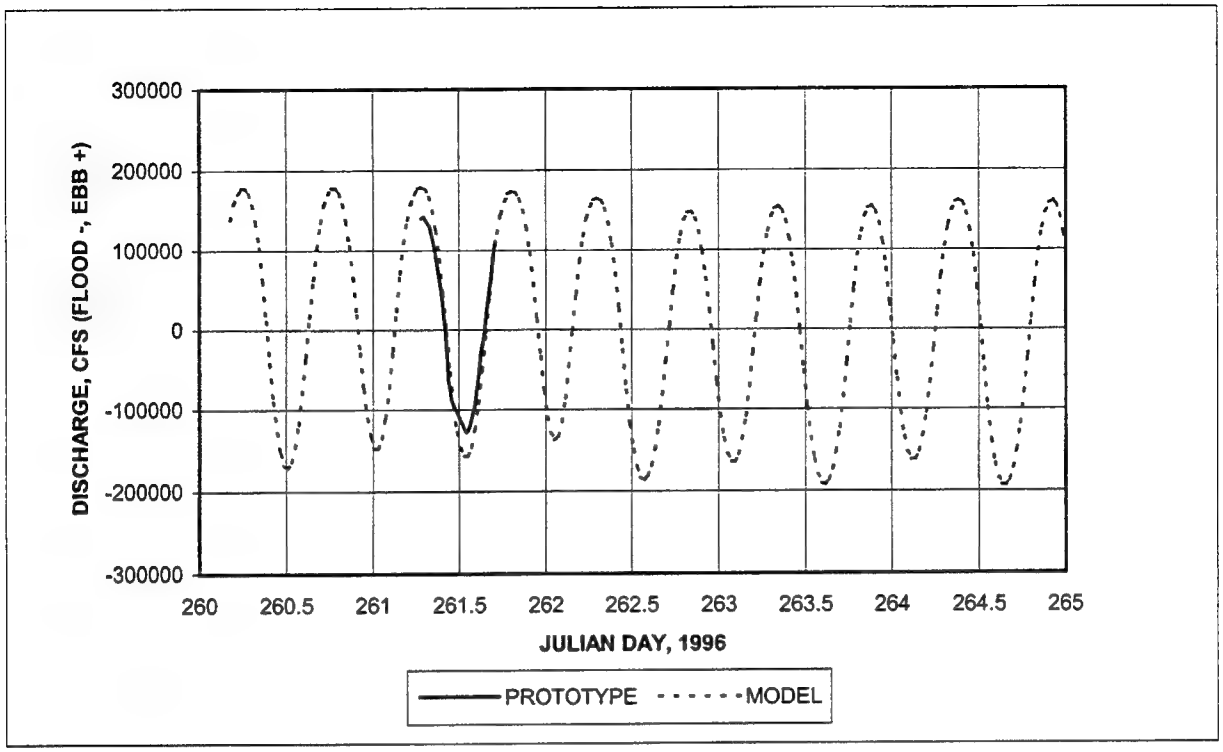

Figure 48. Water discharge at Corps Dock (To convert discharge to cubic meters per second, multiply by 0.02832)

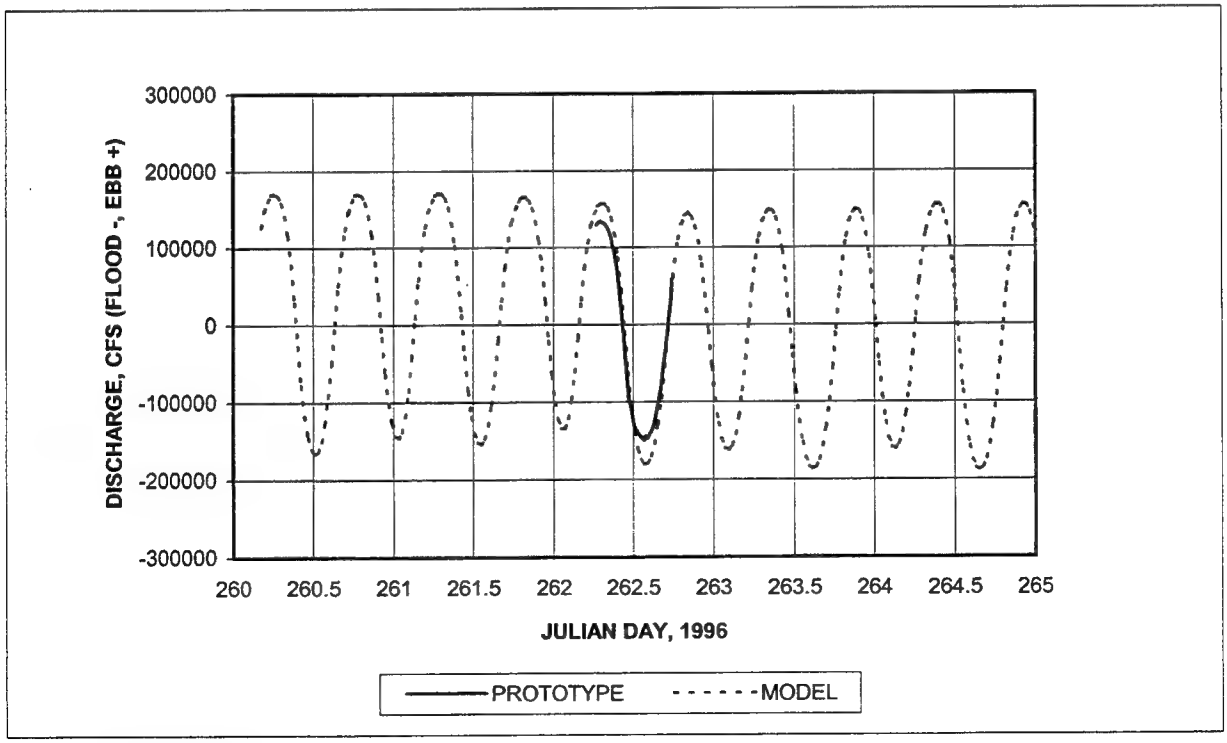

Figure 49. Water discharge at Main Street (To convert discharge to cubic meters per second, multiply by 0.02832)

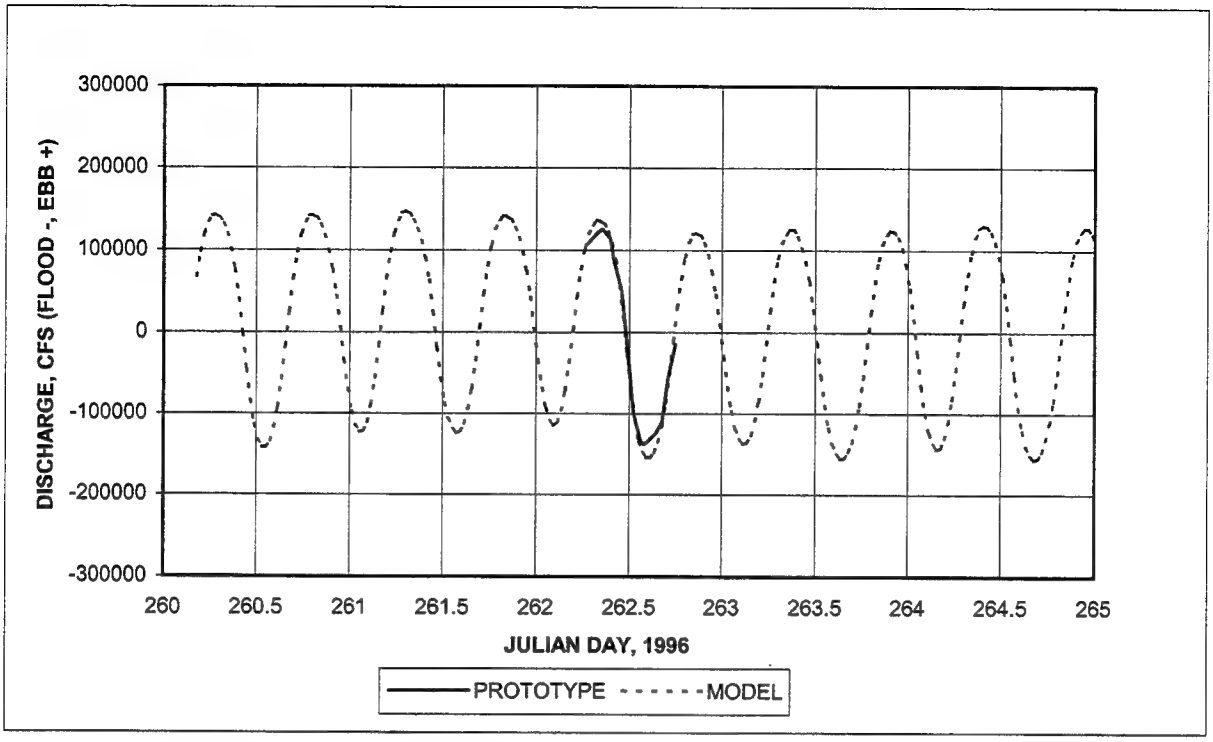

Figure 50. Water discharge at Doctors Inlet (To convert discharge to cubic meters per second, multiply by 0.02832)

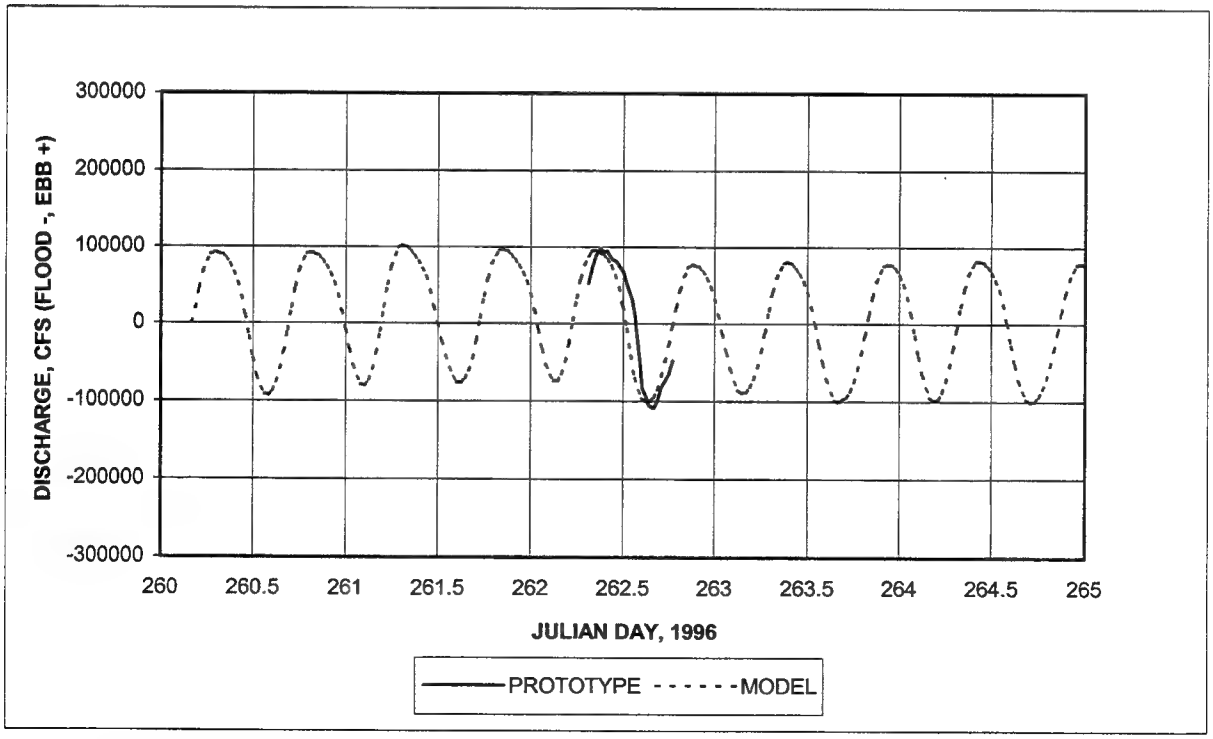

Figure 51. Water discharge at Bayard Point (To convert discharge to cubic meters per second, multiply by 0.02832)

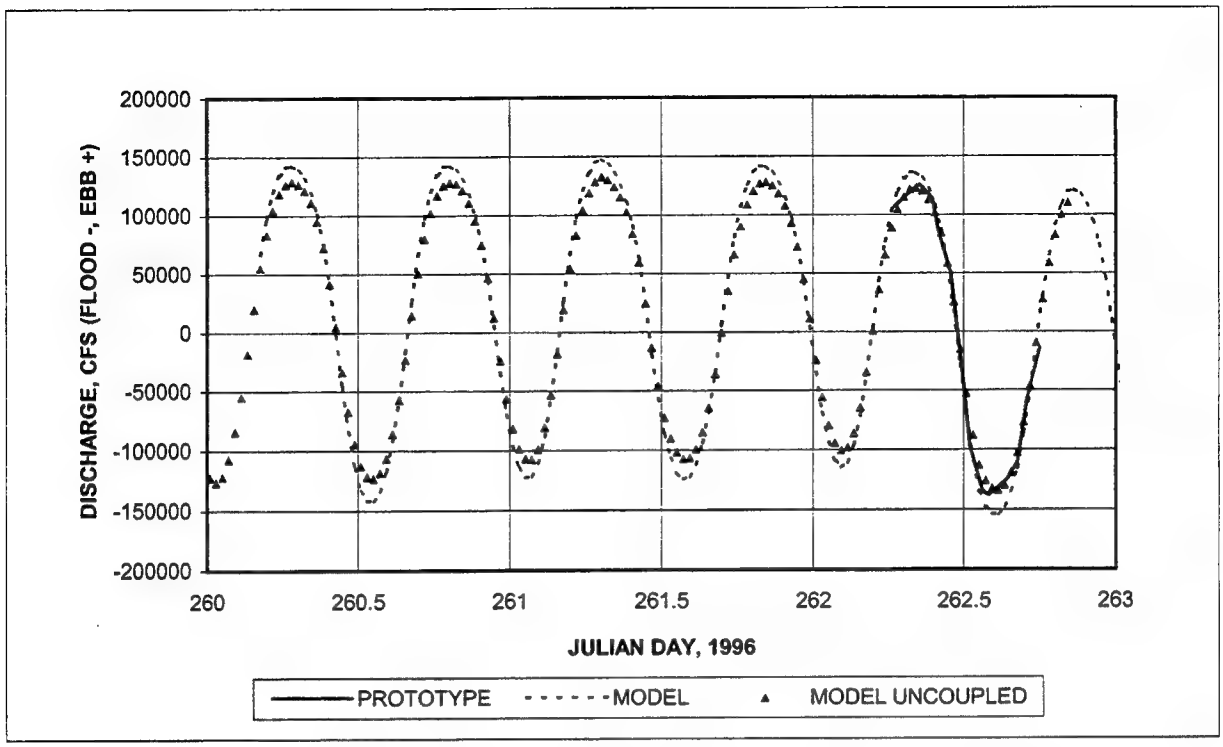

Figure 52. Effect of uncoupling hydrodynamic and salinity computations on water discharge at Doctors Inlet (To convert discharge to cubic meters per second, multiply by 0.02832)

Appendix A

The Finite Elements Approach to Modeling Hydrodynamics and Sediment Transport Using RMA10-WES

Introduction

A model of a particular estuary, river or reservoir, is composed of several parts. There is the geometric description which not only includes the *X*, *Y*, and *Z* locations of points chosen, but also the delineation of bed cover such as grasses, sands, etc. There is also the specification of boundary conditions including all of the forcing mechanisms, tides, wind, inflow, and any constituents. The third part is numerical code. This code has at its core, the basic laws of physics, in particular the relationship between force and acceleration. A consistent model code is a faithful representation of these equations, for sufficient resolution. Since these equations are universal, the range of applicability of the code is limited by the additional empirical relationships to describe turbulent processes, bed roughness, equations of state, and wind stress, and by any simplifying assumptions made in the equations.

There is some degree of uncertainty associated with the geometric description, the boundary conditions and in the numerical code. Often the error indicated by these uncertainties is highest for the specification of the boundary conditions, followed by the geometric description, with the numerical code providing the least of the error. The precise values of inflow and wind fields, particularly in estuarine models, are usually fairly crude. The inflows, for example, are determined by gauges far upstream from the estuary. They leave out large ungauged downstream areas. Also, at the gauge the relationship between gauge elevation and discharge is far from perfect. This relationship changes over time and flow conditions.

These errors can be minimized by careful model verification. Also, modelers can use sound testing procedures to eliminate much of the error from the decision

process. These techniques include plans to base comparisons and sensitivity analysis.

In this paper, one hydrodynamic code is described, RMA10-WES. The Galerkin-based finite element model RMA10-WES is an ERDC adaptation of the RMA-10 code developed by King (1993)[1]. This code computes time-varying open- channel flow and salinity/temperature transport in one, two, and three dimensions. It invokes the hydrostatic pressure and mild slope assumption. Vertical turbulence is supplied using a Mellor-Yamada Level II (Mellor and Yamada 1982) k-ℓ approach modified for stratification by the method of Henderson-Sellers (1984). The salinity/density relationship is based upon Pritchard (1982). The RMA2 code is a predecessor to RMA10-WES but is limited to at most two dimensional cases. The formulation is similar to RMA10-WES and so the only descriptions reported herein will be those of RMA10-WES.

Model Description

The full three-dimensional equations are reduced to a set of two momentum equations, an integrated continuity equation, a convection-diffusion equation, and an equation of state. The simplification is a result of the hydrostatic pressure approximation:

$$\rho \frac{Du}{Dt} - \Delta \bullet \sigma \, x + \frac{\partial P}{\partial x} - \Gamma_x = 0 \tag{1}$$

$$\rho \frac{Dv}{Dt} - \Delta \bullet \sigma \, y + \frac{\partial P}{\partial y} - \Gamma_y = 0 \tag{2}$$

$$\frac{\partial h}{\partial t} + u_\zeta \frac{\partial \zeta}{\partial x} - u_a \frac{\partial a}{\partial x} + v_\zeta \frac{\partial \zeta}{\partial y} - v_a \frac{\partial a}{\partial y} + \int_a^\zeta \left(\frac{\partial u}{\partial x} + \frac{\partial v}{\partial y} \right) dz = 0 \tag{3}$$

$$\frac{Ds}{Dt} - \frac{\partial}{\partial x}\left(D_x \frac{\partial s}{\partial x} \right) - \frac{\partial}{\partial y}\left(D_y \frac{\partial s}{\partial y} \right) - \frac{\partial}{\partial z}\left(D_z \frac{\partial s}{\partial z} \right) = 0 \tag{4}$$

$$\rho = F(s) \tag{5}$$

Elevation-related terms are defined in Figure 1.

[1] References cited in this appendix are listed in the References at the end of the main text.

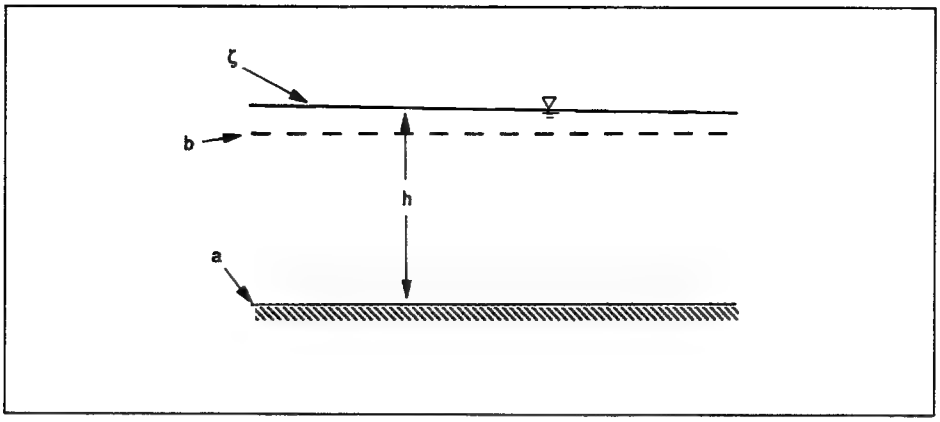

Figure 1. Definitions for elevation terms

where

$$\sigma_x = \left\{ \begin{matrix} E_{xx} & \frac{\partial u}{\partial x} \\ E_{xy} & \frac{\partial u}{\partial y} \\ E_{xz} & \frac{\partial u}{\partial z} \end{matrix} \right\} \quad ; \quad \sigma_y = \left\{ \begin{matrix} E_{yx} & \frac{\partial v}{\partial x} \\ E_{yy} & \frac{\partial v}{\partial y} \\ E_{yz} & \frac{\partial v}{\partial z} \end{matrix} \right\}$$

and

ρ = density

u,v,w = x,y,z velocity components

t = time

P = pressure

$$\Gamma_x = \rho \Omega v - \frac{\rho g u_a (u_a^2 + v_a^2)^{(1/2)}}{C^2} + \psi W^2 \cos(\Theta)$$

$$\Gamma_y = -\rho \Omega u - \frac{\rho g v_a (u_a^2 + v_a^2)^{(1/2)}}{C^2} + \psi W^2 \sin(\Theta)$$

$\Omega = 2\omega\sin(\phi)$

ω = rate of angular rotation of the earth

ϕ = local latitude

g = gravitational acceleration

C = Chezy or Manning friction formulation

ψ = a coefficient from Wu (1980)

W = wind speed

Θ = wind direction counterclockwise from easterly

h = depth

u_ζ, v_ζ = x,y velocity components at the water surface

ζ = water surface elevation

u_a, v_a = x,y velocity

a = bed elevation

s = salinity

D_x, D_y, D_z = diffusion coefficient for salt

E = eddy viscosity components

The continuity equation:

$$\frac{\partial u}{\partial x}+\frac{\partial v}{\partial y}+\frac{\partial w}{\partial z}=0 \tag{6}$$

is solved as a second part of each solution step. Equation 6 is converted to an appropriate boundary value problem through differentiation with respect to z. After rearrangement it takes the form

$$\frac{\partial^2 w}{\partial z^2}=-\frac{\partial}{\partial z}\left(\frac{\partial u}{\partial x}+\frac{\partial v}{\partial y}\right) \tag{7}$$

subject to boundary conditions specified for the water surface and the bed:

$$w_\zeta = u_\zeta \frac{\partial \zeta}{\partial x}+v_\zeta \frac{\partial \zeta}{\partial y}+\frac{\partial h}{\partial t} \quad \text{at the water suface} \tag{8}$$

and

$$w_a = u_a \frac{\partial a}{\partial x} + v_a \frac{\partial a}{\partial y} \quad \text{at the bed.} \tag{9}$$

Note that in these equations the values of u and v will be known at all locations from the previous part of the solution step. Values of w in this solution are used in the next iteration for u, v, h, and s.

The geometric system varies with time; i.e., the water depth h varies during the simulation. To develop an Eulerian form for the solution, it is desirable to transform this system to one that can be described with a constant geometric structure. Early development of the model (King 1982) used a σ-transformation in which the bed and the water surface are transformed to constants. In a later analysis of this method, King (1985) pointed out that at locations where a sharp break in bottom profile occurs, the transformation is not unique and momentum in the component directions may not be correctly preserved. An alternative transformation that preserves the bottom profile as defined, but transforms the water surface to a constant elevation is now used (z^{∇} transformation).

This transformation is defined by:

$$x^{-} = x \tag{10}$$

$$y^{-} = y \tag{11}$$

$$z^{-} = a + (z - a) \frac{(b - a)}{h} \tag{12}$$

where b is the fixed vertical location to which the water surface will be transformed. Equations 1-6 and 7-9 then incorporate the transformation (Equations 10-12).

Another advantage of this transformation is that it produces z^{∇} = constant lines that are close to horizontal, i.e., z = constant lines. This results in less fictitious density-driven currents near bed profile breaks (Stelling and van Kester 1993). Since stratification-related phenomena are usually nearly horizontal, it is important that the transformation leave constant surfaces horizontal. Considering the pressure gradient (due to the density gradient) in this transformation it produces:

$$\frac{\partial P}{\partial x} = \frac{\partial P}{\partial x^{-}} + \frac{\partial P}{\partial z^{-}} \frac{\partial z^{-}}{\partial x} \tag{13}$$

In a strongly stratified stagnant system this pressure gradient should be zero. However, note that Equation 13 in the transformed system is dependent upon two terms (each of which could be large) to cancel each other. This could cause

artificial currents due to truncation and roundoff error. A transformation in which $\partial z^{\nabla}/\partial x \approx 0$, i.e., $z^{\nabla} \approx z$, will reduce this problem. Figure 2 shows an example in which a 12.2-m-deep (40-ft-deep) channel passes through a 2.4-m-deep (8-ft-deep) bay. Here b is chosen to be an elevation of 0 and ζ is 0.6 m (2 ft). Near the break in the bed profile $\partial z^{\nabla}/\partial x$ is fairly small, or z^{∇} surfaces are nearly horizontal. Contrast this with the σ transformation in Figure 3. The σ = constant surfaces are far from horizontal along the channel side slopes. The truncation and roundoff errors tend to drive fictitious currents that cause the denser salt water to leave the channel. The z^{∇} transformation results in:

$$\frac{\partial z^{-}}{\partial x} = 0\,(\zeta - b) \tag{14}$$

whereas the σ transformation is:

$$\frac{\partial \sigma}{\partial x} = 0\,(h) \tag{15}$$

which is much larger.

The Galerkin finite element approximation of Equations 1-4 and 7 uses a quadratic approximation for u, v, w, and s and linear for h and P. The

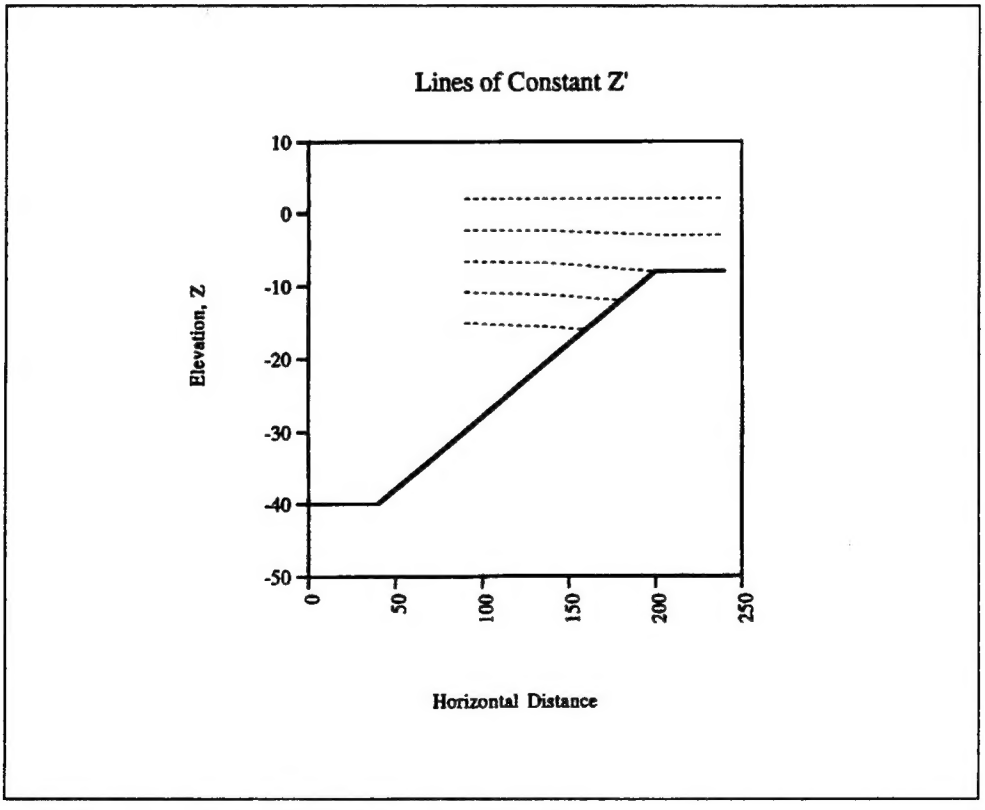

Figure 2. Lines of constant z near a significant grade change

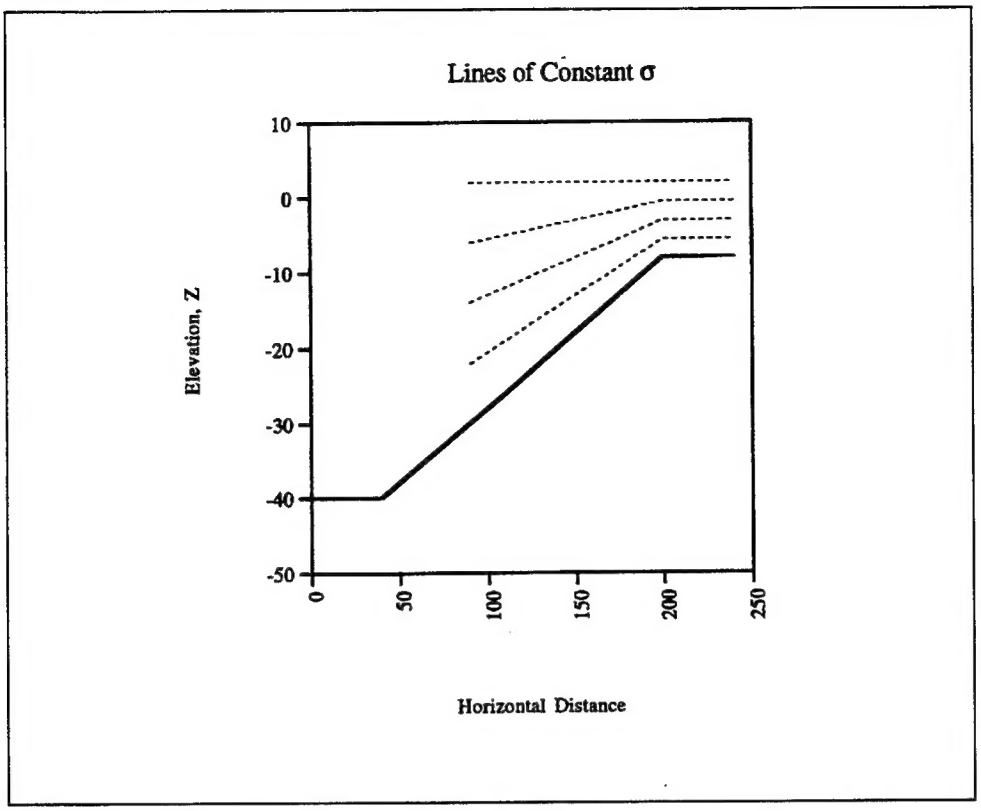

Figure 3. Lines of constant σ near a significant grade change

nonlinearity is addressed by Newton-Raphson iteration at each time-step. Generally the iteration process is split into calculation of Equations 1-3, then 7, followed by 4. This sequence is repeated until sufficient convergence is reached.

Sediment Transport

RMA2 is an ancestor of the RMA10-WES code and is similar in approach. That code was 2-D and 1-D. It did not directly handle sediment transport. Instead, it supplied the currents and water surface elevations to drive a separate sediment transport code, STUDH or SED2D. These sediment transport codes include both cohesive and non-cohesive sediment and the bed interaction algorithms. By separating the hydrodynamics and sediment transport into two codes, the sedimentation process could not directly influence the hydrodynamics. In the development of RMA10-WES, we have included the sediment transport in the hydrodynamic code. At present only cohesive sediments are programmed.

For cohesive sediment the erosion and deposition is described by time rates that are dependent upon the bed shear stress. In RMA10-WES the deposition rate is described Krone (1962).

$$S = -V_s C(1 - \frac{\tau}{\tau_d}) for C \leq C_c \quad (16)$$

$$S = -V_k C^{5}/^{3}(1 - \frac{\tau}{\tau_d}) for C \geq C_c \quad (17)$$

where:

τ = bed shear stress

τ_d= critical shear stress for deposition

V_s= settling velocity

C = the concentration near the bed

C_c= critical concentrarion, 300 *mg/l*

V_k= the hindered settling velocity, $V_s/C_c^{4/3}$

The erosion rate is given by Partheniades (1962).

$$S = P(\frac{\tau}{\tau_e} - 1) \quad (18)$$

where:

P = erosion rate constant

τ_e = the critical shear stress for particle erosion.

The bed algorithim is maintained as a set of fluctuation layers, each with assigned properties. The concentration of the sediment is approximated quadratically over each element in the grid.

REPORT DOCUMENTATION PAGE

Form Approved
OMB No. 0704-0188

1. REPORT DATE *(DD-MM-YYYY)*	2. REPORT TYPE	3. DATES COVERED *(From - To)*
July 2000	Final report	

4. TITLE AND SUBTITLE
Lower St. Johns River and Estuary, Florida, Numerical Model Study

5a. CONTRACT NUMBER

5b. GRANT NUMBER

5c. PROGRAM ELEMENT NUMBER

6. AUTHOR(S)
Jose A. Sanchez , Robert A. Evans, Jr.

5d. PROJECT NUMBER

5e. TASK NUMBER

5f. WORK UNIT NUMBER

7. PERFORMING ORGANIZATION NAME(S) AND ADDRESS(ES)

U.S. Army Engineer Research and Development Center
Coastal and Hydraulics Laboratory
3909 Halls Ferry Road
Vicksburg, MS 39180-6199

U.S. Army Engineer District, Jacksonville
P.O. Box 4970
Jacksonville, FL 32232-0019

8. PERFORMING ORGANIZATION REPORT NUMBER

ERDC/EL TR-00-10

9. SPONSORING / MONITORING AGENCY NAME(S) AND ADDRESS(ES)
U.S. Army Engineer District, Jacksonville
P.O. Box 4970
Jacksonville, FL 32232-0019

10. SPONSOR/MONITOR'S ACRONYM(S)

11. SPONSOR/MONITOR'S REPORT NUMBER(S)

12. DISTRIBUTION / AVAILABILITY STATEMENT

Approved for public release; distribution is unlimited.

13. SUPPLEMENTARY NOTES

14. ABSTRACT

The U.S. Army Engineer Research and Development Center (ERDC) developed a multidimensional hydrodynamic and salinity model of the Lower St. Johns River and Estuary (LSJRE) Florida. The developed model was intended as a general planning tool to gain insight inot the hydrodynamics and transport mechanisms of the system. Model results were verified against prototype hydrodynamic and salinity data. The model satisfactorily reproduces tidal elevations, discharges, and salinity trends.

15. SUBJECT TERMS
Hydrodynamic, Jacksonville, Florida, Numerical Model, RMA10, Salinity, St. Johns River

16. SECURITY CLASSIFICATION OF:			17. LIMITATION OF ABSTRACT	18. NUMBER OF PAGES	19a. NAME OF RESPONSIBLE PERSON
a. REPORT	b. ABSTRACT	c. THIS PAGE			19b. TELEPHONE NUMBER *(include area code)*
UNCLASSIFIED	UNCLASSIFIED	UNCLASSIFIED		96	